

Electronic Thesis and Dissertation Repository

4-22-2013 12:00 AM

Mapping and Zircon Geochronology of the Lyon Inlet Boundary Zone, Nunavut; a Crustal Scale Break in the Churchill Province

Nikolas B. Ganderton
The University of Western Ontario

Supervisor
Dr Desmond Moser
The University of Western Ontario

Graduate Program in Geology
A thesis submitted in partial fulfillment of the requirements for the degree in Master of Science
© Nikolas B. Ganderton 2013

Follow this and additional works at: <https://ir.lib.uwo.ca/etd>



Part of the [Geochemistry Commons](#), and the [Geology Commons](#)

Recommended Citation

Ganderton, Nikolas B., "Mapping and Zircon Geochronology of the Lyon Inlet Boundary Zone, Nunavut; a Crustal Scale Break in the Churchill Province" (2013). *Electronic Thesis and Dissertation Repository*. 1318.
<https://ir.lib.uwo.ca/etd/1318>

This Dissertation/Thesis is brought to you for free and open access by Scholarship@Western. It has been accepted for inclusion in Electronic Thesis and Dissertation Repository by an authorized administrator of Scholarship@Western. For more information, please contact wlsadmin@uwo.ca.

MAPPING AND ZIRCON GEOCHRONOLOGY OF THE LYON INLET
BOUNDARY ZONE, NUNAVUT; A CRUSTAL-SCALE BREAK IN THE
CHURCHILL PROVINCE

(Thesis format: Monograph)

by

Nikolas Ganderton

Graduate Program in Geology

A thesis submitted in partial fulfillment
of the requirements for the degree of
Master of Science

The School of Graduate and Postdoctoral Studies
The University of Western Ontario
London, Ontario, Canada

© Nikolas B. Ganderton 2013

Abstract

An important aspect of geology is the understanding of processes that created and modified continents and their resources. Knowledge of the age of formation and metamorphism of crystalline crust is thus important, and has been pursued in a recently discovered crustal-scale boundary on the southern Melville Peninsula (Nunavut, Canada) through field mapping, U-Pb zircon geochronology and electron beam analysis. This >250km-long crustal feature is here termed the Lyon Inlet Boundary Zone (LIBZ). Three samples from a 15 by 20 km map area reveal a complex Archean history with the dominant granitoid unit crystallizing at 2770 ± 38 Ma and metamorphosed at 2670 ± 36 Ma. All samples exhibit a range of Paleoproterozoic metamorphic zircon growth events ranging from 1842 ± 14 Ma to 1802 ± 10 Ma. The youngest event is a minimum age for amphibolite facies metamorphism, and presumably deformation, in the LIBZ, temporally linking it to the terminal stages of Trans-Hudsonian mountain-building in arctic Canada.

Keywords

Zircon, Churchill Province, Rae sub-province, U-Pb geochronology, mapping, craton formation, Trans-Hudson.

Acknowledgments

I am thankful to the GSC's Geo-mapping for Energy and Minerals (GEM) Melville Peninsula project and the Research Affiliate Program (RAP), which provided me with the opportunity, logistical support, and funding to work on this project. The summer field season was a fantastic experience where I met a group of wonderful people and began work on this fascinating project.

I appreciate the assistance I received from Natasha Wodicka, Tom Pestaj, Bill Davis, and Nicole Rayner at the GSC SHRIMP Lab. You made my first SHRIMP experience very smooth, and taught me some valuable lessons. I would like to say a special thank-you to Natasha – you have been exceedingly helpful throughout this project, whether providing me with supplementary data, or giving suggestions.

Throughout my many years at Western, I have encountered a number of people who have offered me support, encouragement, and inspiration. I am grateful for the friendship and support I have received from many past and present graduate students, especially Devrim Husrevoglu, Sonya Corker, Kyle Frank, Keith Landon, and Nicolle Bellissimo. Thank-you all for the many chats, beers, and adventures. I would also like to thank the many Earth Sciences staff and faculty who have helped shape my interests over the years, especially Phil McCausland, Roberta Flemming, Patricia Corcoran, Neil Banerjee, Norm Duke, and Bill Church.

My research experience would not have been the same without the constant support and assistance from everyone in the Zircon and Accessory Phase Lab (ZAPLab). I am deeply grateful for all of the help I have received over the years from Duane Petts, Ivan Barker, Lisa Cupelli, and James Darling. Each of you taught me numerous skills, offered great advice, and taught me invaluable lessons about the world of geochronology and research. Your constant friendship, mentorship, and assistance made this project an amazingly enjoyable and interesting experience.

I would also like to express my gratitude to my family and friends who have supported and encouraged me throughout this challenging journey. You were always there for me in every situation, lending a helping hand or offering inspiration and reassurance. I am especially grateful to Jill and Rik Ganderton for always supporting my every endeavour and encouraging me to push my own limits. I also thank Scott Messenger, Akos Solti, Chris Wonnell, H  l  ne LeVasseur, Tom Ganderton, and all of the McKibben crew for their friendship throughout my university career – I am extremely fortunate to have met such great friends as you.

Finally, I would like to thank my supervisors, Des Moser and David Corrigan for their support, dedication and assistance throughout this project. I would like to thank David for the invaluable assistance in the field and onwards. Your infectious kindness, help defining and organizing the initial project, logistical support, constant advice, and sharing of extra materials truly made this project a pleasure to work on. Above all, I would like to thank Des for his unending support and encouragement. Your constant mentorship, guidance, and kindness have made this project a delight to work on, and I am especially thankful that you were so involved even during your sabbatical. I have thoroughly enjoyed working with you for these past few years, and I am eternally grateful for the countless opportunities you have provided me. I couldn't have asked for a better experience. Thank you.

Table of Contents

Abstract.....	ii
Acknowledgments.....	iii
Table of Contents.....	v
List of Figures.....	viii
List of Appendices.....	xii
1 Introduction.....	1
2 Geochronological Theory and Geologic Setting.....	2
2.1 Geochronological Theory.....	2
2.1.1 Zircon.....	2
2.1.2 Monazite.....	2
2.1.3 U-Pb Geochronology.....	3
2.1.4 Concordia Plots.....	4
2.1.5 Lead Loss.....	4
2.1.6 Migmatites.....	5
2.2 Geologic Setting.....	6
3 Methods.....	13
3.1 Sampling and Mapping.....	13
3.2 Thin Sections.....	13
3.3 Mineral Separation.....	13
3.3.1 Hand Crushing.....	14
3.3.2 Shatter Box.....	14
3.3.3 Wilfley Table Density Sorting.....	14
3.3.4 Frantz Magnetic Separation.....	15

3.3.5	Heavy Liquid Separation	16
3.3.6	Picking	18
3.4	SHRIMP U-Pb Analysis and FEG-SEM Imaging	18
3.4.1	SHRIMP U-Pb Analysis	18
3.4.2	FEG-SEM Imaging	18
4	Results	21
4.1	Mapping	21
4.1.1	Carbonates.....	21
4.1.2	Aluminous Gneisses and Migmatites.....	24
4.1.3	Pegmatites	25
4.1.4	Granitoids.....	26
4.2	Sampling Rationale.....	27
4.3	Sample 10644 (G060A1)	27
4.3.1	Sample Description.....	27
4.3.2	EDS Phase Mapping and BSE-EDS “Feature” Mapping	29
4.3.3	BSE and SE of Zircon in Thin Section	31
4.3.4	Zircon in Separates	33
4.3.5	SE and Colour-CL of SHRIMP Mount.....	34
4.3.6	U-Pb Isotopic Data and Th/U Ratios	34
4.4	Sample 10645 (G067A1)	39
4.4.1	Sample Description.....	39
4.4.2	EDS Phase Mapping and BSE-EDS “Feature” Mapping	40
4.4.3	BSE and SE of Zircon in Thin Section	41
4.4.4	Zircon in Separates	43
4.4.5	SE and Colour-CL of SHRIMP Mount.....	43

4.4.6	U-Pb Isotopic Data and Th/U Ratios	45
4.5	Sample 10646 (G071A1)	48
4.5.1	Sample Description	48
4.5.2	EDS Phase Mapping and BSE-EDS “Feature” Mapping	49
4.5.3	BSE and SE of Zircon in Thin Section	51
4.5.4	Zircon in Separates	52
4.5.5	SE and Colour-CL of SHRIMP Mount.....	52
4.5.6	U-Pb Isotopic Data and Th/U Ratios	53
5	Discussion	57
5.1	U-Pb Chronology of Individual Samples.....	57
5.1.1	History of Sample 10644 (G060A1).....	57
5.1.2	History of Sample 10645 (G067A1).....	63
5.1.3	History of Sample 10646 (G071A1).....	66
5.2	Chronology of the LIBZ	67
5.3	Relating the LIBZ to the Churchill Province	69
5.3.1	Archean Activity	69
5.3.2	Proterozoic Activity	70
5.4	Age Bracket on Ductile Strain in the LIBZ	71
5.5	Suggestions for Future Work	73
6	Conclusions	74
6.1	Conclusions.....	74
	References	76
	Appendices.....	79
	Curriculum Vitae	87

List of Figures

Figure 2.1 Map of the Hudson Bay area, Canada, showing the location of the Churchill Province and its major constituents..	7
Figure 2.2 Bedrock geology map of the Melville Peninsula	9
Figure 2.3 Legend for bedrock geology map of the Melville Peninsula	10
Figure 2.4 Aeromagnetic map of the Melville Peninsula.	11
Figure 2.5 Magnetotelluric geophysical data and accompanying index map of the Melville Peninsula	12
Figure 3.1 Photograph of the Wilfley table..	15
Figure 3.2 Photograph of the Frantz L1 Isodynamic Separator.....	16
Figure 3.3 Photograph of the heavy liquid separation process..	17
Figure 3.4 Photograph of the Hitachi SU-6600 Field Emission Gun-Scanning Electron Microscope in the Zircon and Accessory Phase Laboratory at Western University.	19
Figure 4.1 Surface geology map of the Lyon Inlet Boundary Zone study area.....	22
Figure 4.2 Field photos showing carbonate rocks from the LIBZ study area.....	23
Figure 4.3 Field photos of aluminous gneisses and migmatites from the LIBZ.....	25
Figure 4.4 Field photos of LIBZ granitoids	26
Figure 4.5 Field and hand sample photos of sample 10644.....	28
Figure 4.6 Petromicrographs of sample 10644.....	29
Figure 4.7 MicroGIS map of a large thin section from sample 10644	30

Figure 4.8 Backscatter (left side) and Secondary (right side) Electron images of select grains found during the feature scan of a sample 10644 thin section.....	32
Figure 4.9 Transmitted light image of some mounted zircon grains (sample G060A1 - 10644)	33
Figure 4.10 SE and colour-CL images of mounted zircon grains (sample G060A1 - 10644).	35
Figure 4.11 Concordia plot of Pb^{207}/Pb^{206} apparent ages for sample 10644 with unforced intercepts.	36
Figure 4.12 A graph showing the Th/U ratio vs. the Pb^{207}/Pb^{206} apparent ages for sample 10644.....	37
Figure 4.13 Colour-CL images of representative grains from each age grouping for sample 10644 (G060A1).....	37
Figure 4.14 Concordia plot for the Proterozoic (1842 Ma and 1804 Ma) populations in sample 10644 with unforced intercepts	38
Figure 4.15 Probability density plot and histogram for the Proterozoic populations of sample 10644 based on Pb^{207}/Pb^{206} age.	38
Figure 4.16 A: Field photo of sample 10645 showing the strong foliation and leucocratic pockets of quartzo-feldspathic composition.. ..	39
Figure 4.17 Petromicrographs of sample 10645.	40
Figure 4.18 MicroGIS map of a large thin section from sample 10645.. ..	41
Figure 4.19 Zircon and Monazite (sample 10645) in contact.	42
Figure 4.20 Transmitted light image of some mounted zircon grains (sample G067A1 - 10645)	43

Figure 4.21 SE and colour-CL images of mounted zircon grains (sample G067A1 - 10645).	44
Figure 4.22 Concordia plot for sample 10645 with unforced intercepts.	45
Figure 4.23 A graph showing the Th/U ratio vs. the Pb^{207}/Pb^{206} apparent ages for sample 10645.....	46
Figure 4.24 Colour-CL images of representative grains from each age grouping for sample G067A1 (10645).....	46
Figure 4.25 Probability density plot and histogram for the Proterozoic population of sample 10645 based on Pb^{207}/Pb^{206} age.	48
Figure 4.26 Field and hand sample photos of sample 10646.....	49
Figure 4.27 Petromicrographs of sample 10646.	49
Figure 4.28 MicroGIS map of a large thin section from sample 10646	50
Figure 4.29 SE and BSE images of a typical zircon from sample 10646.	51
Figure 4.30 Transmitted light image of some mounted zircon grains (sample G071A1 - 10646).	52
Figure 4.31 SE and Colour-CL images of mounted zircon grains (sample G071A1 - 10646).....	53
Figure 4.32 Concordia plot of Pb^{207}/Pb^{206} apparent ages for sample 10646.	54
Figure 4.33 A graph showing the Th/U ratio vs. the Pb^{207}/Pb^{206} apparent ages for sample 10646.....	55
Figure 4.34 Colour-CL images of representative grains from each age grouping for sample G071A1 (10646).....	55

Figure 4.35 Probability density plot and histogram for the Proterozoic population of sample 10646.	56
Figure 5.1 Concordia plot for the 2770 Ma population in sample 10644.....	58
Figure 5.2 Concordia plot for 2670 Ma population in sample 10644.....	59
Figure 5.3 Concordia plot for 1842 Ma population in sample 10644.....	60
Figure 5.4 Concordia plot for 1802 Ma population in sample 10644.....	61
Figure 5.5 Concordia plot for core analyses from sample 10645.....	64
Figure 5.6 Concordia plot for rim analyses from sample 10645.	65
Figure 5.7 Concordia plot of Pb207/Pb206 model ages for sample 10646 with unforced intercepts.	67
Figure 5.8 Magnetotelluric geophysical data and accompanying index map of the Melville Peninsula.	72

List of Appendices

Appendix A - Thin Section Descriptions..... 79

Appendix B - SHRIMP U-Pb Data for Zircon..... 82

**Appendices C,D,E included as separate .pdf files due to large file size

Appendix C - FEG-SEM Images of Thin Sections

Appendix D - Pre-SHRIMP Imaging

Appendix E - Post-SHRIMP Imaging

1 Introduction

This U-Pb geochronological study of zircon grains and their mineral and lithologic context is the first of its kind from a recently discovered crustal-scale boundary in the Rae domain of the western Churchill Province, Nunavut, Canada. This boundary is referred to here as the Lyon Inlet Boundary Zone (LIBZ), after the large marine coastal feature along which it is well exposed. The Churchill Province is the result of a style of continental tectonics that is enigmatic in that a large volume of Archean lithosphere, normally resistant to deformation and heating, has been pervasively re-worked by tectonic processes over a nearly 2 billion year period. Understanding this style of continental tectonics requires knowledge of the absolute timing of the many metamorphic and crustal deformation events during this period. Consequently, the main goal of this study is to characterize the nature and timing of crust formation and the latest metamorphic activity in the LIBZ. This research is conducted in order to enhance the understanding of the tectonothermal evolution of the Hudsonian orogeny that affected much of the bedrock of the Canadian Arctic and its considerable mineral resources.

Sample collection, mapping, and preliminary data collection took place during July and August 2010 as a part of the Geological Survey of Canada's GEM project (Geomapping for Energy and Minerals) on the southern portion of the Melville Peninsula. Funding for this project is provided by Natural Resources Canada as a part of their Research Affiliate Program. Through the integrated use of field mapping, optical microscopy, FEG-SEM imaging, and SHRIMP analysis, this study generates and presents a data set for a group of previously undocumented rocks, presents first-order interpretations for the genesis of the LIBZ, and considers their implications on the crustal evolution of the western Churchill Province.

2 Geochronological Theory and Geologic Setting

2.1 Geochronological Theory

2.1.1 Zircon

Zircon (ZrSiO_4) is an orthosilicate mineral in the tetragonal system with $4/m\ 2/m\ 2/m$ symmetry. It is common to many rocks in the continental crust where it occurs as an accessory mineral. It usually forms prismatic crystals, but sometimes irregular prisms, and is typically several hundred microns in size. Zirconium is in eight-fold coordination with Oxygen in distorted cube-like polyhedra, where the eight Oxygen atoms belong to six different SiO_4 tetrahedra (Klein, 2001). It has a hardness of approximately 7.5 and a specific gravity equal to 4.2. Zircons are often brown, but can be green, gray, red, or colourless, exhibiting a colourless streak (Wenk & Bulakh, 2004).

By weight percent, an ideal zircon crystal will typically contain 67.2% ZrO_2 and 32.8% SiO_2 . However, the element Hafnium is always present, typically in the range of 1 – 4 weight percent, although it can be far higher (Klein, 2001). Th and U are present in small amounts in most zircons, and these elements can self-irradiate the crystal, forming an isotropic glass, lowering the refractive index and reducing the density by as much as 16%. Zircon is a common accessory mineral in igneous and crystalline metamorphic rocks. Due to its high chemical stability and hardness, it is also common in many sedimentary rocks, as it can withstand many rock cycles (Klein, 2001).

2.1.2 Monazite

Monazite is a monoclinic mineral with $2/m$ symmetry and the chemical formula $(\text{Ce,La,Y,Th})\text{PO}_4$. It usually exhibits a yellow to reddish-brown colour, resinous lustre, and an elongated to granular habit. As monazite is essentially a phosphate of the rare-earth elements (REEs), it often contains U and can contain as much as 20% Th. The mineral structure is comprised of REEs in nine-coordination with oxygen, linking six PO_4 tetrahedra. Akin to zircon, it has a high chemical stability and specific gravity, allowing it to withstand multiple rock cycles (Klein, 2001).

2.1.3 U-Pb Geochronology

Zircon and monazite are extremely useful and accurate geochronometers of high temperature geologic processes, as they contain three unique radioactive decay systems. Each system involves a series of intermediate steps which produce short-lived isotopes, along with alpha and beta particles. The three parent isotopes are ^{238}U , ^{235}U , and ^{232}Th , whose stable daughter isotopes are ^{206}Pb , ^{207}Pb , and ^{208}Pb respectively (Harley & Kelly, 2007). Since the final step in the decay chain is many orders of magnitude greater than the previous intermediate steps, the entire decay process can be expressed using a single equation (using ^{238}U as an example):

$$^{206}\text{Pb}^*/^{238}\text{U} = e^{\lambda^{238}t} - 1$$

where t is time, λ is the decay constant, and $^{206}\text{Pb}^*$ is the amount of ^{206}Pb created by the decay of ^{238}U . Each decay system uses this same equation, substituting in the corresponding isotope ratios and their related decay constants (Harley & Kelly, 2007). Time is expressed in units of millions of years (Ma) or billions of years (Ga).

In an ideal closed system, it would be possible to use both U systems in tandem with the ^{232}Th , and they would all yield the same age within error. However, in nature, a crystal will not be equally closed to Th and U during post-crystallization effects. As a result, the two U systems can be used in tandem as an internal self-checking mechanism, but the Th system cannot be used in this way (Harley & Kelly, 2007). An ideal zircon or monazite would also contain no Pb at its time of formation; all Pb present would be a result of radiogenic decay. Any measured Pb which was included in the crystal at the time of formation will lead to an erroneously old age. Fortunately, zircon and monazite are only able to incorporate negligible amounts of Pb during crystallization. By measuring the amount of ^{204}Pb , a non-radiogenic isotope, and then subtracting the associated amount of ^{206}Pb and ^{207}Pb , the amount of “common lead” can be subtracted from the measured values to obtain the radiogenic component (Harley & Kelly, 2007).

2.1.4 Concordia Plots

The power of using two isotopic systems in tandem is revealed when the parent/daughter combinations are plotted against one another ($^{207}\text{Pb}^*/^{235}\text{U}$ vs. $^{206}\text{Pb}^*/^{238}\text{U}$), creating a concordia diagram. The concordia curve is the locus of mutually compatible (concordant) isotope ratios, increasing outwards from the origin as the age of crystallization of the zircon increases. At time zero, when the zircon crystal closes to U, the crystal contains no radiogenic Pb*; this value increases with time. If the measured Pb* values for both isotopic systems are the same, then the age of the grain is concordant, and will plot at some point along the concordia curve. The position at which the zircon grain plots is a direct measure of its age (Harley & Kelly, 2007).

In many cases, the measured values for $^{207}\text{Pb}^*/^{235}\text{U}$ and $^{206}\text{Pb}^*/^{238}\text{U}$ will be different. This means that the age of the grain will not plot directly on the concordia line. If it plots below concordia, it is termed *normally discordant*; if it plots above concordia, it is *reverse discordant*. Reverse discordance is usually a result of analytical and/or statistical error. Normal discordance is usually caused by a significant geological event which occurred after the crystal originally closed to U. This event may involve the growth of new zircon zones, as well as the loss of radiogenic Pb* (Harley & Kelly, 2007). Since lead-loss can occur at variable rates in some small microdomains of a crystal, it is important to use several analyses from a variety of grains. If all analyzed grains have experienced the same events, they may spread out along a line of discordia which will intersect the concordia curve at two points. The upper intercept is the age of crystallization of the grain, and the lower intercept is age of the more recent event where lead loss and/or new zircon growth occurred (Harley & Kelly, 2007).

2.1.5 Lead Loss

Normal discordance is often attributed to the loss of radiogenic Pb from a crystal. There are a multitude of factors which control the occurrence and rate of Pb loss, including crystallographic orientation, mineral composition, the presence of hydrous species, temperature, pressure, and time. Under most geological conditions, zircon and monazite exhibit extremely slow rates of Pb diffusion, although this can be drastically

increased by introducing radiation damage (metamictization) or strain. Metamict zones (usually high-U zones) can begin to lose Pb at temperatures several hundred degrees lower than undamaged zones (Cherniak & Watson, 2000). Metamictization can take significant time periods to accumulate in zircon, as radiation self-anneals over geologic timescales if thermal conditions permit. If a grain remains above a critical amorphization temperature, it will not suffer radiation damage. This temperature is related to the age and U content of a grain, where a crystal with 1000ppm U will self-anneal above 360°C, and grains with 10,000 ppm U will self-anneal above 380°C. Below this critical amorphization temperature, a crystal will accumulate radiation damages over long time scales (Cherniak & Watson, 2000). When dealing with highly discordant analyses, it is important to check the U content and degree of metamictization in order to properly interpret the results.

2.1.6 Migmatites

A migmatite is “a rock found in medium- and high-grade metamorphic areas that can be heterogeneous at the microscopic to macroscopic scale and that consists of two, or more, petrographically different parts. One of these parts must have formed by partial melting and contain rocks that are petrographically related to each other (called the neosome) and to their protolith through partial melting or segregation of the melt from the solid fraction. The partially melted part typically contains pale-coloured rocks that are quartzo-feldspathic, or feldspathic, in composition, and dark-coloured rocks that are enriched in ferromagnesian minerals. However, the partially melted part may simply have changed mineralogy, microstructure, and grain size without developing separate light or dark parts” (Sawyer, 2008).

Migmatitic rocks can be subdivided into smaller parts. The neosome is the part of the migmatite newly formed by or partially reconstituted by partial melting. It may or may not have undergone segregation in which the melt and solid fractions are separated. Based on colour, the neosome can be further broken down to melanosomes and leucosomes. Melanosomes are the dark-coloured part of the neosome in a migmatite that is rich in dark minerals such as biotite, garnet, cordierite, orthopyroxene, hornblende, clinopyroxene, and olivine. It is the solid residual fraction left after some or the entire

melt fraction has been extracted. Microstructures indicating partial melting may be present. Leucosomes are the lighter coloured part of the neosome in a migmatite, consisting dominantly of quartz and feldspar. The leucosome is that part of the migmatite derived from segregated partial melt; it may contain microstructures that indicate crystallization from a melt or magma. Leucosomes may not necessarily have the composition of an anatectic melt, as fractional crystallization and separation of the fractional melt may have occurred. A paleosome is the non-neosome part of a migmatite that was not affected by partial melting, and in which structures (such as foliations, folds, layering) older than the partial melting are preserved. The microstructure (size, form, and orientation of grains) is either unchanged, or only slightly coarsened, compared to that in similar rocks just outside the region affected by anatexis (Winter, 2001; Sawyer, 2008).

2.2 Geologic Setting

The Churchill Province, one of the largest and least explored Archean crustal blocks the Canadian Shield, extends from Baffin Island, Nunavut to western Canada, where it lies beneath Phanerozoic strata. Regionally, the Churchill Province is comprised of Neoproterozoic gneissic and supracrustal rocks with Neoproterozoic plutonic intrusions, overlain by extensive Paleoproterozoic metasediments. Based on differences in lithology, age, and petrogenesis, the Churchill Province is divided into several smaller sections (see Figure 2.1); the Rae sub-province, Hearne Province, and Chesterfield Domain. These domains record a variety of shared and unique geologic events involving magmatism related to craton formation (2.8-2.6 Ga), post-cratonic orogenesis, regional magmatism, and crustal extension (2.5-1.8 Ga) (Hanmer et al., 1995; Sandeman et al., 2001a, 2001b; Martel et al., 2008).

The detailed crustal evolution and economic mineralization potential of the Churchill Province is generally poorly constrained. However, existing surficial geology and geochronological data indicate a complex tectonothermal history. Current information suggests initial craton formation during the Meso- and Neoproterozoic in the Rae sub-province and Chesterfield Domain, and in the Neoproterozoic for the Hearne Province. During the Neoproterozoic, the Rae and Chesterfield regions amalgamated, leading to reworking along their margins (Peterson, 2006; Rainbird et al., 2006; Petts, 2012).

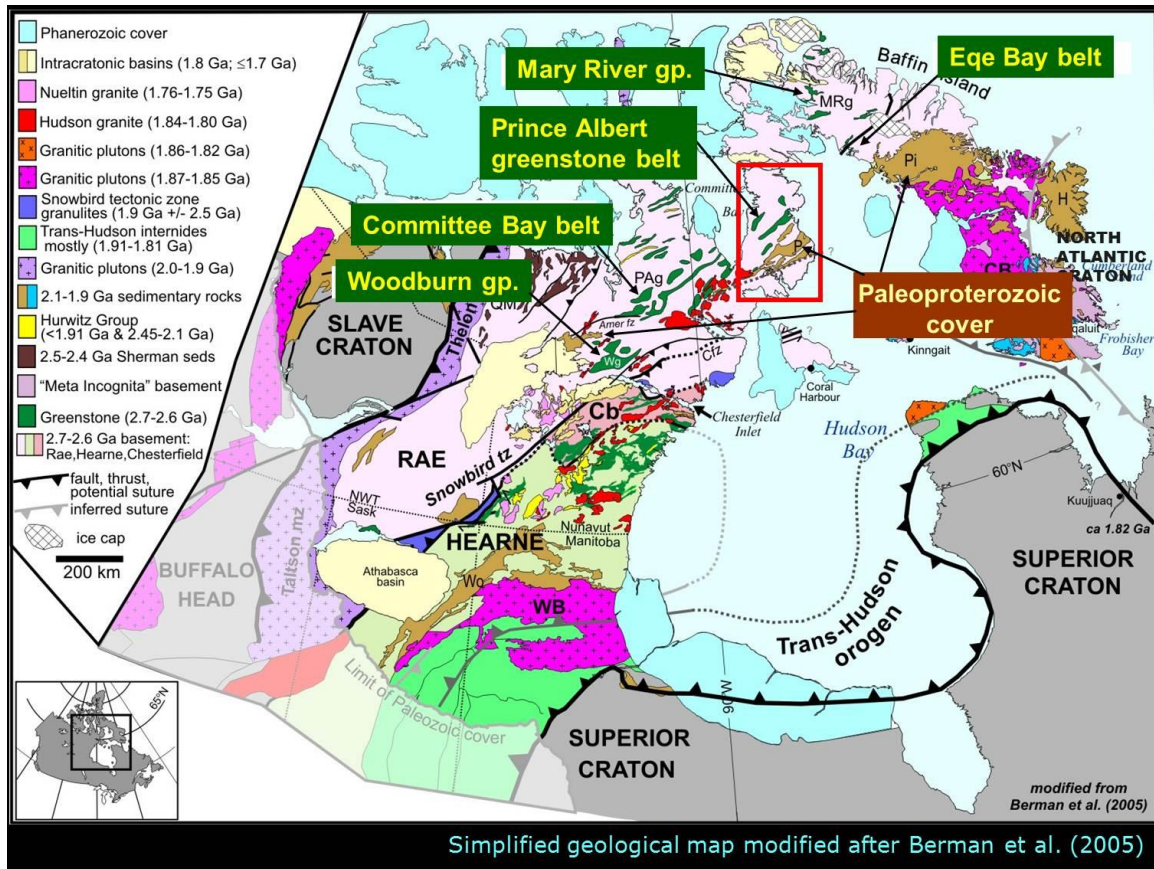


Figure 2.1 Map of the Hudson Bay area, Canada, showing the location of the Churchill Province and its major constituents. Note the Piling Group (Pi) on central Baffin Island, and the Penrhyn Group (Pe) along strike to the southwest, in southern Melville Peninsula. The red box indicates the location of Melville Peninsula. The Lyon Inlet Boundary Zone study area is marked by the red star (modified from Berman et al, 2005 by Corrigan, personal communication).

During the Trans-Hudson Orogen (2.0-1.8 Ga), the Churchill Province experienced widespread crustal shortening, leading to intrusive magmatism and tectonic-related metamorphism (Hanmer et al., 1995; Corrigan et al., 2005; Flowers et al., 2006; Martel et al., 2008; Petts, 2012). The Hearne Province amalgamated to the Rae-Chesterfield composite at ca. 1.92 Ga (Davis et al., 2006). This was followed by the ca. 1.84-1.81 Ga terminal collision of the western Churchill Province with the Superior Province and Sask craton, as demonstrated by the 1.85-1.81 Ga Hudson plutons (Aspler et al., 2002). Following these collisions and amalgamations, intracratonic magmatism occurred, represented by the 1.76-1.75 Ga Nuelin granites, with widespread upper-

crustal extension expressed by the deposition of the 1.83-1.70 Dubawnt Supergroup (Peterson, 2006; Rainbird et al., 2006; Petts, 2012).

The Penrhyn Group is a supracrustal assemblage of Paleoproterozoic age, located in the southern portion of Melville Peninsula (see figure 2.1, 2.2, 2.3). It is comprised of metasedimentary rocks, predominantly paragneisses, with local schist, amphibolite, quartzite, and marble. During the Trans-Hudsonian Orogeny, the Penrhyn Group was extensively folded resulting in prominent northeast trending synclines and anticlines, with most rocks reaching amphibolite to granulite facies metamorphism. Late into the Trans-Hudson, the Penrhyn Group was intruded by small bodied, high-U granitic plutons (Reesor et al., 1975; Okulitch et al., 1978a,b; Maurice, 1979; Henderson, 1983, 1988).

The Lyon Inlet Boundary Zone (referred to in this paper as the LIBZ) was first recognized in the aeromagnetic survey map of Melville Peninsula (figure 2.4). The aeromagnetic map shows that the southern portion of Melville Peninsula is heterogeneously magnetic at map scale. Moving north, a strong northeast-southwest trending fabric with a dextral component suddenly appears. This marks the beginning of the LIBZ, which increases in thickness from about 10 km to 40 km moving from west to east, potentially continuing northward into the southernmost exposure of the Penrhyn Group.

Further investigation of this feature involved a magnetotelluric geophysical survey (conducted by Jessica Spratt, summer 2009, see figure 2.5) which shows a large scale crustal break in the same area as the dextral fabric seen in the aeromagnetic maps. This supports the hypothesis that the LIBZ is a significant crustal scale feature which warrants investigation of its time of formation relative to other tectonic boundaries related to the Trans Hudson orogen.

The study area was selected in order to map and sample a representative portion of the LIBZ, using aeromagnetic maps to define the desired target area and air photos to select the location with the most accessible outcrop. The outcome of mapping and sampling can be found in Chapter 4. The purpose of the study is to use field mapping,

optical petrography, micro-textural analysis, and U-Pb geochronology in order to define the nature and timing of the latest activity in the LIBZ.

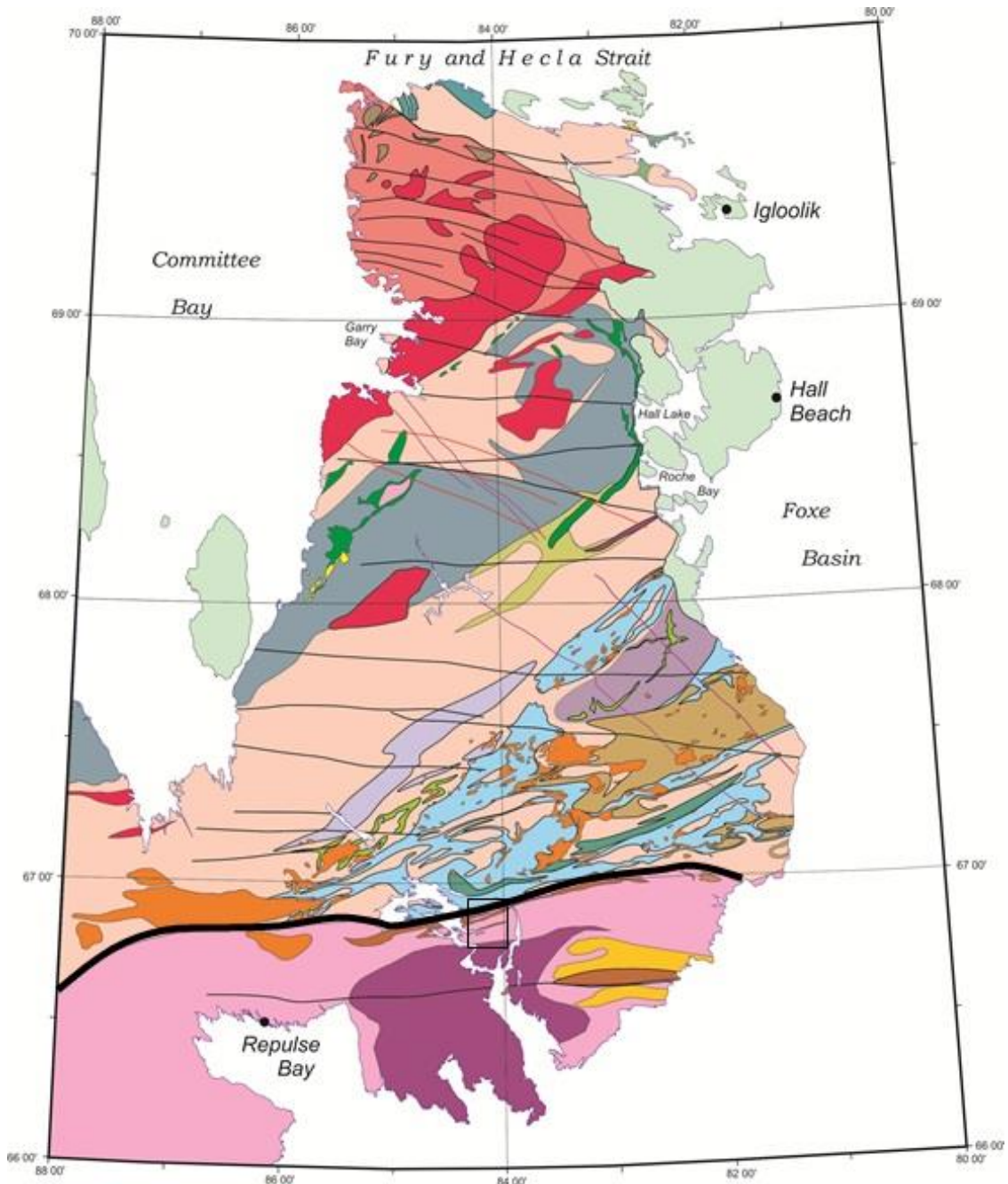


Figure 2.2 Bedrock geology map of the Melville Peninsula; for legend, see figure 2.3 below (from Corrigan, personal communication). The black rectangle marks the location of the LIBZ study area, the black line shows the area of most intense dextral shear.



Figure 2.3 Legend for bedrock geology map of the Melville Peninsula for figure 2.2 (from Corrigan, personal communication)

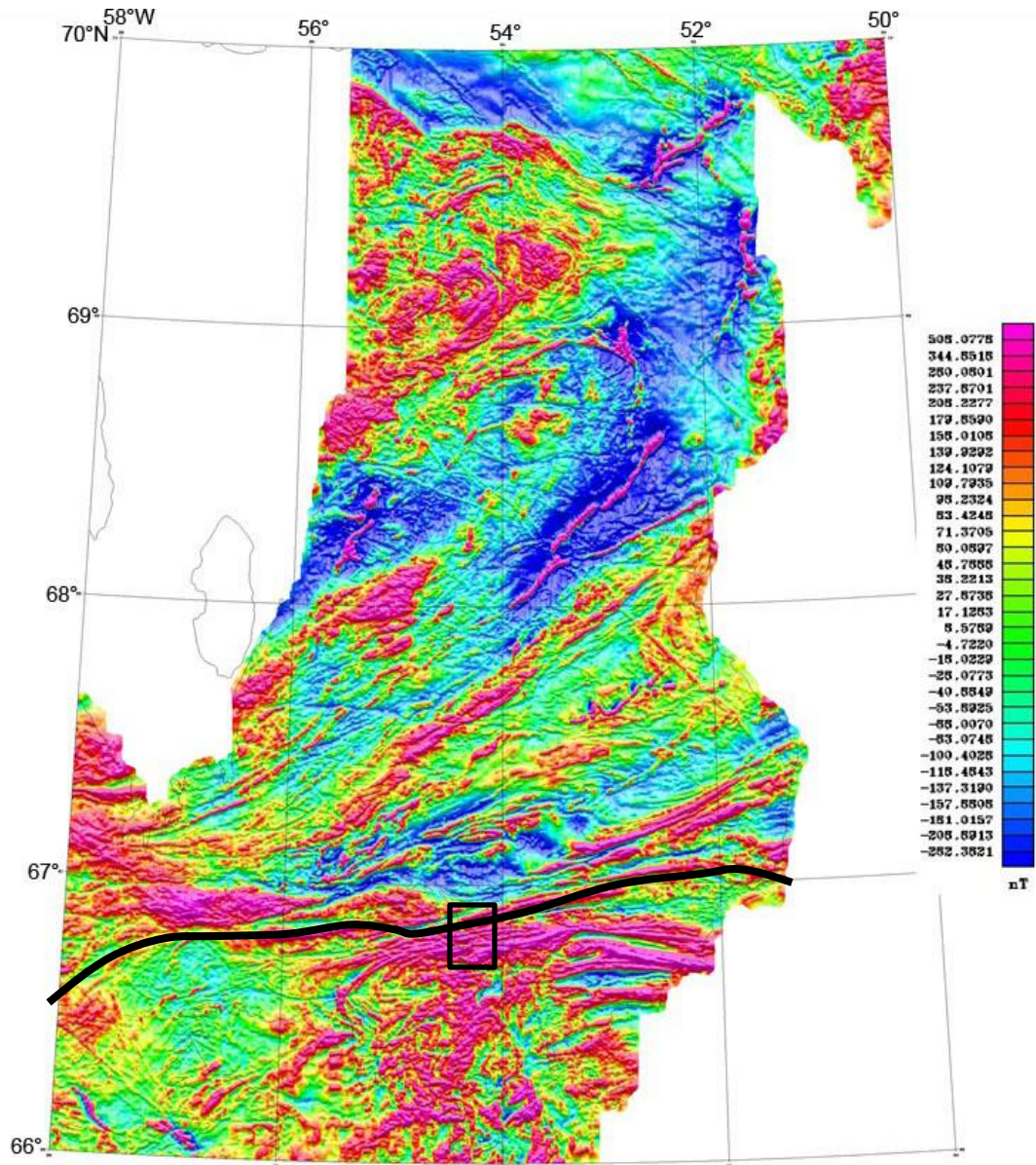


Figure 2.4 Aeromagnetic map of the Melville Peninsula (from Corrigan, personal communication). The black rectangle marks the location of the LIBZ study area, the black line shows the area of most intense dextral shear.

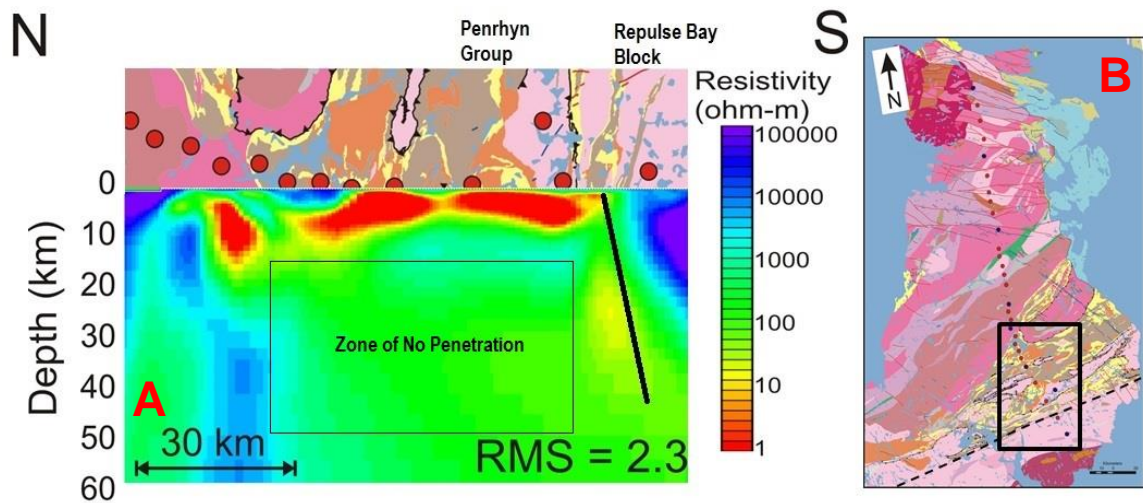


Figure 2.5 Magnetotelluric geophysical data (A) and accompanying index map (B) of the Melville Peninsula (conducted by Dr. Jessica Spratt, summer 2009, 2010) showing the location and depth of the crustal break which defines the LIBZ (modified from Corrigan, 2011, personal communication)

3 Methods

3.1 Sampling and Mapping

Samples were collected by the author during the summer of 2010 as part of the Geological Survey of Canada's GEM-Melville project (July-August 2009, 2010). Representative photographs of the outcrop were taken, and the samples were removed from outcrop using a standard six pound sledge hammer. Weathered and altered surfaces were removed in the field. The samples and their locations were described and noted in a field book, and entered into the GSC's ArcGIS database using a hand-held GPS (WGS 84). Personal field notes and a variety of datasets collected during the GEM-Melville project were combined, and a local geology map was created using Esri ArcGIS 10 (see figure 4.1 in Results).

3.2 Thin Sections

Polished thin sections for each sample were made at Western University. These thin sections were investigated and described using a stereomicroscope (descriptions included in Appendix A). They were then polished with a Buehler Ecomet III Grinder/Polisher using progressively finer grits, from 1.0 μm down to 0.25 μm . After each stage, the sections were checked using a stereomicroscope to ensure no grains were being plucked and the relief between grains and grain boundaries was decreasing. After the final polish with the fine grit, the sections were polished using a vibratory polisher, inspecting the progress every 30 minutes. Samples required 60 to 120 minutes to reach an ideal finish with minimal plucking and low overall relief.

3.3 Mineral Separation

All mineral separation was carried out in the Zircon and Accessory Phase Laboratory (ZAPLab) at Western University.

3.3.1 Hand Crushing

Samples were crushed on a steel plate within a cardboard box lined with brown craft paper. To prevent ripping of the paper, a 3cm thick steel plate was then placed into the box, with the sample placed on top. A standard 22oz geology hammer and short-handled two pound sledge hammer were used to crush the sample until the approximate diameter of all fragments was less than 5 mm.

In order to reduce the possibility of contamination, all materials were cleaned with compressed air before and after each sample was crushed. Craft paper was replaced for each sample. The steel plate and hammers were washed with soap and water, thoroughly scoured using a power-drill with a wire brush attachment, again cleaned with soap and water, then cleaned with ethanol and compressed air.

3.3.2 Shatter Box

Once all fragments of a sample had been reduced to a diameter of approximately 5mm or less, they were transferred to a shatter box in order to mechanically powder the sample. The shatter box was run for 20 second intervals, inspecting the grain size visually between each interval. A total of 40 to 60 seconds was sufficient to powder all materials.

Before and after each sample, a pure quartz sand was run for 60 seconds to scour the surface of the milling discs. Each component was then washed with soap and water, then ethanol, and then blown off with compressed air.

3.3.3 Wilfley Table Density Sorting

Once the samples had been through the complete crushing process, they were run on a Wilfley table in order to separate the heavy and light fractions from one another. Prior to introducing the sample, the frequency of oscillations, table tilt, and water flow were adjusted to ensure the table was maintaining water flow in all areas where the sample may reach in order to prevent sticking and build-up. Once the sample was introduced, small corrections were made in order to maximize the efficiency of separating the heavy fraction. Figure 3.1 depicts a sample being processed on the Wilfley table. Before and after each sample, the table was carefully cleaned with compressed air,

soap, and water. Once the samples had been fully separated, the excess water in the collection cups was decanted off, and the samples were placed in a low temperature (35-40°C) oven until fully dry.

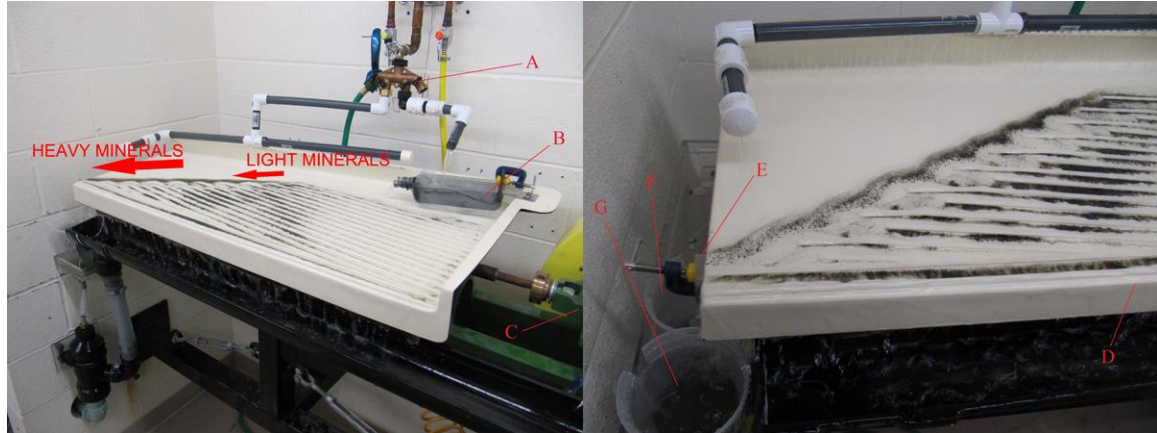


Figure 3.1 Photograph of the Wilfley table. Heavy minerals are preferentially forced to the left side of the table where they are trapped in collection cups. A) Water flow controls; B) sample introduction container; C) motor controlling the frequency of oscillation; D) ultra-fine minerals are washed off the bottom; E) splitter at the end of the table is placed manually in order to most efficiently collect the heavy minerals; F) heavy mineral collection cup; G) light mineral collection cup.

3.3.4 Frantz Magnetic Separation

Once dried, the heavy mineral portion was then run through a Frantz L1 Isodynamic Magnetic Separator. A first pass was made with the magnets turned on with the amperage set to 0 in order to remove any highly magnetic fragments. After this pass, each sample was run at 15° side tilt, starting at 0.1A and progressing upwards at 0.2A to 0.4A intervals until the maximum power of the magnets was reached at approximately 1.6A. The magnetic portion of each pass was collected and stored separately; the non-magnetic portion was passed through again at increased amperage. Samples with larger volumes of material were given a second pass at 1.6A with 10° side tilt in order to further refine the magnetic portion. Feeder tube and ramp vibration frequency were carefully monitored visually throughout each pass in order to maintain a constant flow rate. Figure 3.2 depicts a sample being processed on the Frantz.

Before and after each use, the Frantz was disassembled and its individual components were cleaned. All components were first cleaned with compressed air. Small components (feeder tubes) were then cleaned in a Branson 3510 Sonicator. Larger components (ramp, collection dishes) were cleaned by hand using soap and water, followed by ethanol.

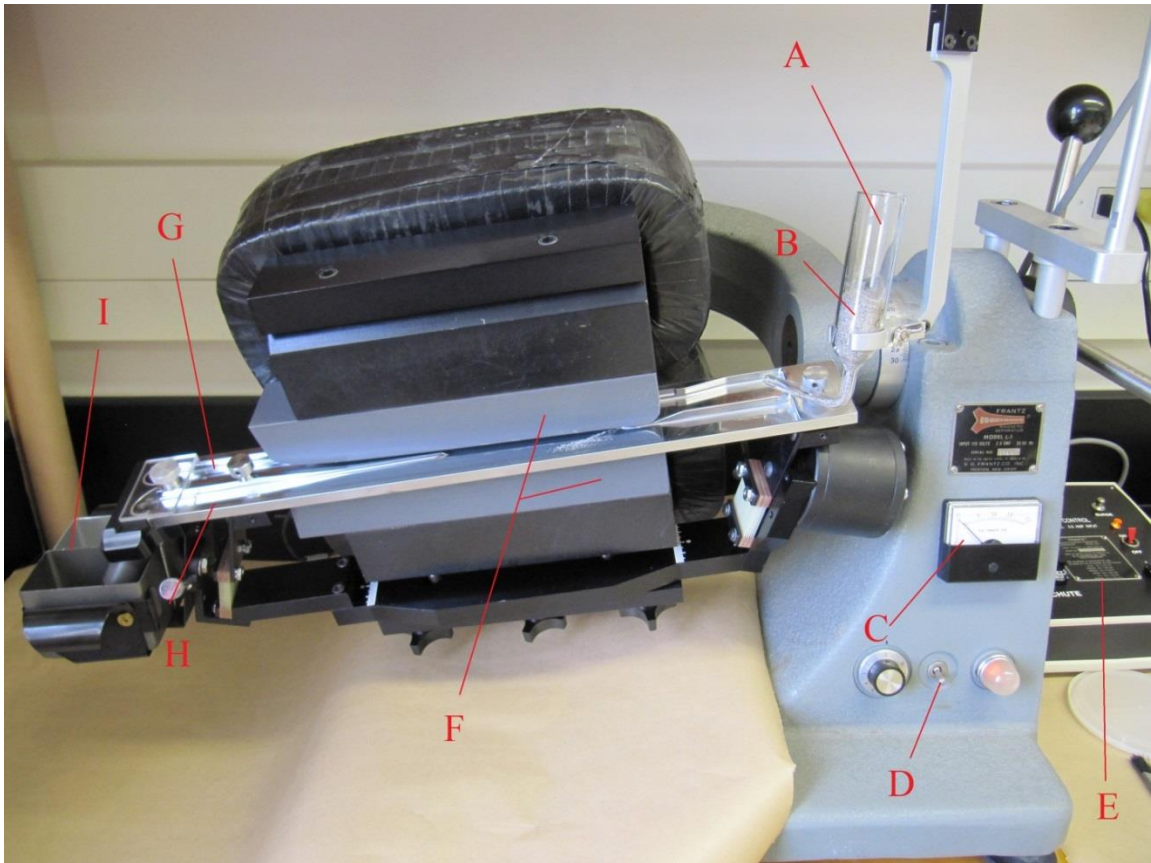


Figure 3.2 Photograph of the Frantz L1 Isodynamic Separator. A) Feeder tube; B) sample; C) amperage read-out; D) magnet on/off switch; E) vibration frequency controls for sample release container and ramp; F) magnets; G) end of ramp – grains magnetic at current amperage; H) end of ramp - grains non-magnetic at current amperage; I) sample collection boxes.

3.3.5 Heavy Liquid Separation

After magnetic separation, individual fractions were further refined using heavy liquid density sorting. The heavy liquid used was Lithium Sodium Polytungstate (LST), which has a density of 2.8g/mL. The LST was poured into a flask, and the sample was inserted into the top, stirred thoroughly to mix the grains evenly throughout the LST, and

then allowed to settle (See Figure 3.3). Once most grains had settled to the bottom or floated to the top, small amounts of the LST with the dense grains were released through the valve and captured in filter paper (coarse porosity, fast flow rate). Once all of the dense grains had been collected in this manner they were washed with distilled water, then dried under a heat lamp. This process was then repeated into a different filter for the remaining light grains. All components were carefully cleaned with compressed air, soap, water, and ethanol before and after each sample was processed.

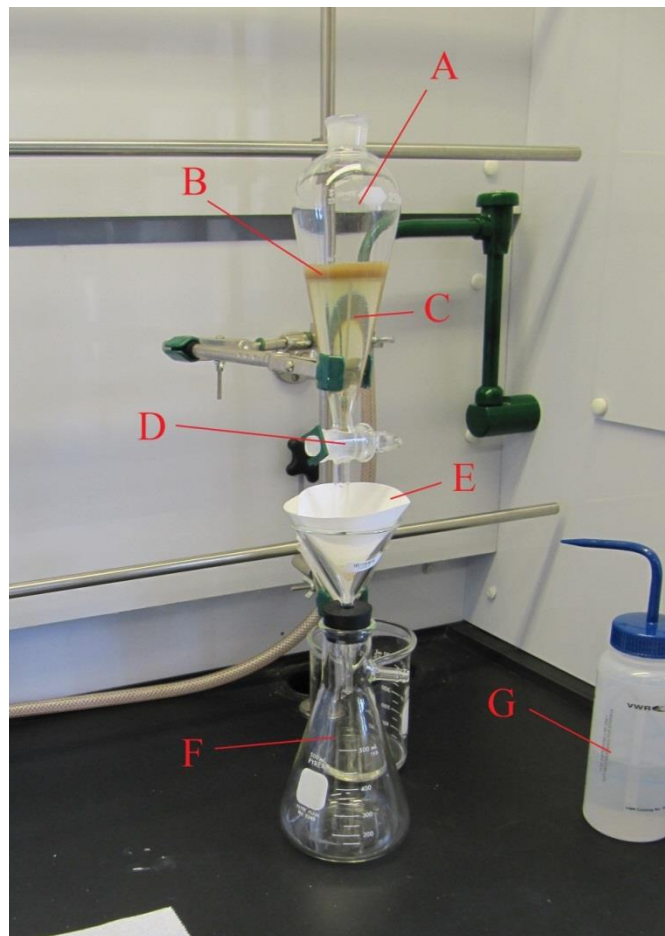


Figure 3.3 Photograph of the heavy liquid separation process. The sample is added to the LST in the flask on the top, agitated, and allowed to settle. Once settled, the heavy grains are carefully released through the valve and collected in the filter paper. A) Flask containing LST and sample; B) light minerals floating on the top of the LST; C) heavy minerals sinking through LST; D) heaviest minerals at the bottom of the flask, near the valve; E) filter paper to collect heavy minerals; F) flask to collect filtered LST; G) distilled water to wash the minerals after they have been filtered out of the LST.

3.3.6 Picking

Once dried, individual separate fractions were collected in small petri dishes, and partially filled with ethanol. The dishes were then investigated for zircon grains using a stereomicroscope. Individual grains were collected using jewellers tweezers, and transferred to a separate petri dish using a micro-pipette. In all samples, a variety of zircon morphologies were selected in order to prevent population bias.

3.4 SHRIMP U-Pb Analysis and FEG-SEM Imaging

3.4.1 SHRIMP U-Pb Analysis

U-Pb geochronology was performed using a SHRIMP-II ion probe at the Geological Survey of Canada (Ottawa, Canada) under the supervision of Dr. Natasha Wodicka. Zircon separates from each sample were sent to the GSC, where they were mounted on a 2.5 cm diameter epoxy disc, along with GSC zircon standards 6266 ($^{206}\text{Pb}/^{238}\text{U}$ age = 559 Ma) and 1242 ($^{206}\text{Pb}/^{238}\text{U}$ age = 2673 Ma). The disc was then polished in order to expose the interior of the zircon crystals. A total of 195 zircon analyses were completed in February 2012 (see Appendix B); 142 on unknowns, 53 on standards. Ages cited in this text correspond to $^{207}\text{Pb}/^{206}\text{Pb}$ model ages, and include associated 2σ analytical uncertainties.

3.4.2 FEG-SEM Imaging

Prior to SHRIMP analysis, the epoxy mount was examined in the ZAPLab at Western University using a Hitachi SU-6600 Field Emission Gun SEM (FEG-SEM, see figure 3.4). The stub was imaged using backscatter electrons (BSE), secondary electrons (SE), and colour cathodoluminescence (colour CL) in order to pre-select potential sites for SHRIMP analysis. Ideal sites were free of holes and cracks (best seen in SE and sometimes BSE), and were contained to a single zircon domain (best seen in BSE and colour CL). After SHRIMP analysis was completed, the grains were imaged a second time using the same techniques, in order to verify that these ideal conditions were met. Any SHRIMP pits that were found to cross zircon zoning boundaries, holes, or cracks were noted, and their corresponding data points were scrutinized.



Figure 3.4 Photograph of the Hitachi SU-6600 Field Emission Gun-Scanning Electron Microscope in the Zircon and Accessory Phase Laboratory at Western University.

Zircon and monazite crystals in thin section were imaged using BSE and SE simultaneous image capture, utilizing a working distance of 9.7 mm to 9.8 mm, accelerating voltage of 15000 Volts, and magnification ranging from 900X to 20,000X. BSE and SE images of individual crystals on the SHRIMP mount were taken in the same manner, with a working distance of 10.4 mm to 10.5 mm, accelerating voltage of 15000 Volts, and magnification ranging from 150X to 1500X. In order to view internal zoning within monazite crystals, some images were taken using a low accelerating voltage (5000 Volts), with a working distance ranging from 7.1mm to 8.6 mm, and magnification from 450X to 3000X.

The FEG-SEM was also used to image the polished thin sections. Automated “Feature” mapping and chemical abundance mapping were performed on samples of interest. “Feature” mapping uses BSE image capturing with user defined parameters for

brightness, contrast, and greyscale to locate and record all locations on a thin section which meet the requirements. These locations are checked for their chemical content with a quick EDS analysis. The program was instructed to search for zircon, baddeleyite, and monazite, and to acquire BSE images and EDS spectra upon the discovery of any of these mineral phases. Data on the approximate dimensions and orientation of the grains was recorded. Images were taken using a working distance of 9.8mm, with an accelerating voltage of 15kV.

In addition, the FEG-SEM was used to generate chemical abundance maps (“Phase Maps”) of representative portions of thin sections. This automated technique uses energy dispersive X-ray spectroscopy (EDS) to create a chemical map of the individual elements contained within the sample. Combined with SE, BSE, and optical techniques, the chemical map can be used to generate a map of the minerals with the thin section. Phase maps were generated at a working distance of 9.8mm, using an accelerating voltage of 15000 Volts, and a pixel resolution of 256x192.

Both the feature map and phase map were geo-referenced to a scanned image of the thin section. These were all imported into ArcGIS to create a micro-GIS map of each thin section. This allowed for a closer investigation into the relationships between the locations of U-Pb bearing minerals and the minerals surrounding them. These maps can be found in the Chapter 4.

4 Results

4.1 Mapping

The compilation of field mapping data allowed for the creation of a bedrock geology map of the LIBZ study area (figure 4.1). The bedrock in the area can be subdivided into four broad and distinct units based on composition, mineralogy, and field mapping. These units have a regional foliation striking northwest-southeast, dipping to the northeast at an average angle of 70° . The area has undergone significant metamorphism, as shown by a series of tight, sub-vertically plunging isoclinal folds, a migmatitic texture in most lithologies, and an average metamorphic grade of upper amphibolite to lower granulite facies. The four broad units are described in this chapter.

4.1.1 Carbonates

Carbonate rocks in the study area consist of marble and calc-silicate gneiss that occur exclusively in the northern portion of the map. The marble units weather to a medium grey colour and have well-rounded surfaces. In some cases, outcrops are extremely friable, often with a weathered “crust” several centimetres thick. The marbles have a mineral assemblage of calcite (80%), diopside (15%), and graphite (5%). In some cases, diopside concentrations can be as high as 30%, and marbles occasionally contain minor concentrations of titanite. The marbles have a fine to medium grained granoblastic texture, with grain sizes on the order of 1 mm to 3 mm, though graphite grains tend to be slightly smaller. Foliation is generally weak to absent and is parallel to the regional trend, except in some outcrops which display extremely convoluted fold structures (see figure 4.2 photo A).

Calc-silicate gneiss units in the LIBZ are more heterogeneous in composition compared to the marble, and consist of evenly spaced alternating layers of marble and more silica-rich layers of “dirty” marble, or siliciclastic rocks such as metapelites. Individual layers vary in thickness from approximately 5 cm to 80 cm. Due to these differences in silica content, the calc-silicates are easily recognized by their alternating light and dark grey “ribbed” appearance, arising from differential weathering (see figure 4.2 photo B). The siliceous layers are usually composed of variable amounts of calcite

(30-60%), diopside (15-60%), quartz (5-40%), and plagioclase (5-40%). Grains vary in size from approximately 1 mm to 4 mm, with occasional large diopside crystals, and display a granoblastic texture. The gneissic layering follows the regional trend for foliation.

Surface Geology: Lyon Inlet Boundary Zone Study Area

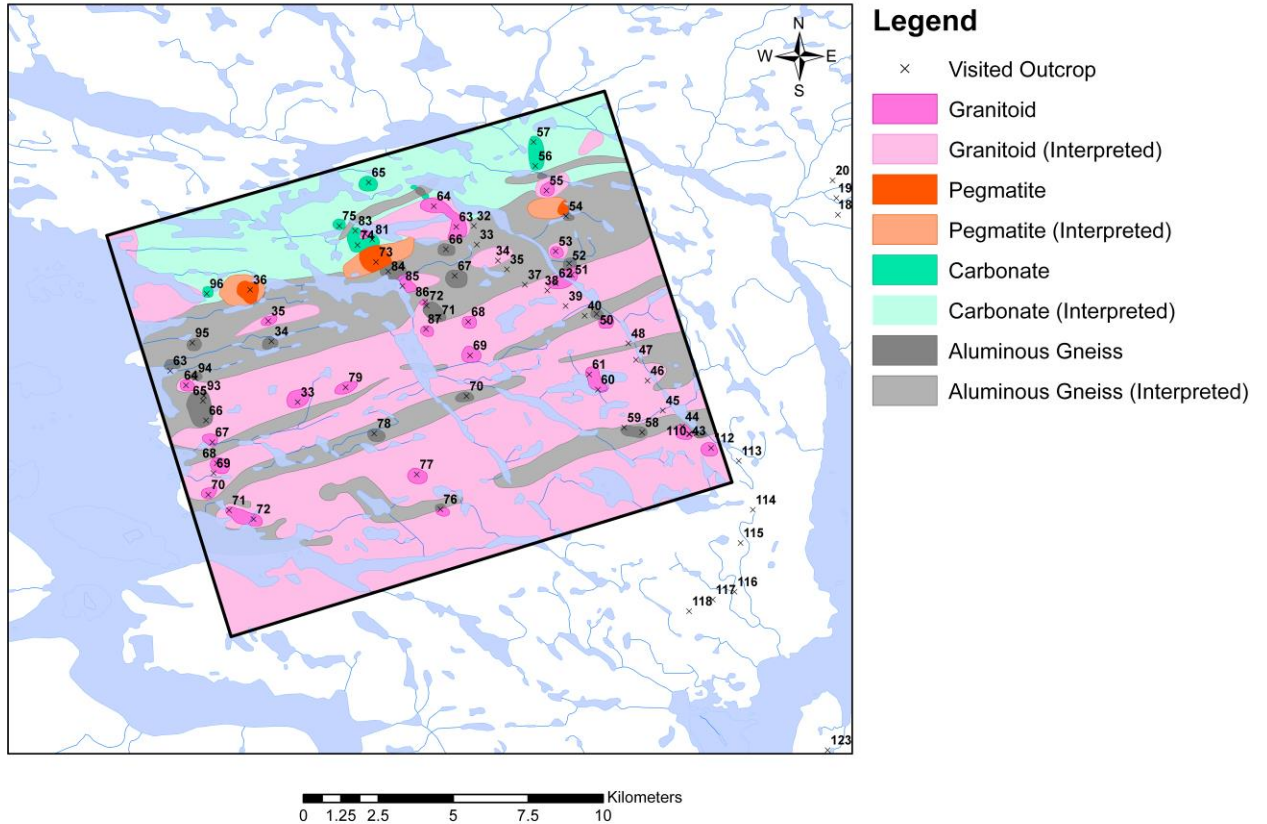


Figure 4.1 Surface geology map of the Lyon Inlet Boundary Zone study area. A detailed description of each unit is provided in this chapter. Unit boundaries are inferred from field observations, air photos, and aeromagnetic patterns. Station/Sample numbers are labeled.



Figure 4.2 Field photos showing carbonate rocks from the LIBZ study area. A: Marble showing the light grey weathered surface and convoluted folding. Folds encompass a quartz nodule to the left of centre of the image. B: A typical calc-silicate rock displaying differential weathering. The darker, negative relief layers are diopside-rich marble; the lighter, more resistant layers contain quartz and plagioclase.

4.1.2 Aluminous Gneisses and Migmatites

Several quartzo-feldspathic units in the area are distinguished by their more aluminous (mica-rich) mineral assemblages. The Al enrichment is inferred to be due to past weathering, and consequently the units are termed “siliciclastic.” The siliciclastic rocks in the LIBZ are metapsammites, meta-semi-pelites, and metapelites, which follow the regional trend for foliation. The metapsammites are weathered to a medium grey, and can be difficult to distinguish from the other siliciclastics at a distance due to heavy lichen cover. They are typically composed of >40% quartz, with the remainder composed of equal parts of biotite and plagioclase, and grain size varying from approximately 1 mm to 4 mm (see figure 4.3). The metapsammites typically contain a minor volume (on the order of 10%) of centimetre wide lenses of quartzo-feldspathic material.

The meta-semi-pelites are very similar to the metapsammites on the weathered surface, obscured even further by heavy lichen cover. Their typical mineralogy is biotite (15%-35%), quartz (25%-40%), plagioclase (10%-25%), with occasional K-feldspar (<1%-25%) and minor cordierite (<1%-5%). Grains range in size from 1 mm to 4 mm, and show a migmatitic texture. Cordierite and K-feldspar grains are usually found within the centimetre scale quartzo-feldspathic leucosome lenses.

The metapelites have a dark grey weathered surface, and an average composition of biotite (>50%), quartz (10%-25%), plagioclase (5%-15%), garnet (<1%-10%), cordierite (<1%-5%). The degree of remelting ranges from approximately 5% to 15%, with garnet mostly occurring in quartzo-feldspathic leucosome lenses.

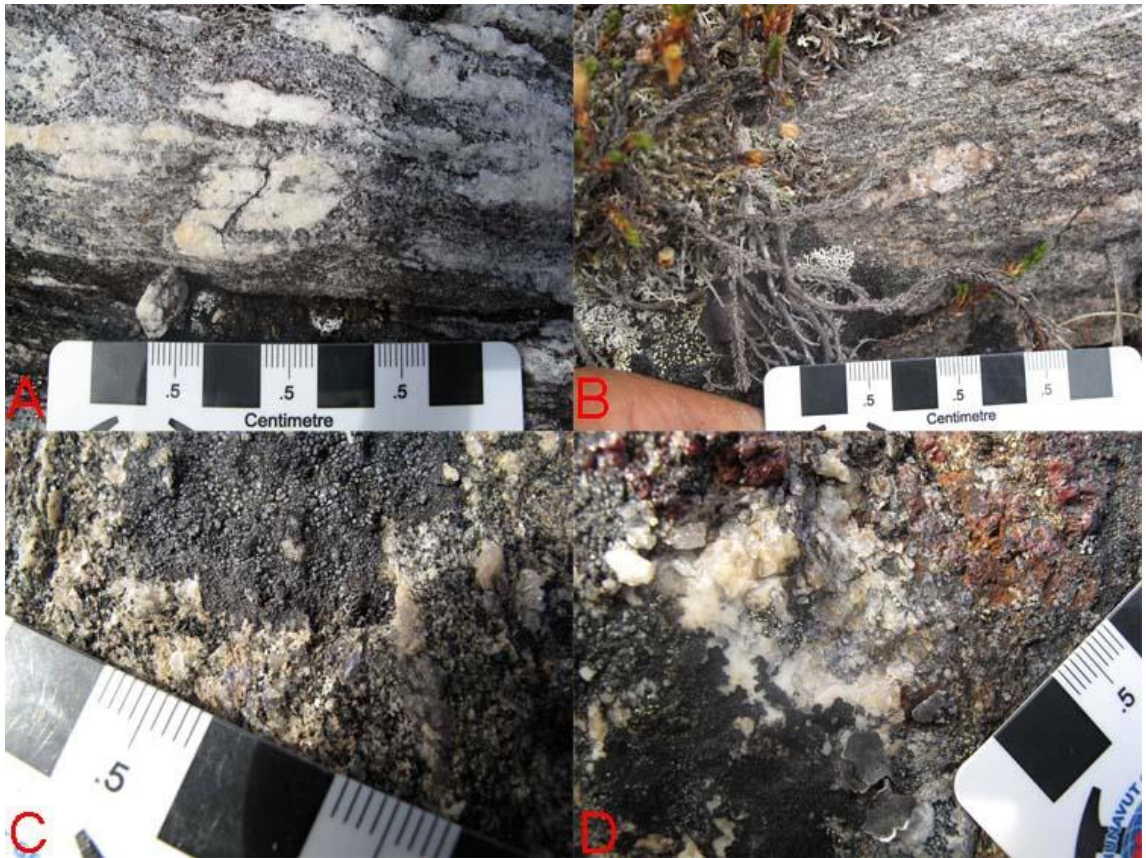


Figure 4.3 Field photos of aluminous gneisses and migmatites from the LIBZ. A: Close-up photo of a metapsammite showing the migmatitic texture; B: A meta-semi-pelite with quartz, K-feldspar, and plagioclase in small leucosome lenses; C: Close-up image of a cordierite-bearing leucosome in a meta-semi-pelite; D: Close-up image of a garnet-cordierite leucosome from a metapelite.

4.1.3 Pegmatites

The pegmatitic granitoid bodies of the LIBZ study area are uncommon, mostly occurring as sheets and dikes metres to tens of metres thick, in the northern portion of the map area where the carbonate rocks first appear. They are extremely friable and weather to a rusty orange-brown. The composition is granitic, with 3 cm to 8 cm grains of quartz (30%), plagioclase (30%), biotite (15%), and K-feldspar (25%). Foliation is generally difficult to determine due to the friable and highly weathered texture; when it is visible, it follows the regional trend, though it is possible that some bodies may be undeformed.

4.1.4 Granitoids

The LIBZ study area contains three major granitoid lithologies with phaneritic textures: tonalite, granite, and quartz monzonite (see figure 4.4). The main minerals are quartz (15%-40%), plagioclase (20-45%), K-feldspar (<5%-15%), biotite (10%-30%), and hornblende (0%-15%), ranging in size from 1 mm to 4 mm. Accessory phases include zircon, monazite, apatite, and iron sulphides. Each lithotype is heterogeneous at the outcrop scale, displaying a migmatitic texture with 5 cm to 50 cm leucocratic and melanocratic lenses. The foliation ranges from moderately foliated to strongly gneissic, and follows the regional trend.

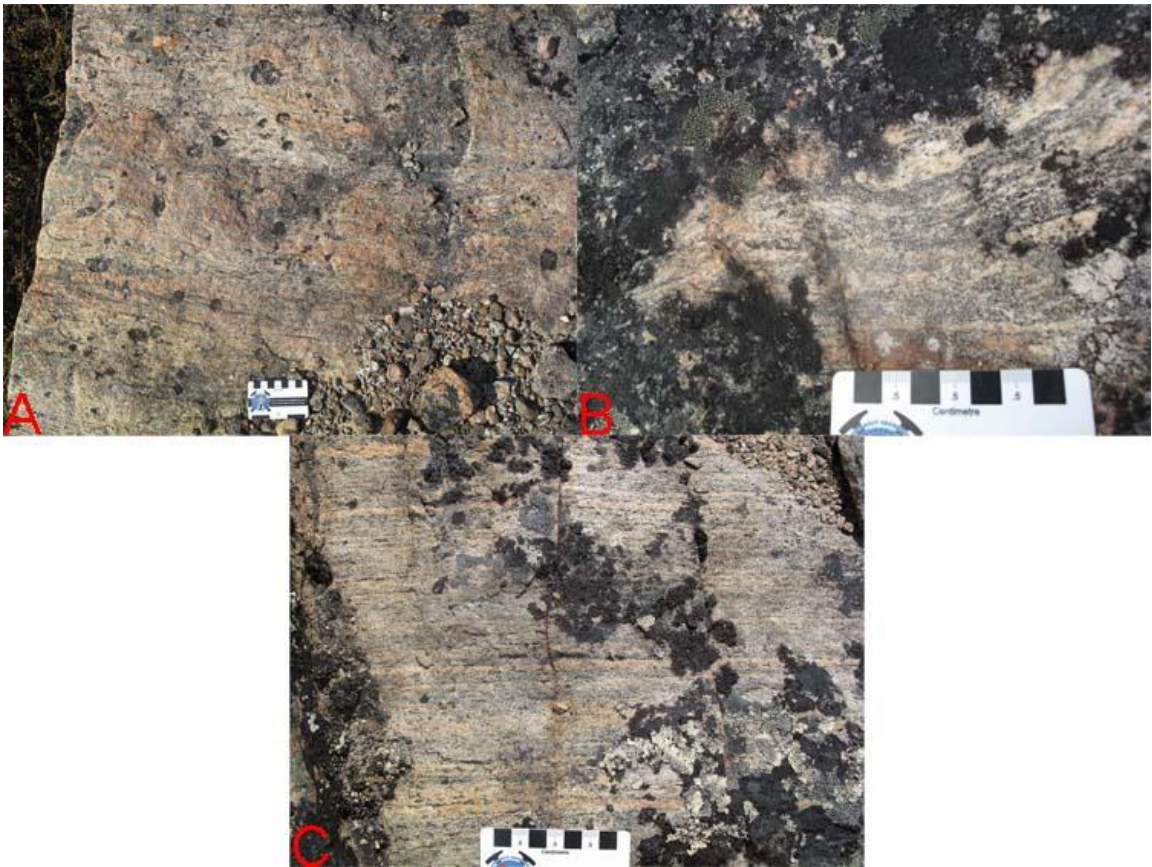


Figure 4.4 Field photos of LIBZ granitoids. A: A biotite granite; B: A close-up image of a biotite-hornblende tonalite outcrop; C: A biotite-hornblende monzogranite.

4.2 Sampling Rationale

Samples for this study were collected during the second field season of the GEM-Melville project (July-August 2010) as part of the regional mapping program. Additional sampling for geochronology was carried out in an effort to determine the final stages of metamorphic activity and mineral fabric development in the Lyon Inlet Boundary Zone for the purpose of regional reconstruction of crustal history. From this suite of samples, three representative and distinctive samples were selected for detailed study. These were chosen to represent the dominant lithologies observed in the study area while exhibiting a range of visible strain (weakly, moderately, and strongly foliated). The mineralogy, petrology, and U-Pb zircon geochronology of these samples is presented below.

4.3 Sample 10644 (G060A1)

4.3.1 Sample Description

Sample 10CXA-G060A1 (GSC internal SHRIMP mount number IP629-10644) is a foliated, medium grained, phaneritic biotite hornblende granitoid (for location, see figure 4.1). It has a moderate to strong foliation defined by biotite and hornblende alignment, with 1 mm to 5 mm thick quartzo-feldspathic and biotite-hornblende rich bands. It is classified as a granodiorite (after the IUGS classification scheme in Winter, 2001) based on its modal mineralogy of plagioclase (30%), quartz (45%), hornblende (15%), K-feldspar (5%), and biotite (5%). The sample outcrop exhibits numerous 1 cm to 4 cm thick K-feldspar rich veins that typically follow the foliation, occasionally cross-cutting it at low angles. At the outcrop scale, some small (usually on the order of 10-30 cm) fine grained amphibolitic lenses can be observed (see figure 4.5).

In thin section (see figure 4.6), a moderate to strong foliation and K-feldspar rich vein can be observed. The predominant composition of the host rock is anhedral plagioclase (35%), quartz (40%), and hornblende (15%), with minor K-feldspar (5%) and biotite (5%). The grain size varies between <1 mm and 4 mm. Iron sulphides and other accessory phases such as titanite, apatite, and zircon can also be observed. In some rare grains, the plagioclase displays a myrmekitic texture.

No hornblende or biotite grains are present in the K-feldspar rich vein. The vein consists of <1 mm to 4 mm anhedral K-feldspar (55%) and quartz (35%), with occasional plagioclase grains (10%). As seen in figure 4.7, all but one of the zircon and monazite grains are found outside or on the margin of the vein.

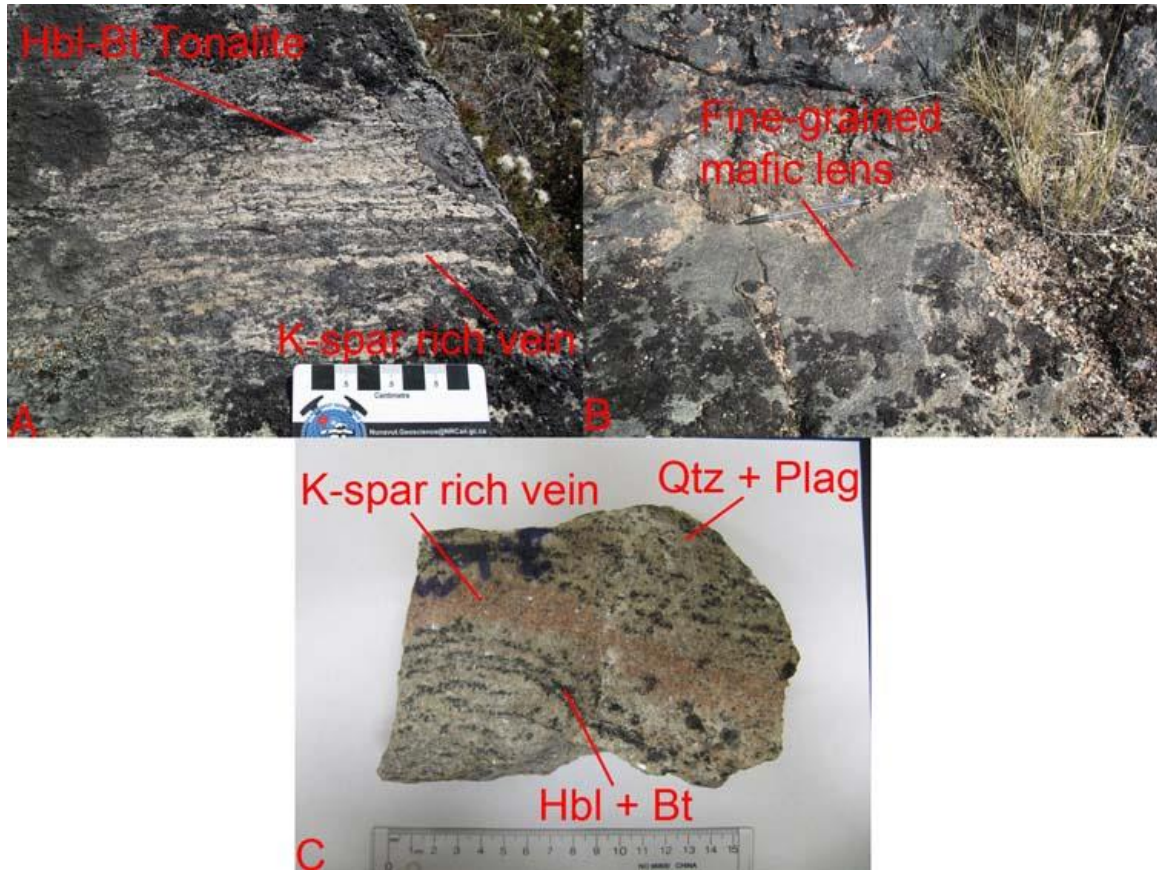


Figure 4.5 Field and hand sample photos of sample 10644. Top left: Outcrop photo showing the foliation and k-spar rich veins. Top right: Outcrop photo showing a relatively large mafic lens. Bottom: Hand sample photo showing the dominant mineralogy and clearly showing the K-Feldspar rich vein.

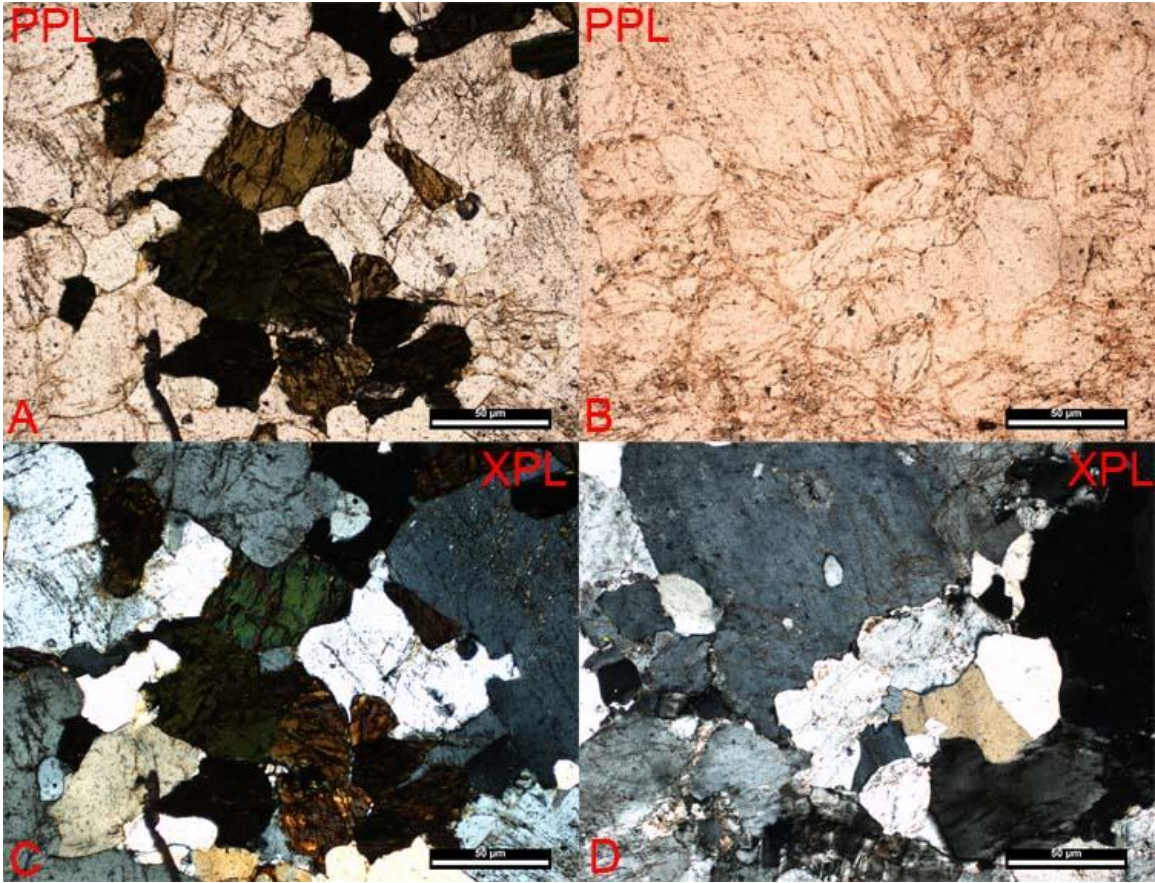


Figure 4.6 Petromicrographs of sample 10644 with a side-by-side comparison of the mineral composition of the bulk-rock (left) and the K-feldspar rich vein (right). A and B are taken in Plane-Polarized Light, C and D are taken in cross-polarized light. The slide was not moved or rotated when switching polarization,

4.3.2 EDS Phase Mapping and BSE-EDS “Feature” Mapping

FEG-SEM EDS data was used to create a chemical map of a representative portion of the thin section (figure 4.7). This was done in order to more easily assess the modal abundance of each mineral phase, and to ascertain whether or not zircon and monazite growth can be related to certain mineral phases. The major mineral phases, defined based on abundance of three chemical elements (see Methods) and confirmed with optical petrography, are Si+Al+Na (plagioclase, 50%), Si+Al+K (K-feldspar, 20%), Mg+Ca+Fe (hornblende and biotite, 15%), Si+O (quartz, 10%), and Fe+S (various iron sulphides, <1%). Accessory phases including zircon, monazite, titanite, and apatite are also present, together comprising <1% total modal abundance. They are not shown as individual phases due to the lack of spatial resolution used for the EDS scan.

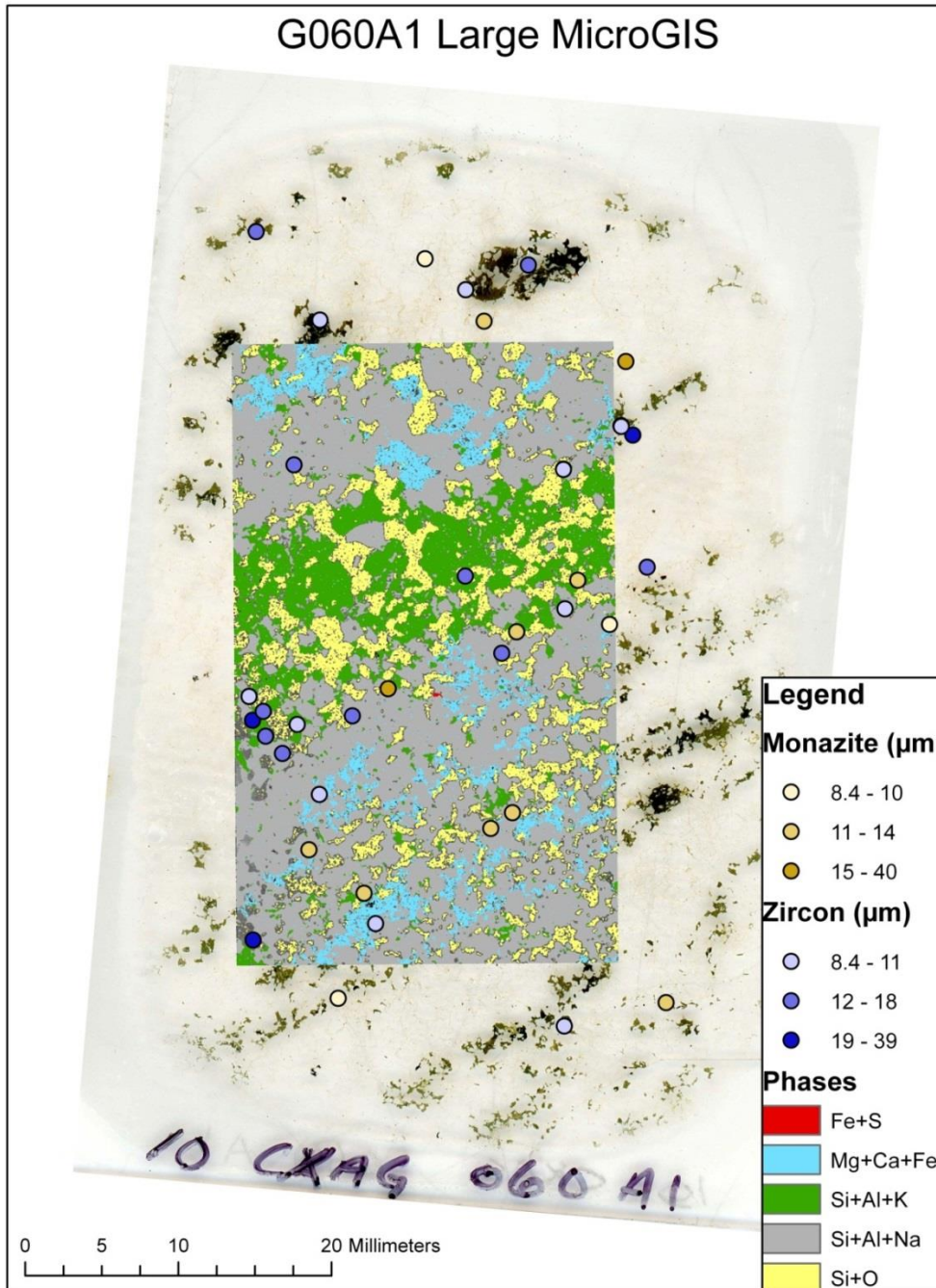


Figure 4.7 MicroGIS map of a large thin section from sample 10644. Monazite and Zircon are split into three size categories, represented by the different shades of blue and orange. The phases represent locations in the thin section where EDS data exists for a unique combination of chemical elements (mineral phase). F+S = iron sulphide phases, Mg+Ca+Fe = biotite and hornblende, Si+Al+K = K-feldspar, Si+Al+Na = plagioclase, Si+O = Quartz. An image with numbered grains and images of select grains can be found in Appendix C.

The results of automated “Feature” mapping (see Methods) are also included in figure 4.7. A total of 25 zircon grains were found, ranging in length from 8 μm to 40 μm , and area from 40 μm^2 to 664 μm^2 . The largest zircon grains are usually in contact with, or in close proximity to K-feldspar. Medium to small grains may also follow this relationship, though they can also be found in or near biotite, hornblende, and occasionally quartz grains.

A total of 13 Monazite grains were found, ranging in length from 8 μm to 40 μm , and area from 40 μm^2 to 511 μm^2 . Monazite grains have the same spatial associations as zircon, with the largest grains tending to be related to K-feldspar, and the medium to small grains being found in close proximity to K-feldspar, biotite, hornblende, and occasionally quartz.

4.3.3 BSE and SE of Zircon in Thin Section

Backscatter and Secondary Electron images were taken of the largest zircon grains in the thin section. Most zircon crystals appear to be relatively damaged, with many cracks and holes. Despite this, it is still possible to observe several different features within the grains. In BSE (and sometimes SE), some grains exhibit relatively bright, planar growth banding (figure 4.8). Other grains show similar planar structures in the core, with the addition of discontinuously zoned rims. Some grains display bright, irregularly resorbed cores, with bright, discontinuously zoned rims.

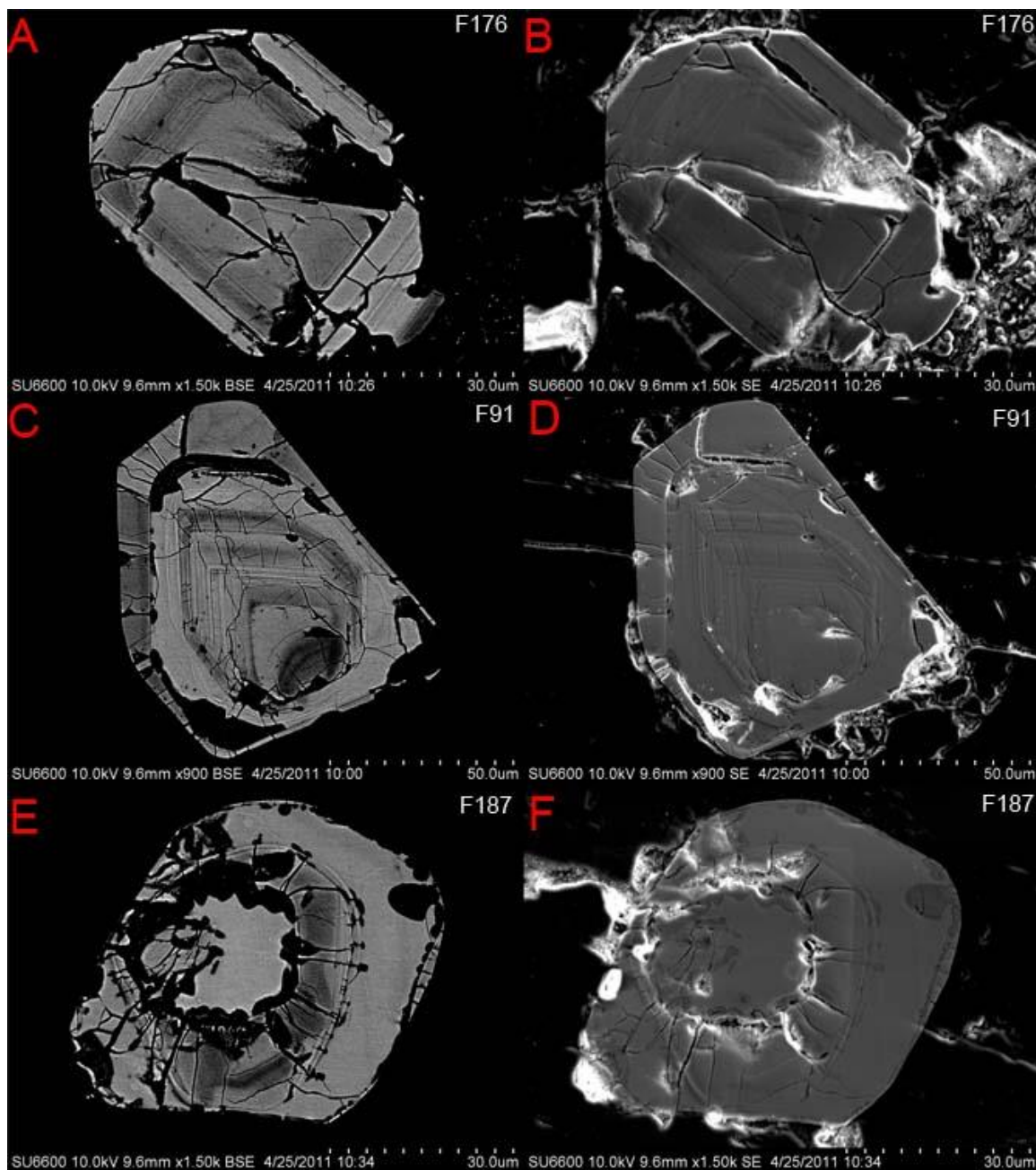


Figure 4.8 Backscatter (left side) and Secondary (right side) Electron images of select grains found during the feature scan of a sample 10644 thin section. The feature number is listed in the upper right corner of each image. The full image set can be found in Appendix C. Magnification, scale, and important imaging conditions are listed below each image. A and B: Planar growth banding; B and C: planar growth banding and a discontinuously zoned rim; E and F: A resorbed core and discontinuously zoned rim.

4.3.4 Zircon in Separates

After whole-rock mineral separation and electromagnetic filtering to isolate the least paramagnetic grains, high quality zircons were hand-picked and cast in epoxy along with SHRIMP standards. These grains were polished to mid-plane in order to expose any internal zoning, and to create an ideal surface for ion microprobe imaging and SEM analysis. Images of the 68 mounted grains were taken in transmitted light (see figure 4.9). Individual grains vary in length from approximately 75 μm to 500 μm . A few grains exhibit euhedral to subhedral prismatic crystal form; many are subhedral, often rounded to well rounded, giving a “potato-like” appearance. The majority of grains are relatively translucent, often with highly visible internal zoning or core-rim structures, and varying degrees of radial and/or transverse fractures. Other grains are tinted brown to orange; these are typically larger than the more translucent grains, and generally contain a higher concentration of cracks, though internal zoning can still be observed.

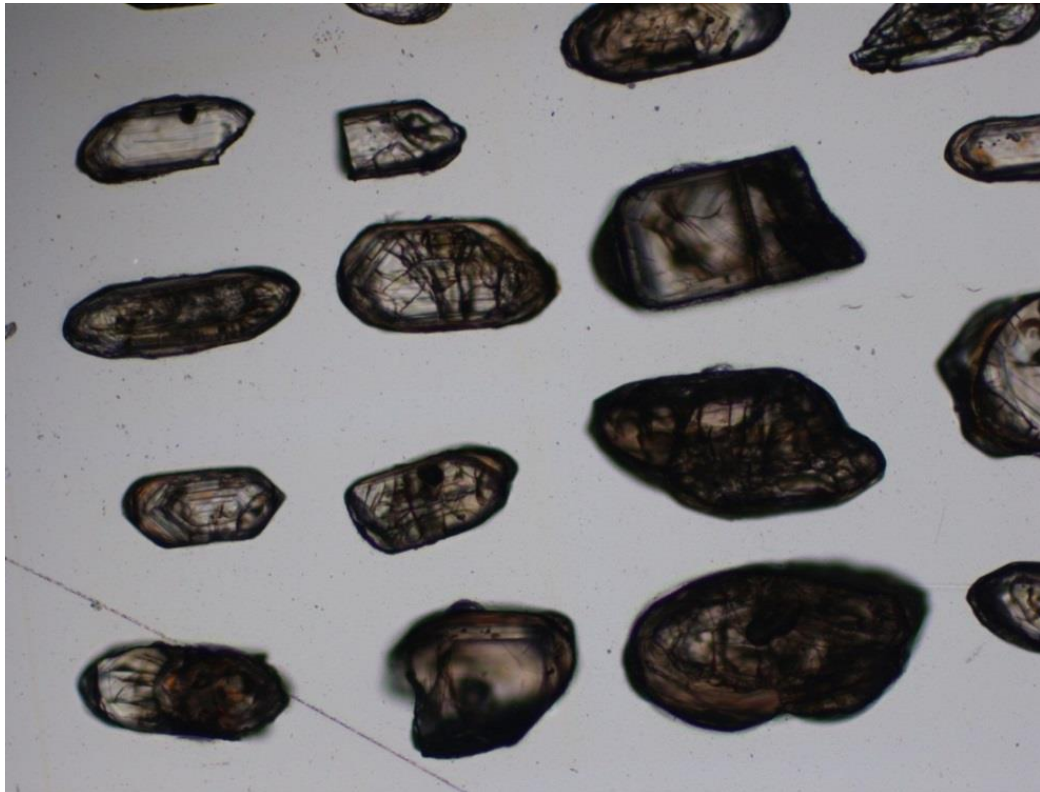


Figure 4.9 Transmitted light image of some mounted zircon grains (sample G060A1 - 10644), showing the variance in size, shape, colour, and internal zoning.

4.3.5 SE and Colour-CL of SHRIMP Mount

Zircon grains on the SHRIMP mount are of the same size range and morphology as those in the separates and in thin section. SE images reveal that most grains have a minor amount of cracks and holes, with few dark inclusions. Colour-CL imaging reveals several different internal structures which can be observed among all the mounted grains. Approximately 80% of grains exhibit a bright, discontinuously zoned core, which may have bright, planar growth banded rims, or dark, discontinuously zoned to homogeneous rims. The remaining 20% of grains usually display dark, homogenous cores, sometimes with medium to bright discontinuous rims, and dark homogeneous outer rims. Representative grains of each morphology are displayed in figure 4.10.

4.3.6 U-Pb Isotopic Data and Th/U Ratios

The results of SHRIMP-II U-Pb analysis for sample 10644 give a broad range of $^{207}\text{Pb}/^{206}\text{Pb}$ model ages, spanning from 2796 ± 20 Ma to 1795 ± 10 Ma. The analyses are generally near concordia, with an average discordance of 1% (See figure 4.11). The data can be separated into four groups based on apparent age, chemistry, and colour-CL microstructure. The mean $^{207}\text{Pb}/^{206}\text{Pb}$ model ages for these groups are 2770 Ma, 2670 Ma, 1842 Ma, and 1802 Ma. Some grains with multiple zones had several U-Pb analyses made, revealing Archean cores with Proterozoic rims (eg. grains 24, 25, see Appendix D for images of all grains), while others give apparent ages which are entirely Archean (eg. grain 12) or entirely Proterozoic (eg. grain 5). The Th/U ratios in this sample are highly varied relative to $\text{Pb}^{207}/\text{Pb}^{206}$ ages, ranging from 0.03 to 1.2, but correlating with the four age groupings present (see figure 4.12) and CL zoning.

The oldest grouping (at 2770 ± 38 Ma) consists of cores which are bright in colour-CL and exhibit planar to discontinuous zoning. They have an average Th/U ratio of 0.6 and minimum Th/U ratio of 0.18. The cores are typically crystalline and free of cracks (see figure 4.13 for a representative grain from each age group).

The zircon grains in the 2670 ± 36 Ma group are rims which are dark in colour-CL with discontinuous zoning. They have an average Th/U ratio of 0.1 and maximum

Th/U ratio of 0.2. They are crystalline and mostly free of cracks, though several grains exhibit moderate cracking around the boundary between core and rim.

The youngest $\text{Pb}^{207}/\text{Pb}^{206}$ apparent ages in this sample can be considered as two separate groupings, at 1842 ± 14 Ma and 1802 ± 10 Ma. The ca. 1842 Ma grouping is consists of whole grains and rims which are very dark in colour-CL and discontinuously zoned. These rims are crystalline, free of cracks, and have high U content (over 1000 ppm) with an average Th/U ratio of 0.1. The grouping at 1802 Ma is also comprised of whole grains and rims which are dark in a colour-CL and discontinuously zoned. This group can be distinguished from the 1842 Ma group by apparent age, by having a much lower U concentration (under 1000 ppm), and a higher Th/U ratio of 0.8. They are crystalline and free of cracks. A concordia plot (figure 4.14) and histogram (figure 4.15) showing both of these populations also allows these two youngest events to be visually distinguished from one another.

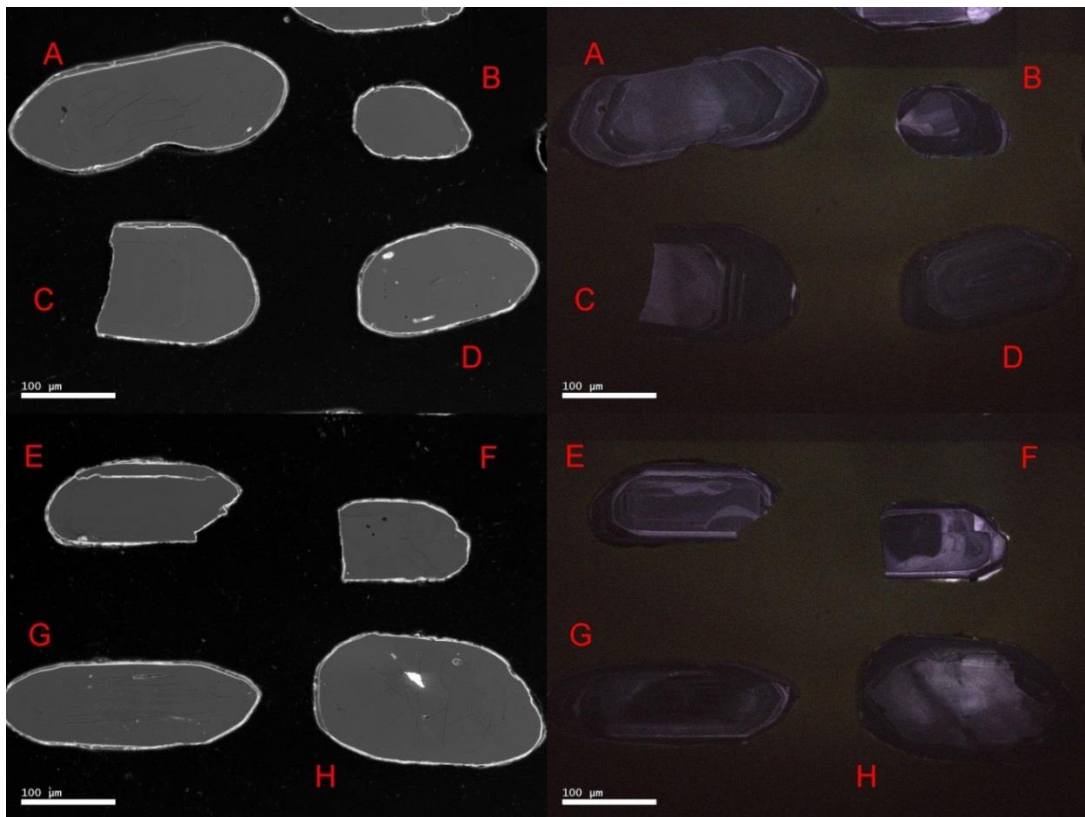


Figure 4.10 SE and colour-CL images of mounted zircon grains (sample G060A1 - 10644) showing the variety of sizes, shapes, and internal structures that can be found

within the sample. A) Bright, discontinuously zoned core with bright planar zoned rims, and a dark, homogeneous outer rim; B and C) Bright, discontinuously zoned core with occasional planar zoning, and a dark, homogeneous rim; D) Medium to dark planar banded core, with dark homogeneous rim; E) Bright, discontinuously zoned core with bright planar zoned inner rim, and dark homogeneous outer rim; F and G) Dark, homogeneous core, with medium to bright discontinuously zoned inner rim and dark, homogeneous outer rim; H) Bright, discontinuously zoned core with dark, homogeneous outer rim.

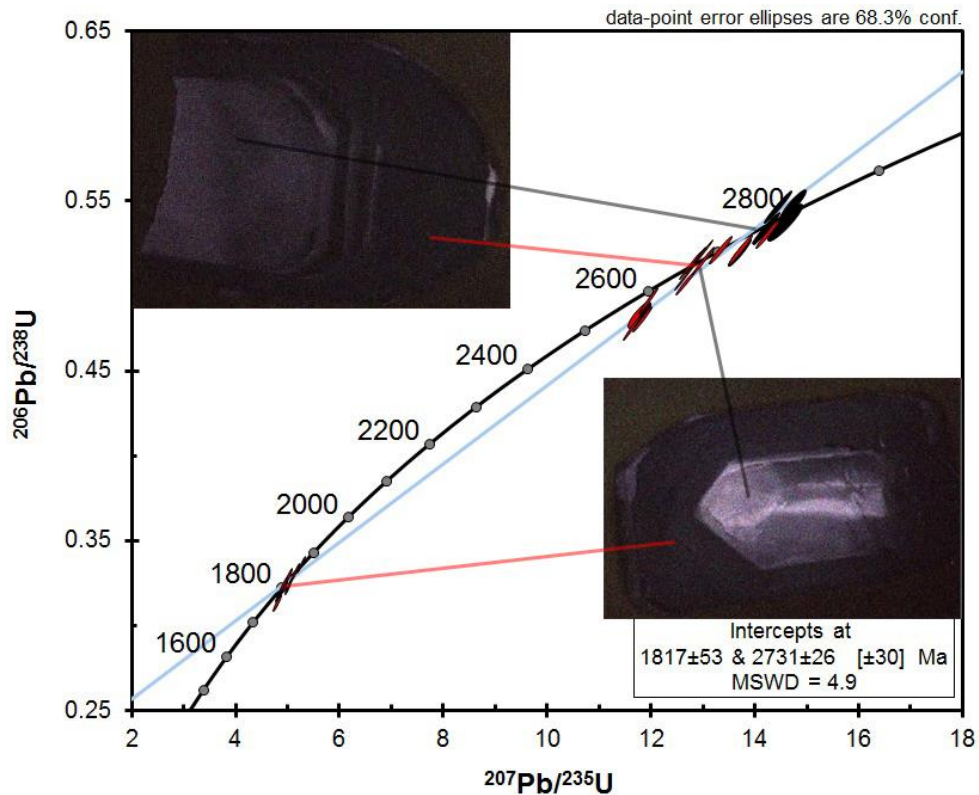


Figure 4.11 Concordia plot of Pb^{207}/Pb^{206} apparent ages for sample 10644 with unforced intercepts, showing several groups (Archean and Proterozoic). Representative grains from several populations are overlain with lines to connect microstructural domains with corresponding isotopic data. Error ellipses are 1σ , ages are Ma, black ellipses represent core analyses, red ellipses represent rim analyses.

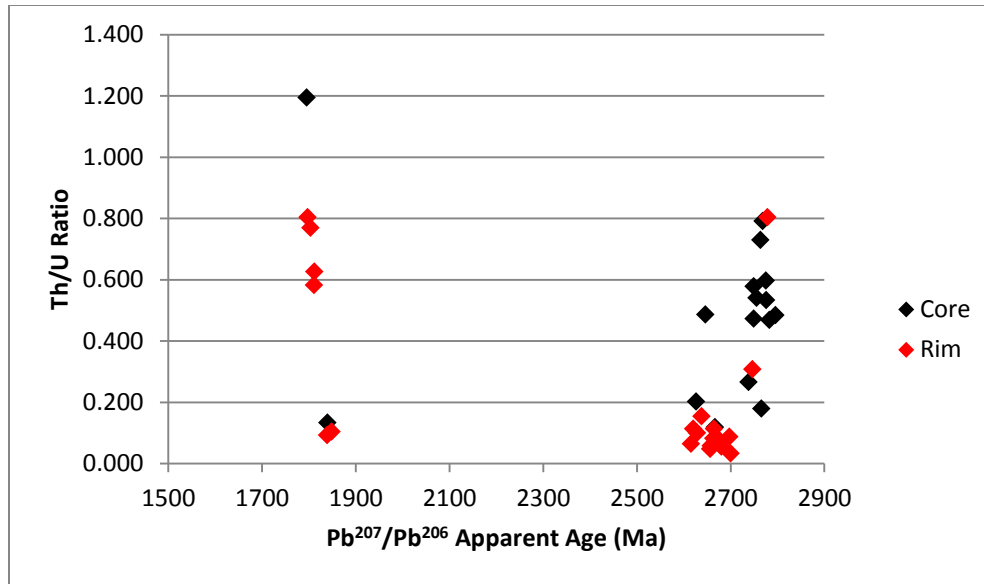


Figure 4.12 A graph showing the Th/U ratio vs. the Pb^{207}/Pb^{206} apparent ages for sample 10644. Note how four separate data clusters can be observed.

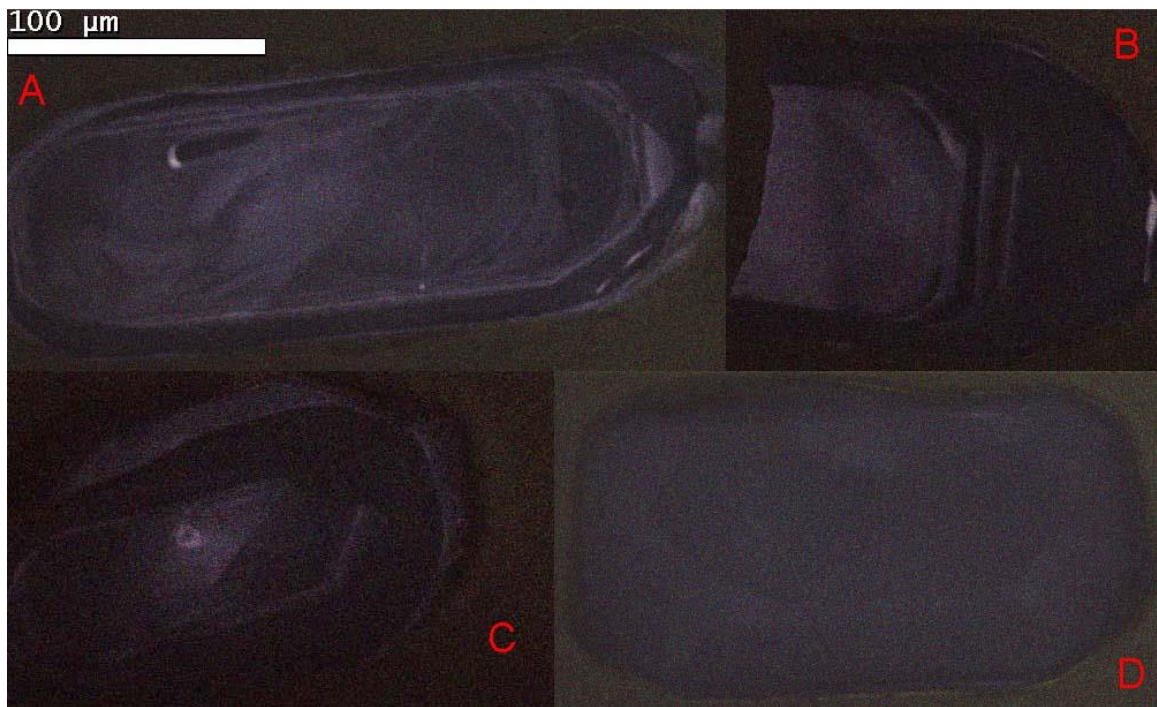


Figure 4.13 Colour-CL images of representative grains from each age grouping for sample 10644 (G060A1). A: 2770 Ma grouping (Grain 14) showing a light, planar to discontinuous core; B: 2670 Ma grouping (Grain 28) showing a dark, discontinuously zoned rim around a light, planar to discontinuous core of the 2770 Ma grouping; C: 1842 Ma grouping (Grain 24) showing a dark, discontinuously zoned rim around an Archean core; D: 1802 Ma grouping (Grain 5) with chemical zoning and no Archean core.

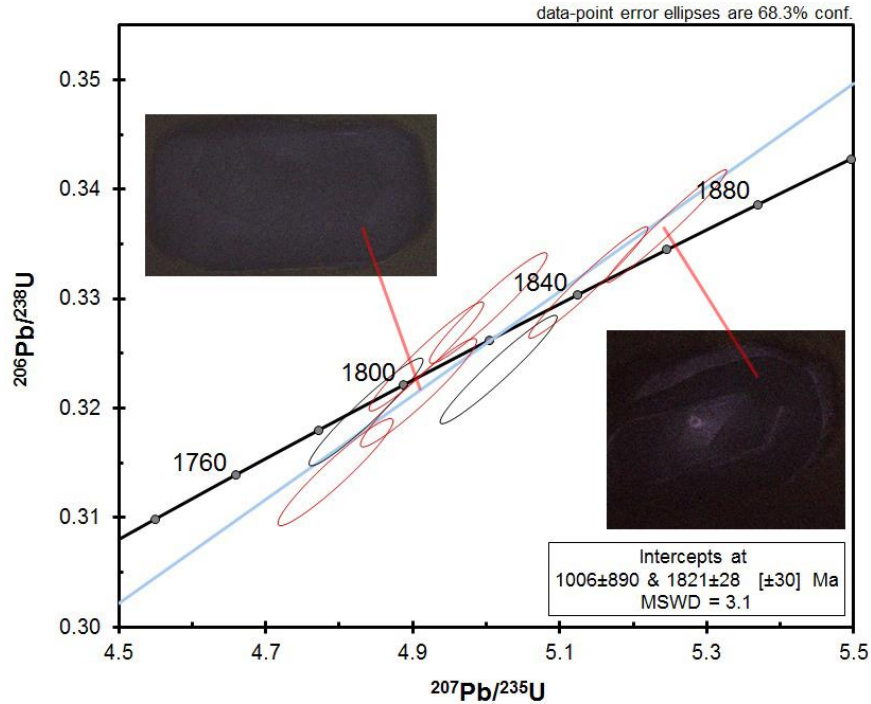


Figure 4.14 Concordia plot for the Proterozoic (1842 Ma and 1804 Ma) populations in sample 10644 with unforced intercepts. Two distinct zircon populations are evident, and a representative grain from each is shown. Data points which are greater than 5% discordant are excluded. Error ellipses are 1σ , ages are in Ma, black ellipses represent core analyses, red ellipses represent rim analyses.

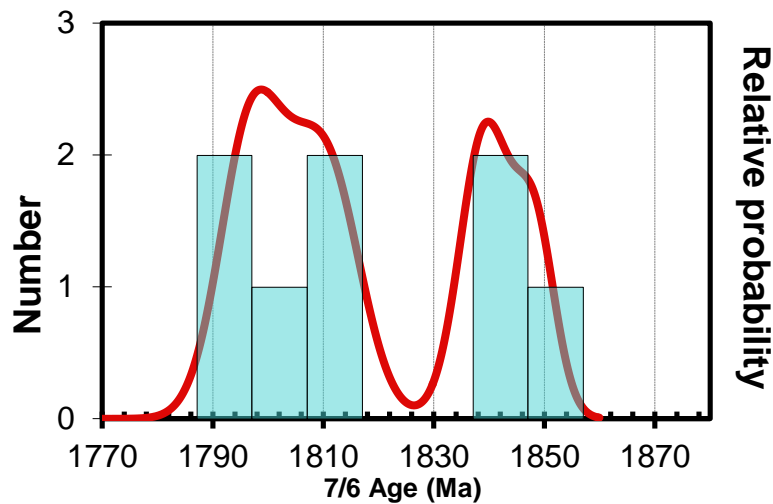


Figure 4.15 Probability density plot and histogram for the Proterozoic populations of sample 10644 based on Pb^{207}/Pb^{206} age. Bin width is set to the average 2-sigma error (10 Ma), bin start is set so that the minimum age attained from concordia (1802 Ma) is at the centroid of a bin. Analyses greater than 5% discordant were excluded.

4.4 Sample 10645 (G067A1)

4.4.1 Sample Description

Sample 10CXA-G067A1 (GSC internal SHRIMP mount number IP629-10645, see figure 4.1 for location) is classified as a medium grained migmatitic biotite, garnet, cordierite gneiss, based on its modal mineralogy of quartz (35%), biotite (30%), plagioclase (20%), K-feldspar (5%), cordierite (5%), and garnet (5%). Accessory phases include sulphides, monazite, apatite, and high quantities of zircon are also present, collectively comprising <1% of the sample. Grain size ranges from <1 mm to 3 mm, and grains are typically anhedral. The sample exhibits a strong foliation defined by biotite alignment and 1 mm to 3 mm thick quartzo-feldspathic and biotite-rich bands. In outcrop, quartzo-feldspathic leucocratic lenses can be seen to sometimes contain garnet (see figure 4.16, 4.17) and occasionally cordierite.



Figure 4.16 A: Field photo of sample 10645 showing the strong foliation and leucocratic pockets of quartzo-feldspathic composition. B: Field photo showing a group of leucocratic quartzo-feldspathic lenses rich in garnet. C: Hand sample photo, G067A1.

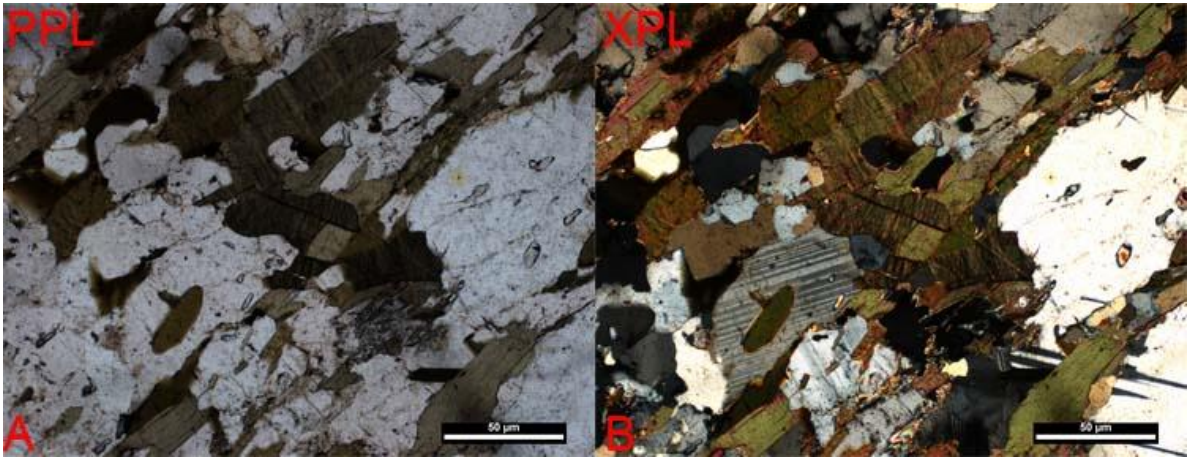


Figure 4.17 Petromicrographs of sample 10645; A: Plane-polarized; B: Cross-polarized. The slide was not moved or rotated when switching polarization.

4.4.2 EDS Phase Mapping and BSE-EDS “Feature” Mapping

Elemental (EDS) mapping of a thin section was used to map the distribution of chemical associations characteristic of certain minerals or phases identified independently by optical microscopy. The major mineral phases present were determined to be Al+low Mg+O (cordierite, 15%), Al+high Mg+O (biotite, 30%), Al+Na+O (plagioclase, 10%), Al+Si+K (K-feldspar, 5%), P+Ca+O (apatite, <1%), Si+O (quartz, 40%). Although accessory minerals are present in the sample (total modal abundance <1%), the resolution of the EDS scan does not show them clearly enough to allow their inclusion in the chemical map.

The results of EDS mapping, along with automated “Feature” mapping are shown in figure 4.18. A total of 167 zircon grains, ranging in length from 9 µm to 94 µm, and area from 44 µm² to 4098 µm² were located. Zircon grains of all sizes occur almost exclusively within biotite grains. 31 Monazite grains were found, ranging in length from 10 µm to 158 µm, and area from 51 µm² to 12371 µm². As with zircon, nearly all monazite grains occur either in or in contact with biotite grains.

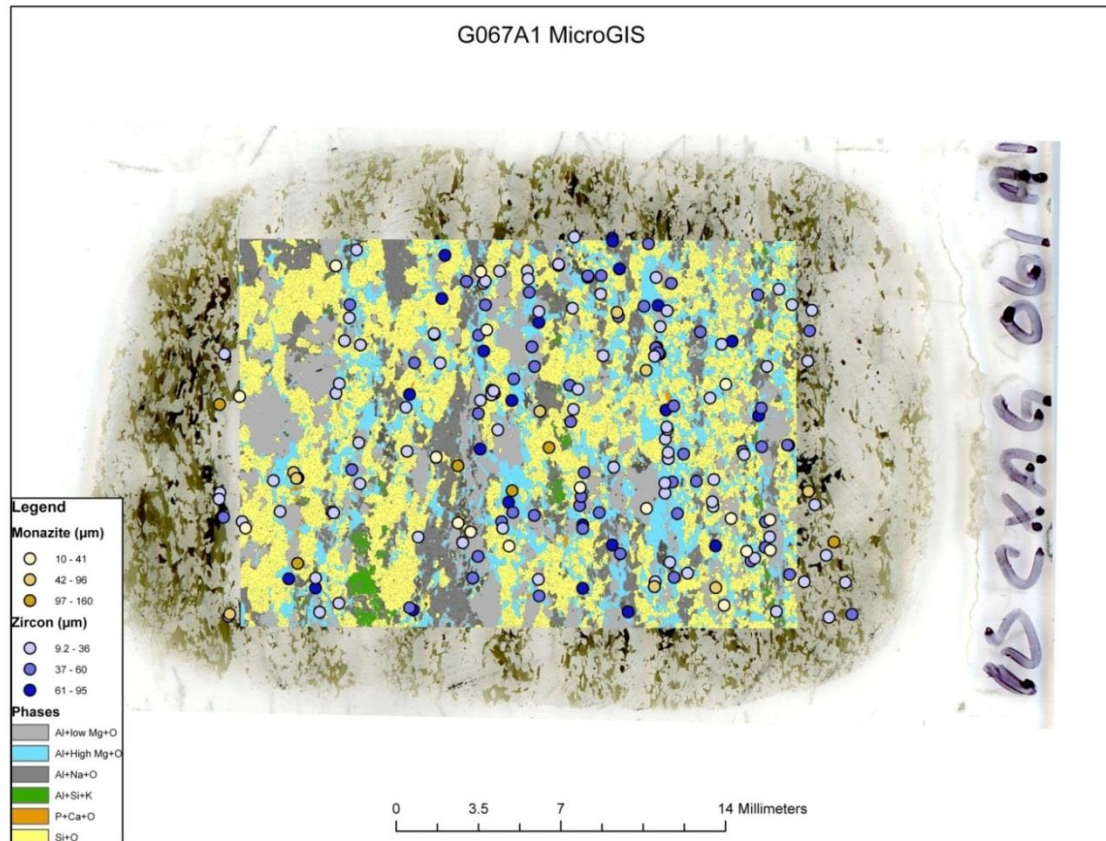


Figure 4.18 MicroGIS map of a large thin section from sample 10645. Monazite and Zircon are split into three size categories, represented by the different shades of blue and orange. The phases represent locations in the thin section where EDS data exist for a unique combination of chemical elements (mineral phase).

4.4.3 BSE and SE of Zircon in Thin Section

The internal structure of the largest zircon and monazite grains were imaged in situ with electron microscopy (BSE and SE). Most crystals are highly fractured and damaged, although some monazite grains are better preserved. In rare cases, zircon and monazite grains can be found in direct contact with each other (see figure 4.19).

In BSE, zircon grains typically have dark, discontinuously zoned cores, with thick, bright, homogeneous rims. In rare cases, some grains contain medium brightness planar growth banded cores. Monazite grains do not always clearly show zoning in BSE, although some grains show bright, irregularly shaped, discontinuously zoned cores, with

thick dark inner rims and thin bright outer rims. Grains display a variety of degrees of transverse fracturing.

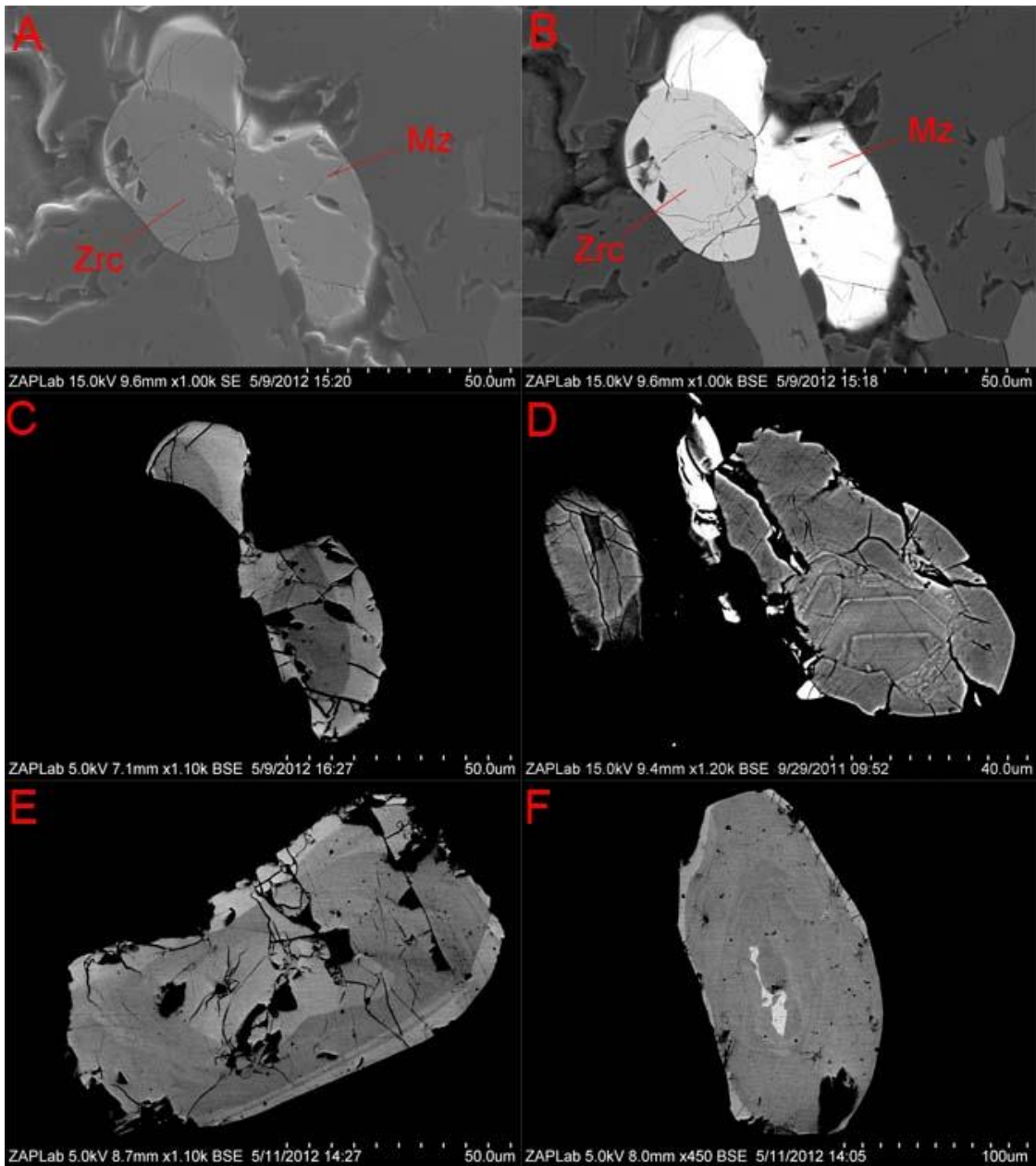


Figure 4.19 Zircon and Monazite (sample 10645) in contact imaged in A: BSE; B: SE; C: A monazite grain with a dark, discontinuous core and bright, continuous rim; D: zircon showing planar growth banding in its core; E and F: two monazite grains with bright, irregularly shaped cores, medium-bright planar to discontinuously zoned bodies, and bright, homogeneous rims. Magnification, scale, and important imaging conditions are listed below each grain.

4.4.4 Zircon in Separates

After whole-rock mineral separation, a population of large, representative high quality zircon (n=103) were cast in epoxy for SHRIMP analysis (see figure 4.20). Individual grains vary in length from approximately 50 μm to 150 μm , though most are on the order of 75-100 μm . Most grains are well-rounded and “potato” shaped, though some are broken, displaying angular edges; occasionally, grains have a relict, slightly prismatic appearance. The vast majority of grains are translucent with varying degrees of transverse and radial fractures, and occasionally display internal zoning and core-rim structures.



Figure 4.20 Transmitted light image of some mounted zircon grains (sample G067A1 - 10645), showing the variance in size, shape, colour, and internal zoning

4.4.5 SE and Colour-CL of SHRIMP Mount

Secondary Electron images of polished grain surfaces occasionally reveal holes (normally $>10 \mu\text{m}$), and usually have a moderate amount of transverse or radial fracturing, although approximately 30% of grains appear relatively well preserved. In colour-CL, many grains display a bright, complex and discontinuously zoned core,

surrounded by a dark, homogeneous zone of varying thickness (typically 10-30 μm), and a bright, discontinuously zoned outer rim ranging in thickness from $<5 \mu\text{m}$ to as much as 40 μm (see figure 4.21). This zoning sequence was observed in approximately 90% of the population. The remaining grains have the same dark and light inner and outer rims, but lack an obvious core.

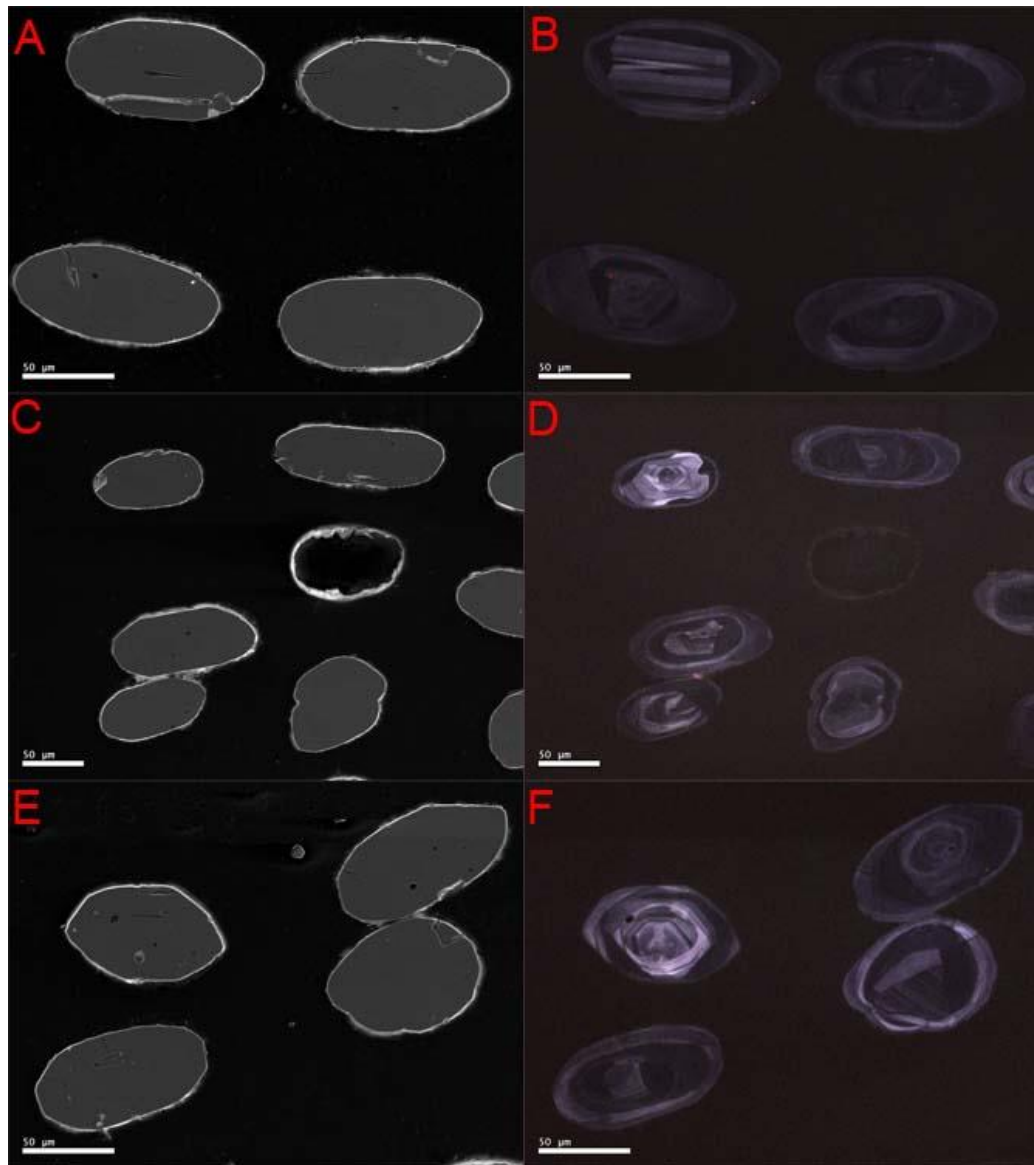


Figure 4.21 SE (A,C,E) and colour-CL (B,D,F) images of mounted zircon grains (sample G067A1 - 10645) showing the variety of sizes, shapes, and internal structures that can be found within the mounted grains from the sample suite. Note how most grains have an obvious core structure that is bright in colour-CL and planar to discontinuously zoned, with a dark, homogeneous “inner rim”, and a bright, discontinuously zoned outer rim.

4.4.6 U-Pb Isotopic Data and Th/U Ratios

U-Pb age data from sample 10645 yield a wide range of minimum $\text{Pb}^{207}/\text{Pb}^{206}$ apparent ages, spanning from 2680 ± 10 Ma to 1764 ± 50 Ma (see figure 4.22), which can be separated into two groups based on apparent age, chemistry, and colour-CL microstructure. The Th/U ratios for all analyses can be seen in figure 4.23. This graph shows a steady decrease in Th/U ratio with decreasing $^{207}\text{Pb}/^{206}\text{Pb}$ apparent age. It also shows the strong relationship between apparent age and grain structure – ages of cores increase from approximately 1850 Ma up to 2690 Ma, while rims are all between 1750 Ma and 1900 Ma (see figure 4.24 for representative grains from each group).

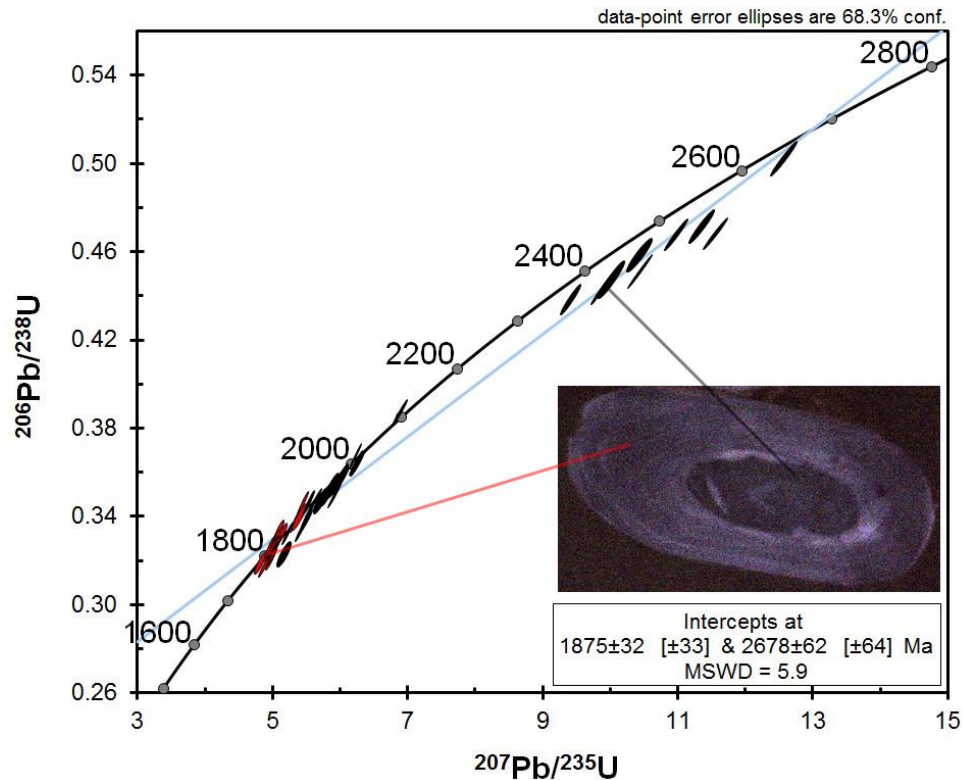


Figure 4.22 Concordia plot for sample 10645 with unforced intercepts showing the wide age variability of the first group, along with a distinct Proterozoic cluster. Data points which are greater than 5% discordant are excluded. An example grain with a partially reset Archean core and Proterozoic rim is overlain. Error ellipses are 1σ , ages are in Ma, black ellipses represent core analyses, red ellipses represent rim analyses.

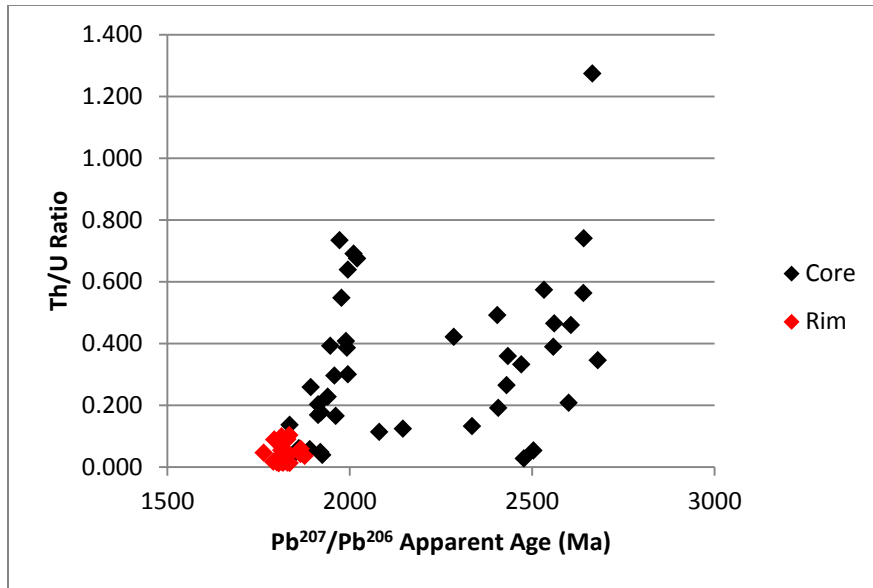


Figure 4.23 A graph showing the Th/U ratio vs. the Pb^{207}/Pb^{206} apparent ages for sample 10645, illustrating how core ages spread over a wide range, while rims are relatively concentrated.

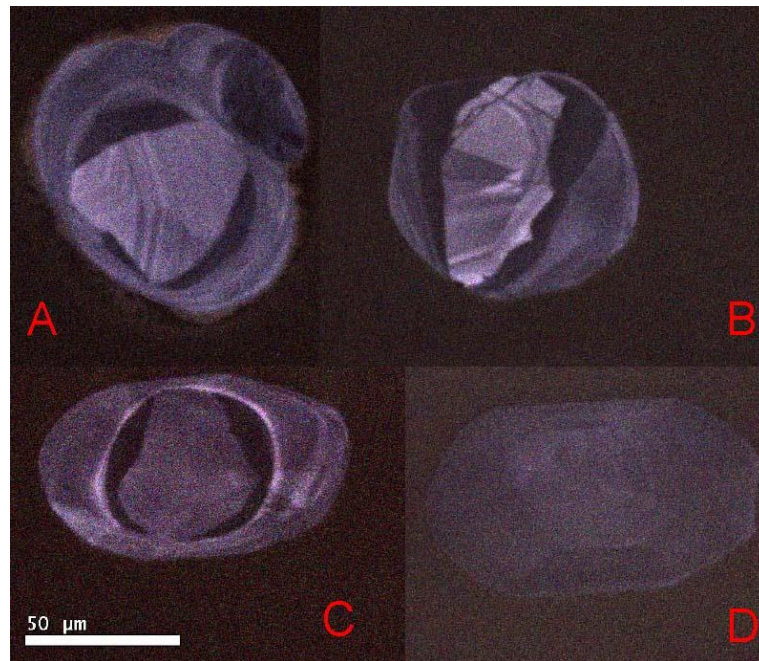


Figure 4.24 Colour-CL images of representative grains from each age grouping for sample G067A1 (10645). A: (Grain 38) Bright, truncated planar Archean core with a dark inner rim and a bright outer rim; B: (Grain 101) Bright, truncated planar core with a dark inner rim and a bright Proterozoic outer rim; C: (Grain 23) Bright, discontinuous Proterozoic rim on an Archean core; D: (Grain 56) Dark chemically zoned Proterozoic grain with no Archean core.

The first group spans a wide range of model ages, from 2680 ± 10 Ma to 1891 ± 10 Ma. This group is comprised of cores which plot almost entirely below concordia, ranging from 1% to 11% discordant. The Th/U ratios for this group range from 0.03 to 1.3, with an average of 0.4. These cores are usually bright in colour-CL, often displaying truncated planar zoning with occasional discontinuous zoning. Many of these cores are surrounded by a discontinuous zone of zircon which is dark in colour-CL, and then a bright, planar to discontinuously zoned rim. U-Pb analyses for this grouping are mostly from the planar to discontinuous central portions of the grains, though some overlap with the darker “inner” rim. These microstructures appear to be consistent throughout the wide range of apparent ages for this group.

The second group of $^{207}\text{Pb}/^{206}\text{Pb}$ apparent ages in this sample are from rims and range from 1877 ± 18 Ma to 1764 ± 50 Ma. Grains in this group are typically concordant or only a few percent discordant, with Th/U ratios of 0.1 or lower, with an average of Th/U ratio of 0.05. The rims are bright in colour-CL, planar to discontinuously zoned, crystalline, and free of cracks and inclusions. Similar grain structure and chemistry within this group suggests that there is only a single Proterozoic population, supported by a probability density plot (see figure 4.25).

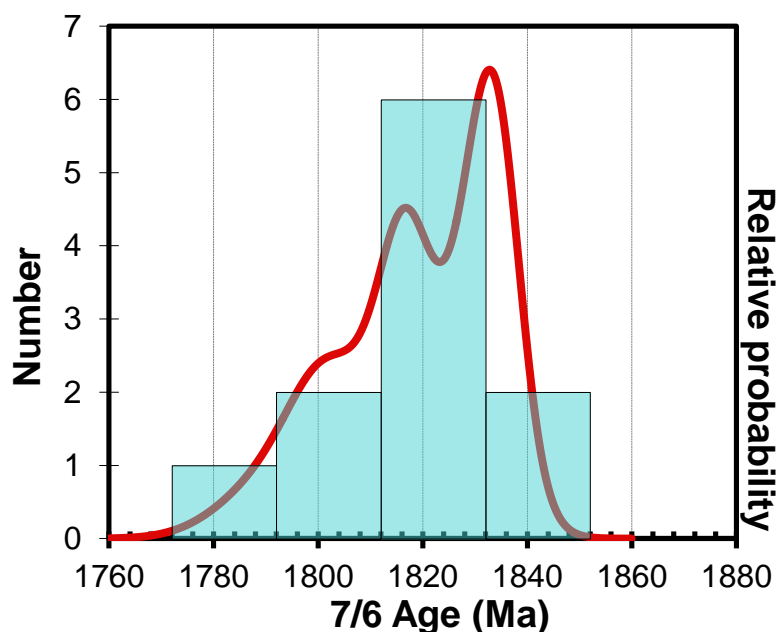


Figure 4.25 Probability density plot and histogram for the Proterozoic population of sample 10645 based on $^{207}\text{Pb}/^{206}\text{Pb}$ age. Bin width is set to the average 2-sigma error (12 Ma), bin start is set so that the minimum age attained from concordia (1822 Ma) is at the centroid of a bin. Analyses greater than 5% discordant were excluded.

4.5 Sample 10646 (G071A1)

4.5.1 Sample Description

Sample 10CXA-G071A1 (GSC internal SHRIMP mount number IP629-10646) has a modal mineralogy of quartz (45%), plagioclase (20%), biotite (20%), K-feldspar (5%), Cordierite (5%), and iron sulphides (5%)(see figure 4.26). Following the classification scheme of Winter, 2001, this rock is named a migmatitic cordierite biotite gneiss. Accessory phases include zircon, monazite, titanite, and apatite, collectively comprising <1% of the sample. Mineral grains are typically anhedral, ranging in size from <1 mm to 4 mm (see figure 4.27). The sample has a moderate foliation defined by biotite alignment and 1 mm to 5 mm thick quartzo-feldspathic and biotite-rich bands. In outcrop, a migmatitic texture can be observed, with quartzo-feldspathic leucosomes occasionally displaying cordierite.

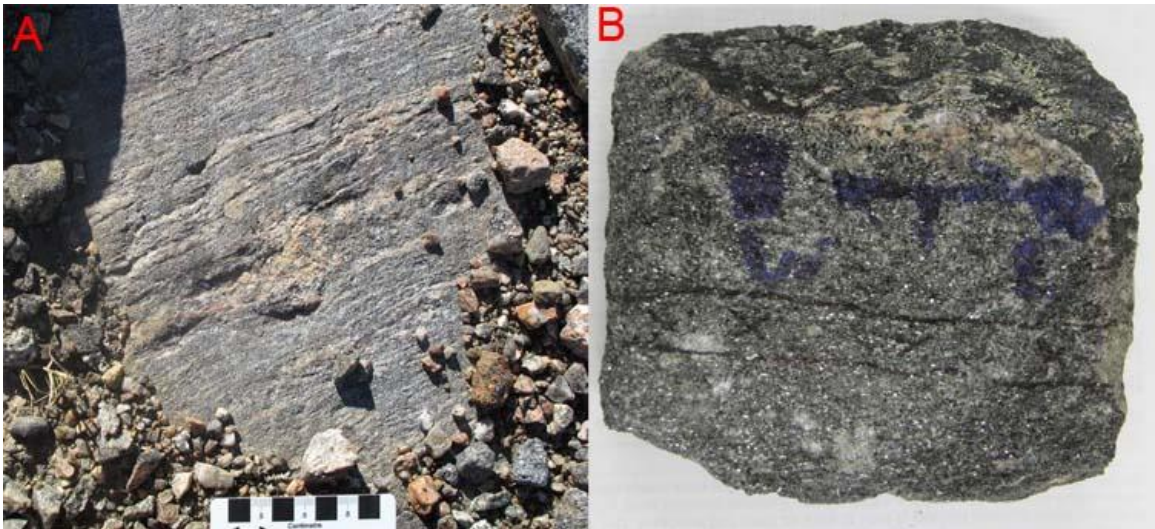


Figure 4.26 Field and hand sample photos of sample 10646. A: Field photo showing the foliation and centimetre scale lenses of leucosome; B: Hand sample photo with small pockets of leucosome visible.

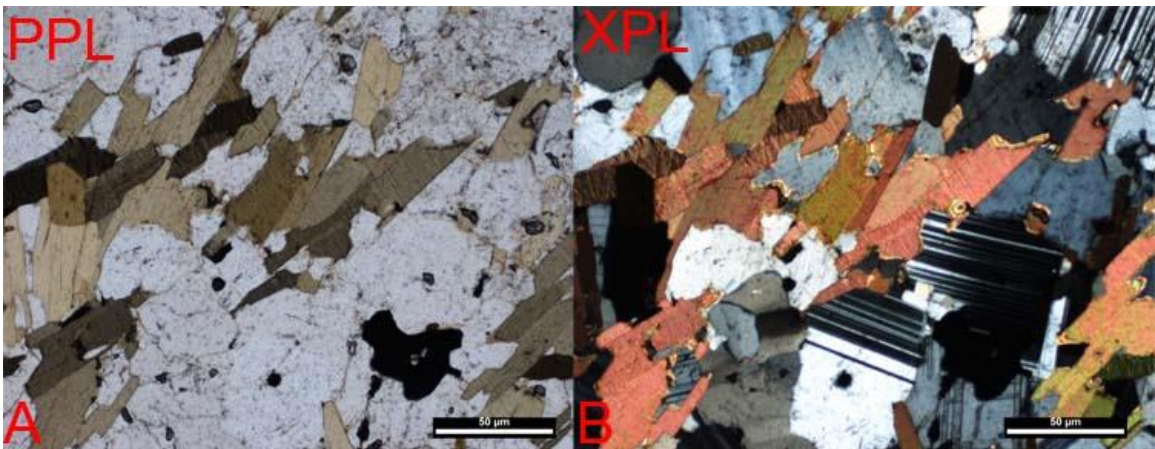


Figure 4.27 Petromicrographs of sample 10646; A: Plane-polarized; B: Cross-polarized. The slide was not moved or rotated when switching polarization.

4.5.2 EDS Phase Mapping and BSE-EDS “Feature” Mapping

EDS mapping, combined with optical microscopy, the major mineral phases present were determined to be Fe+Ti+O (titanite, <1%), K+low Al+Si (K-feldspar, 5%), Si+Al+O (sillimanite, <1%), Si+Ca+Na (plagioclase, 30%), Si+low Mg+Al (cordierite, 35%), Si+Mg+Fe (biotite, 15%), and Si+O (quartz, 20%).

Figure 4.28 shows the results of the chemical mapping, overlain by the results of automated feature scanning. 77 zircon grains were found, ranging in length from 9 μm to 92 μm , and area from 44 μm^2 to 3494 μm^2 . Approximately 90% of zircon grains are located either with or in contact with biotite grains, with the remaining 10% usually found in contact with quartz grains. 46 monazite grains were found, ranging in length from 8 μm to 136 μm , and area from 41 μm^2 to 6823 μm^2 . As with zircon, approximately 90% of monazite grains can be found within or in contact with biotite, and 10% in contact with quartz grains.

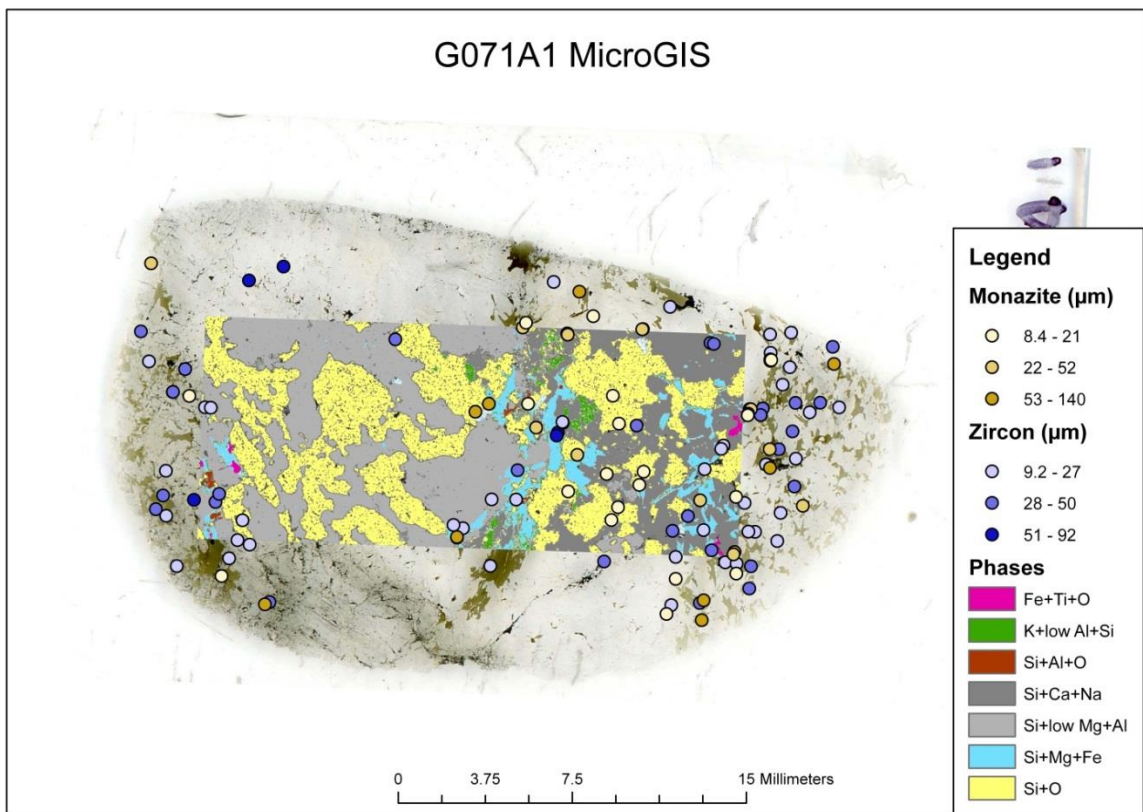


Figure 4.28 MicroGIS map of a large thin section from sample 10646. Monazite and Zircon are split into three size categories, represented by the different shades of blue and orange. The phases represent locations in the thin section where EDS data exists for a unique combination of chemical elements (mineral phase). Fe+Ti+O = titanite, K+low Al+Si = K-feldspar, Si+Al+O = sillimanite, Si+Ca+Na = plagioclase, Si+low Mg+Al = cordierite, Si+Mg+Fe = biotite, Si+O = quartz.

4.5.3 BSE and SE of Zircon in Thin Section

BSE and SE images were taken of the largest zircon grains. SE images (figure 4.29) reveal that most zircon crystals contain a moderate amount of radial fractures, with occasional transverse fractures. Monazite grains display very few radial fractures, but many are severely damaged by transverse fractures.

In BSE, zircon grains display medium brightness planar growth banded cores, with thin, bright, discontinuously zoned rims. Monazite grains show a bright, irregularly shaped homogeneous core, with a thick, dark homogeneous inner rim, and a thin, bright homogeneous outer rim.

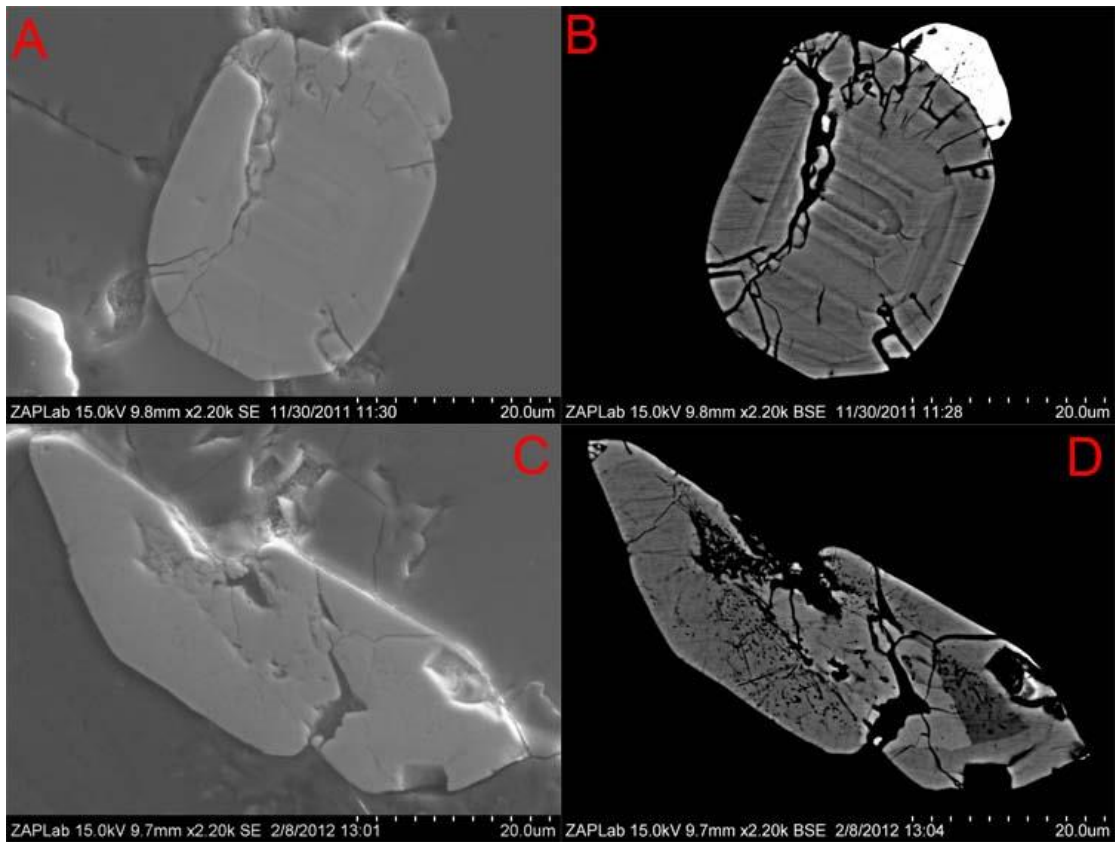


Figure 4.29 A: SE image of a typical zircon from sample 10646, displaying radial and transverse fractures. Internal zoning is also visible; B: BSE image of the same zircon, showing the planar zoning in the core. The small, bright grain attached to the upper right section of the zircon grain is a monazite overgrowth; C: SE image of a typical monazite from G071A1. Transverse fracturing has damaged the grain; D: BSE image of the same monazite grain, showing the bright, irregularly shaped core, dark inner rim, and bright outer rim.

4.5.4 Zircon in Separates

Images of the 144 mounted grains were taken in transmitted light (see figure 4.30). Individual grains vary in length from approximately 75 μm to 250 μm . Grains are typically anhedral, well rounded and “potato” shaped, although approximately 10% have a vaguely prismatic appearance. Most (approximately 95%) grains are translucent, with minimal to moderate degrees of fracturing, and highly visible core-rim structures. The remaining 5% have a slight brown tint.

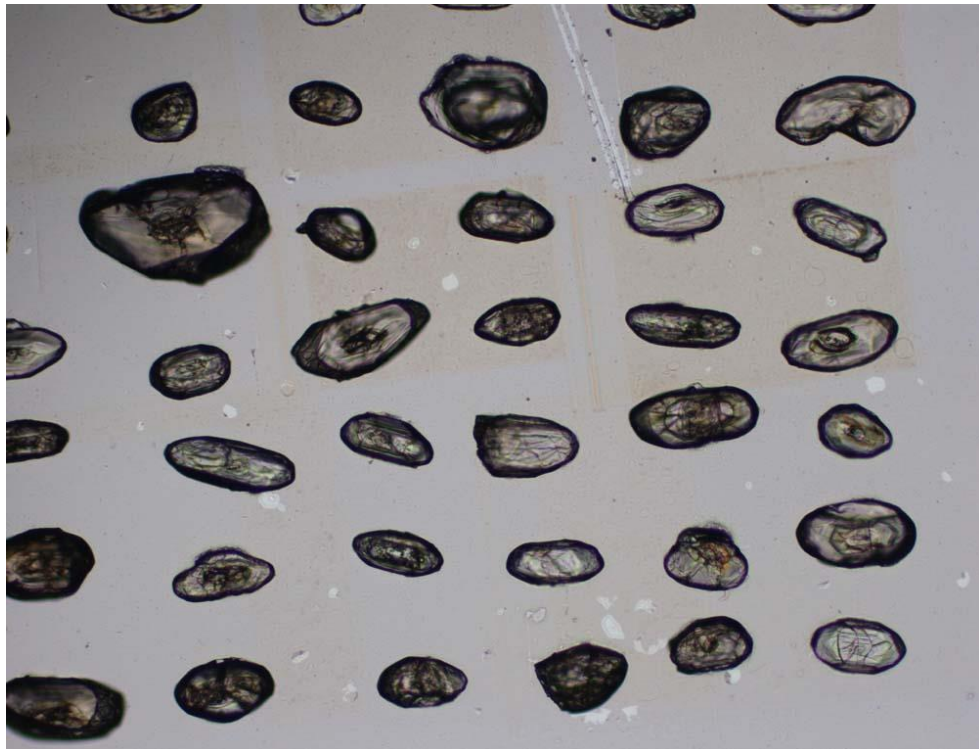


Figure 4.30 Transmitted light image of some mounted zircon grains (sample G071A1 - 10646), showing the variance in size, shape, colour, and internal zoning.

4.5.5 SE and Colour-CL of SHRIMP Mount

Secondary Electron images of polished cross-sections of the grain mount reveal that most grains are free of holes. Approximately 60% of grains exhibit moderate degrees of radial fracturing, with occasional transverse fracturing. Approximately 30% of grains are free of cracks and holes. In colour-CL, approximately 65% of zircon grains show an

irregular or discontinuously zoned core, with a thick, dark, homogeneous inner rim, and a bright, discontinuously zoned rim, which is typically very thin. The rest of the grains display this same morphology without the core structure (see figure 4.31).

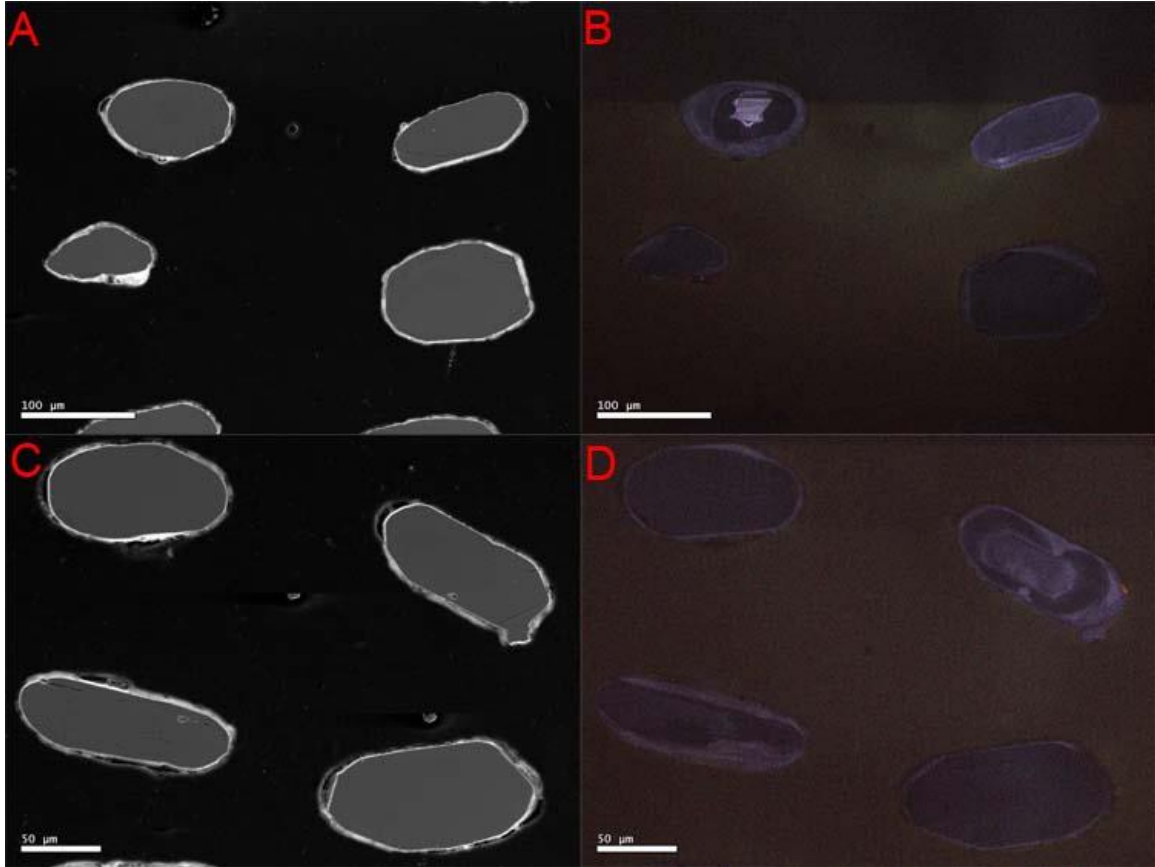


Figure 4.31 SE and Colour-CL images of mounted zircon grains (sample G071A1 - 10646) showing the two dominant zircon morphologies: A bright, planar to discontinuously zoned core with a dark, homogeneous inner rim, and a thin, bright, discontinuously zoned outer rim (eg. top-left grain in A,B; top right in C,D), as well as the same morphology without an obvious core (eg. bottom-left grain in C,D).

4.5.6 U-Pb Isotopic Data and Th/U Ratios

The results of SHRIMP-II U-Pb analysis for sample 10646 give a comparatively restricted range of minimum Pb^{207}/Pb^{206} apparent ages, ranging from 1846 ± 6 Ma to 1800 ± 12 Ma, with a single outlier at 2022 ± 6 Ma. The analyses are generally near concordia, with an average discordance of 1% (See figure 4.32). The Th/U ratios in this

sample are relatively much lower than in the other samples; almost all grains are below 0.08, with a cluster of grains below 0.02 (see figure 4.33).

Zircon zones which are dark in colour-CL have very low Th/U ratios, usually around 0.01. The lighter zones have higher Th/U ratios, averaging approximately 0.05, ranging from 0.008 to 0.08. Variations in Th/U ratios occur independent of changes in Pb^{207}/Pb^{206} apparent age. Grains are crystalline and free of cracks.

Some grains have truncated planar zoned cores, which are often highly resorbed, and sometimes contain large inclusions which stand out in colour-CL (see figure 4.34). These resorbed cores appear structurally similar to cores in sample 10645, though the lack of chemical data from cores in this sample prevents a meaningful comparison. The single outlying apparent age for this population is taken from one of these cores, while the remaining analyses are taken from rims. Analyses in this sample cannot be separated into chemically or structurally distinct groupings. A probability density plot (figure 4.35) also suggests that this group of analyses represents a single zircon growth event.

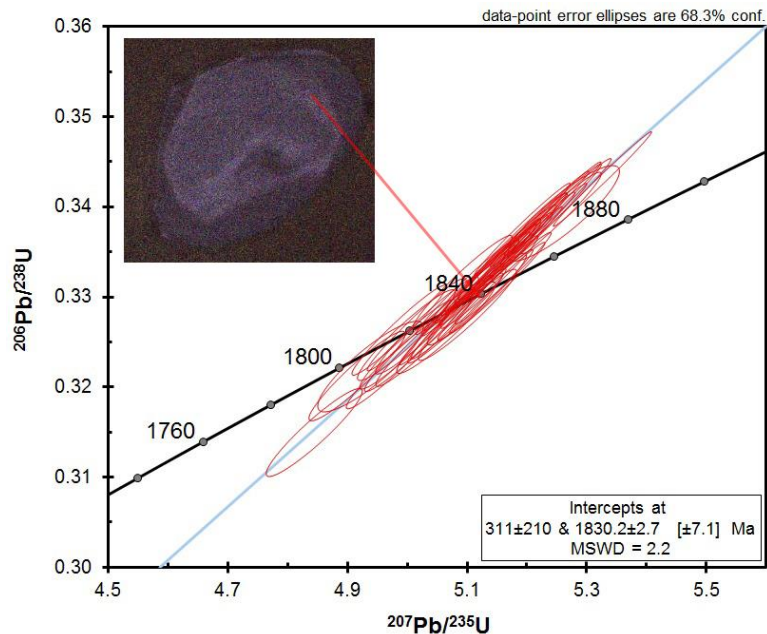


Figure 4.32 Concordia plot of Pb^{207}/Pb^{206} apparent ages for sample 10646 with unforced intercepts. An example grain with a chemically zoned core is shown. Data points which are greater than 5% discordant are excluded. Error ellipses are 1σ , ages are in Ma, black ellipses represent core analyses, red ellipses represent rim analyses.

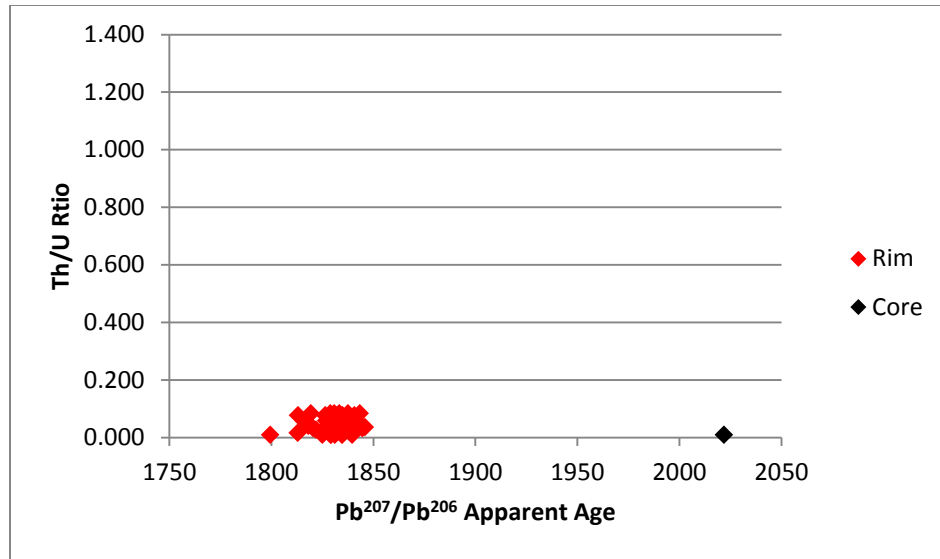


Figure 4.33 A graph showing the Th/U ratio vs. the Pb^{207}/Pb^{206} apparent ages for sample 10646. The scale is kept the same as that in the graphs for the previous samples in order to show how much lower the Th/U ratios are in this sample relative to the other two. The single outlier is the only analysis from a structural core.

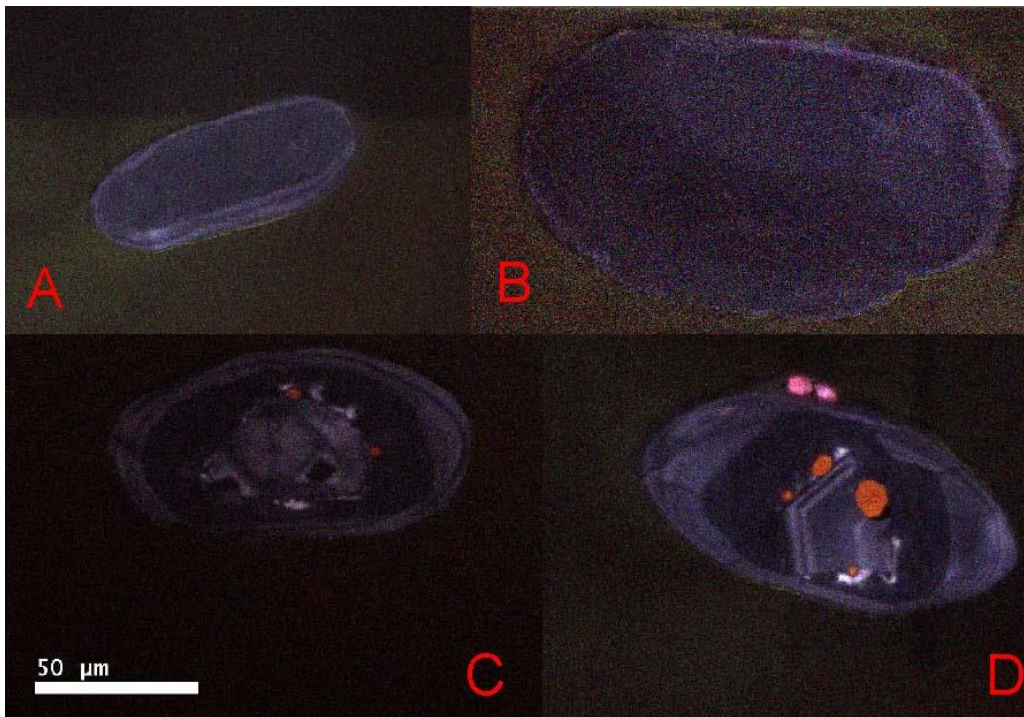


Figure 4.34 Colour-CL images of representative grains from each age grouping for sample G071A1 (10646). A and B: (Grain 24 and Grain 35) Discontinuously and chemically zoned Proterozoic grains with no structural cores; C and D: (Grain 38 and Grain 39) resorbed cores with bright, discontinuous, Proterozoic rims.

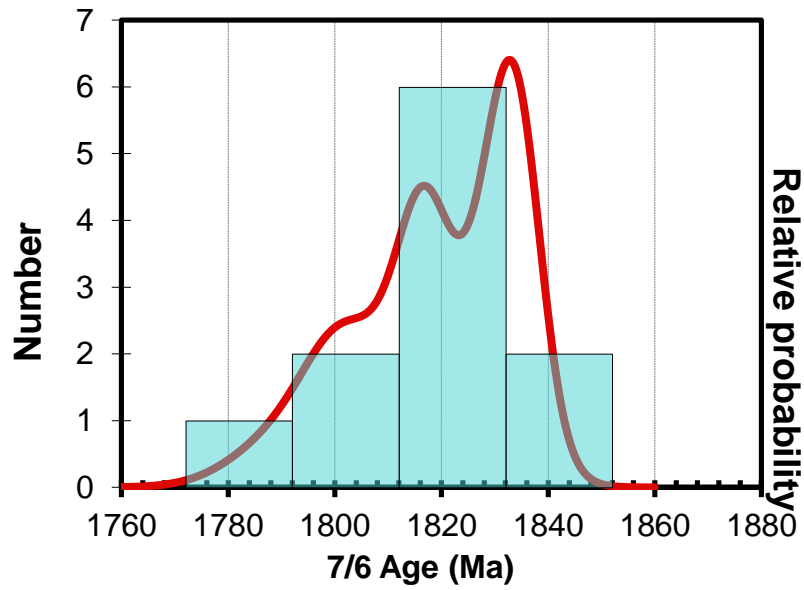


Figure 4.35 Probability density plot and histogram for the Proterozoic population of sample 10646 based on $^{207}\text{Pb}/^{206}\text{Pb}$ age. Bin width is set to the average 2-sigma error (8 Ma), bin start is set so that the minimum age attained from concordia (1830 Ma) is at the centroid of a bin. Analyses greater than 5% discordant were excluded.

5 Discussion

5.1 U-Pb Chronology of Individual Samples

5.1.1 History of Sample 10644 (G060A1)

As described in the Chapter 4, the $^{207}\text{Pb}/^{206}\text{Pb}$ model ages for sample 10644 can be placed into four groups. Each of these groups is interpreted to represent an individual zircon growth event. The geologic significance of each event is interpreted as follows, in order from oldest to youngest.

Zircon zones belonging to the 2770 ± 38 Ma grouping have Th/U ratios greater than 0.5, usually exhibit planar zoning, and are structural cores to zircon rims which are measured to be younger. This evidence allows for this age grouping to be interpreted as a zircon growth event which occurred during the igneous rock forming event that led to the crystallization of this rock's granodioritic protolith. A concordia plot for this grouping with unforced intercepts gives an upper intercept of 2770 ± 38 Ma. Anchoring the lower intercept at 1802 ± 10 Ma, the interpreted timing of the youngest zircon growth event in this sample, changes the upper intercept to 2774 ± 38 Ma (see figure 5.1). This change is within error of the unforced upper intercept, so it is likely that the majority of Pb-loss in this sample would have occurred around the time of this youngest event.

Zircon domains belonging to the 2670 ± 36 Ma age grouping have very low Th/U ratios (average 0.119), appear dark and discontinuously zoned in colour-CL, and are structural rims to cores which are measured to be older. These domains are therefore interpreted to be formed as a result of an Archean metamorphic zircon growth event. Figure 5.2 shows concordia plots for this population with forced and unforced intercepts. The unforced lower intercept is not quite within error of the interpreted age of Pb-loss which occurred at 1802 ± 10 Ma, yielding an absolute minimum age for this population at 2670 ± 36 Ma. Anchoring the lower intercept at 1802 ± 10 Ma increases the minimum age (upper intercept) of the population to 2692 ± 62 Ma, which is within error of the unforced upper intercept. While it is possible that this zircon growth event

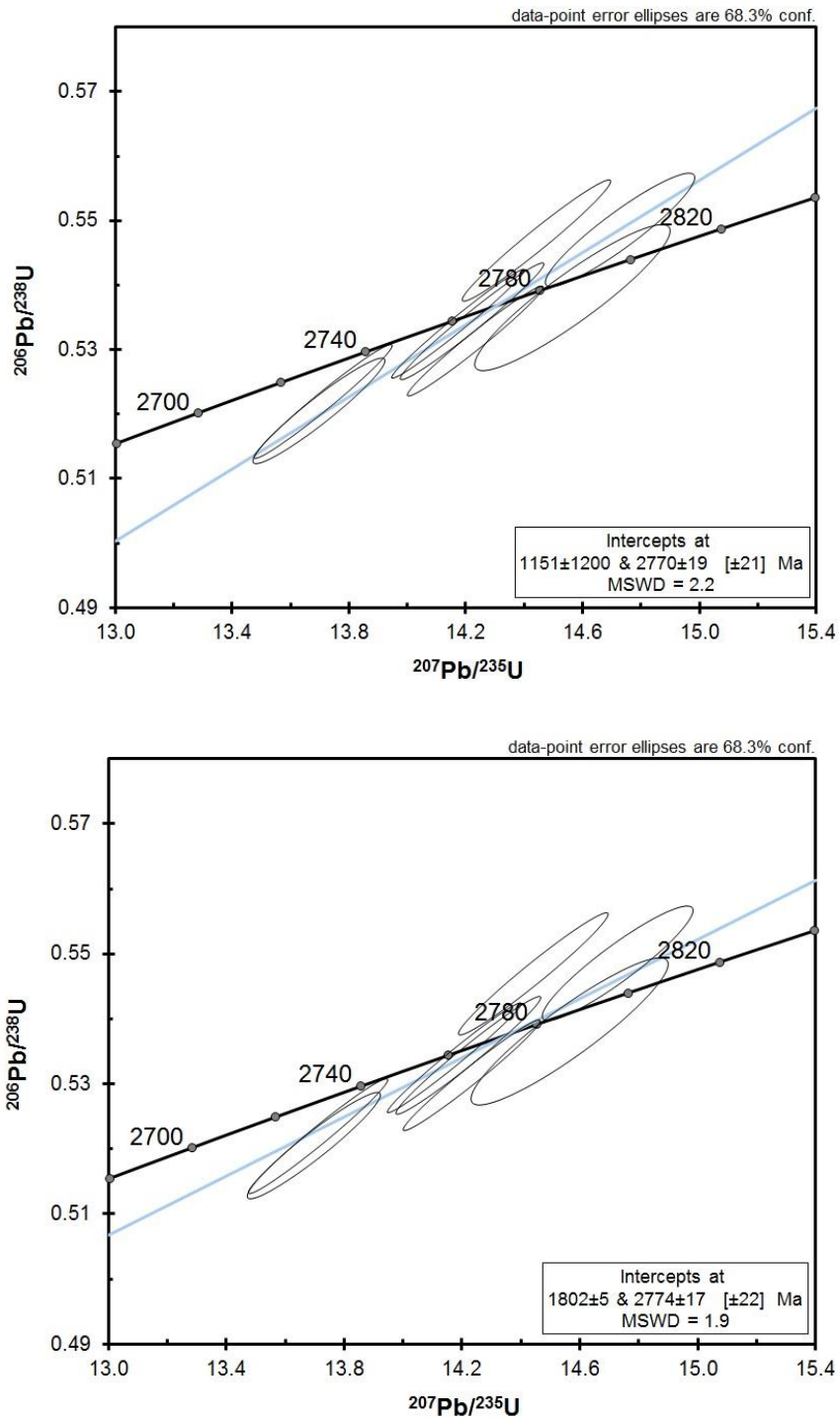


Figure 5.1 Top: Concordia plot for the 2770 Ma population in sample 10644 with unforced intercepts. Bottom: Concordia plot for the 2770 Ma population in sample 10644 with a lower intercept anchored at 1802 ± 5 where the youngest zircon growth event in this sample occurred. Forced and unforced intercepts are within error of each other. Data points which are greater than 5% discordant are excluded. Error ellipses are 1σ , ages are in Ma, black ellipses represent core analyses, red ellipses represent rim analyses.

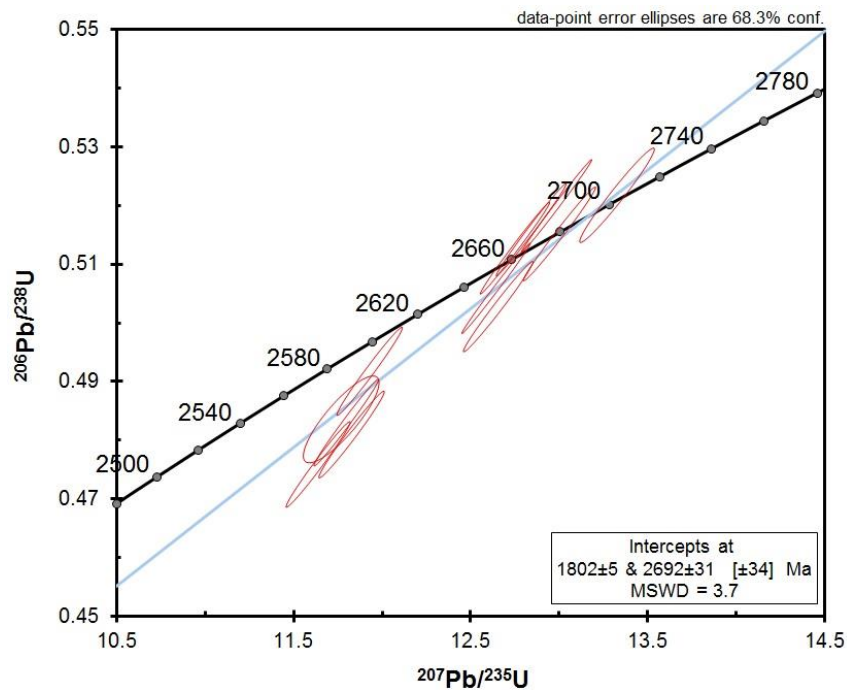
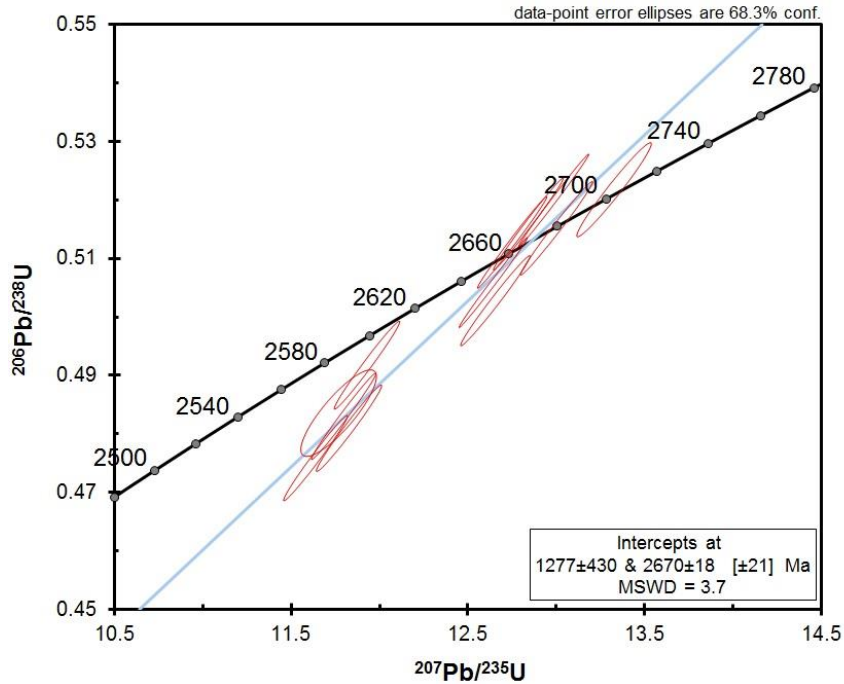


Figure 5.2 Top: Concordia plot for 2670 Ma population in sample 10644 with enforced intercepts. Bottom: Concordia plot for the 2670 Ma population in sample 10644 with a lower intercept anchored at 1802 ± 5 where the youngest zircon growth event in this sample occurred. This anchor is within the broad error of the enforced intercept. Data points which are greater than 5% discordant are excluded. Error ellipses are 1σ , ages are in Ma, black ellipses represent core analyses, red ellipses represent rim analyses.

occurred ca. 2690 Ma, the youngest possible minimum age for this population is measured to be 2670 ± 36 Ma; this youngest age is the one reported in this paper.

Zircon domains belonging to the ca. 1842 ± 14 Ma event occur either as individual grains with no structurally older core (eg. grain 15) or as rims on cores which are measured to be older (eg. grain 24; SE and CL images of specific grains can be found in Appendix D). This, along with their chemistry and colour-CL microstructures, suggest that this population was formed during a Proterozoic metamorphic event. A concordia plot (figure 5.3) with unforced intercepts places the event at 1842.6 ± 6.7 Ma (1σ error). A lower intercept of 447 ± 550 Ma does not give a very meaningful estimate for the timing of any relatively young disturbance as the error is so large.

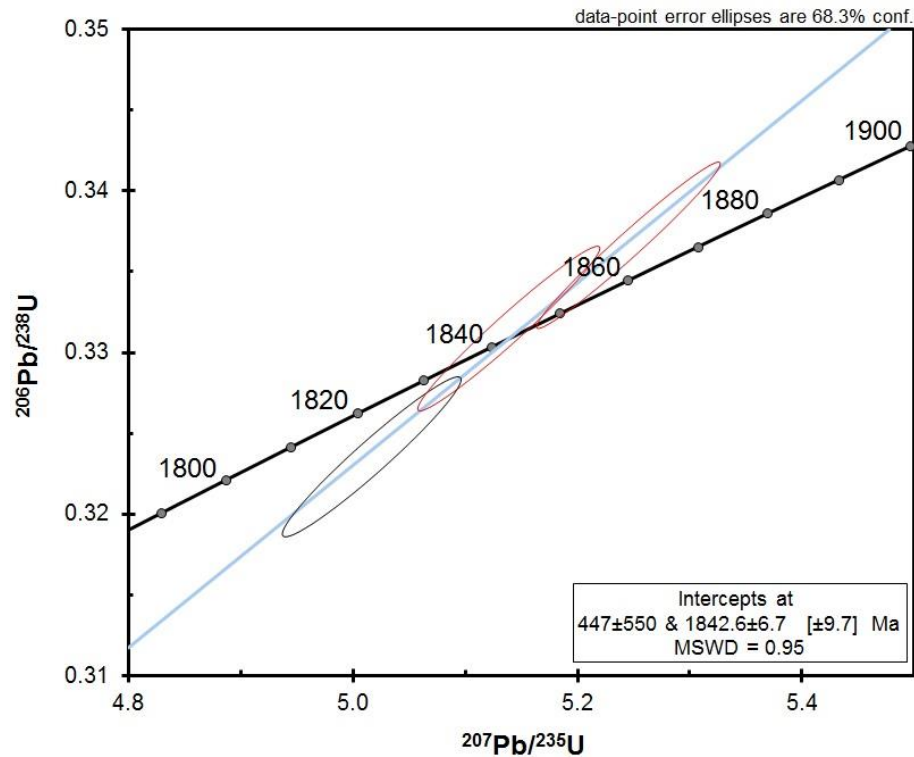


Figure 5.3 Concordia plot for 1842 Ma population in sample 10644 with unforced intercepts. Data points which are greater than 5% discordant are excluded. Error ellipses are 1σ , ages are in Ma, black ellipses represent core analyses, red ellipses represent rim analyses.

The younger, ca. 1802 ± 10 Ma event occurs with the same single grain and rim structures as the 1842 Ma event, but their differences in model age and U concentrations allows for two distinct Proterozoic zircon populations. This second event, the youngest in this sample, is also interpreted to be of metamorphic origin. As this is the youngest zircon growth event, it is used as an anchor for the lower intercepts of the Archean events, as it is a likely cause for disturbance. The concordia plot in figure 5.4 does not give a meaningful lower intercept, as the error is too large. All that can be determined is that disturbance occurred at some point between the closure of the system to Pb ca. 1802 Ma and the present day.

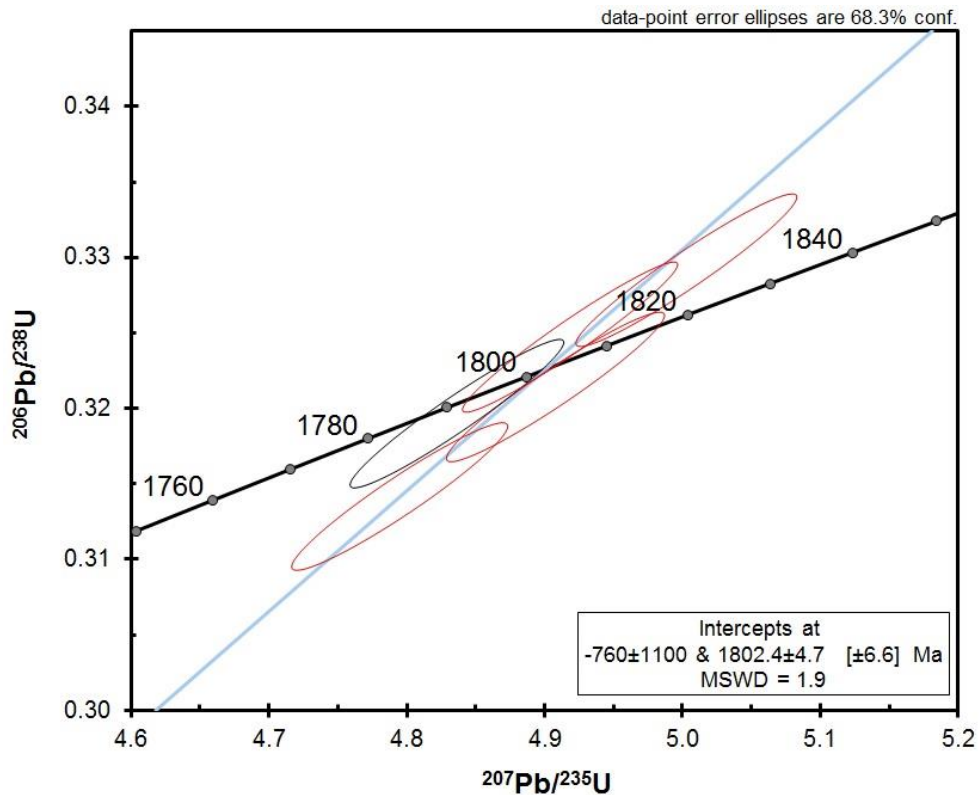


Figure 5.4 Concordia plot for 1802 Ma population in sample 10644 with unforced intercepts, representing the youngest zircon growth in this sample. Data points which are greater than 5% discordant are excluded. Error ellipses are 1σ , ages are in Ma, black ellipses represent core analyses, red ellipses represent rim analyses.

The zircon growth event ca. 2770 Ma marks the crystallization of an igneous melt. If the sample 10644 is representative of all granitoid bodies in the LIBZ, then this event indicates a major rock-forming episode, encompassing 50% of present-day surface

expression in the LIBZ map area. This percentage will be reduced if there is found to be more than one generation of granitoid in the LIBZ map area. Field mapping revealed only minor variability in bulk composition, so the simplest explanation is to assume that 10644 is representative of all LIBZ granitoids.

Following the formation of these igneous zircons is a period with no zircon growth. During this time, the granitoids most likely continued to cool in the crust, until the beginning of a ca. 2670 Ma metamorphic event, when metamorphic zircon rims grew on the existing igneous grains. Following this metamorphic event was a long period with no zircon growth. The Archean zircon grains are mostly well-preserved, showing clear core-rim relationships and often prismatic morphologies, and most grains are within a few percent of concordia. This allows that the protolith stayed fairly warm during this long period of inactivity, at or above zircon's self-annealing temperature of approximately 100-150°C, and was therefore seated in the crust well below the surface. Alternatively, the sample may have resided in the upper crust. Although most grains are metamict and therefore prone to alteration and loss of radiogenic Pb (age re-setting), it did not experience extensive Pb-loss due to an absence of fluids able to leach Pb from zircon.

Metamorphism began once more ca. 1842 Ma, when Proterozoic zircon domains grew as rims on existing Archean grains in addition to entirely new Proterozoic crystals. Where this growth occurs around Archean cores, many of them preserve their prismatic morphology (eg. grains 24, 25). A short period of inactivity followed, and then another small pulse of metamorphic zircon growth occurred at 1802 ± 10 Ma. This marks the youngest zircon growth event in this sample, again occurring around Archean cores (grain 1) and as individual grains (grain 5). The remaining mineral assemblage is biotite-hornblende-quartz-feldspar. At some point between this event and present day, uplift and/or erosion exposed the rock to the surface.

5.1.2 History of Sample 10645 (G067A1)

The minimum $^{207}\text{Pb}/^{206}\text{Pb}$ ages for sample 10645 are separable into two groups. The first group spans a wide range of time, from 2680 ± 10 Ma to 1891 ± 10 Ma. It is possible that these grains all belonged to a single older Archean and most probably igneous rock forming event, and they have subsequently been partially reset (through Pb-loss) to varying degrees. It is also possible that the cores in this sample are representative of both Archean events observable in sample 10644 ca. 2770 Ma and 2670 Ma. The cores of some grains in sample 10645 appear similar in texture and structure to the Archean grains seen in sample 10644. The amount of Pb loss and resetting makes it difficult to determine which case is the most likely. See figure 5.5 for concordia plots for these highly variable cores.

The second group of $^{207}\text{Pb}/^{206}\text{Pb}$ model ages in this sample is comprised of rims ranging from 1877 ± 18 Ma to 1764 ± 50 Ma surrounding cores which are measured to be older. In addition to highly discordant data, the three oldest data points in this sample (at approximately 1870 Ma) which appear to belong to a separate group must be excluded as their model ages are a result of mixed core and rim material in the SHRIMP analysis (see Appendix E for post-SHRIMP imaging). This results in a narrower age range for the group, spanning 1836 ± 8 Ma to 1805 ± 16 Ma, and model age for this population at 1823 ± 34 Ma (see figure 5.6). Due to their chemistry and microstructure, it is probable that these rims were formed during a Proterozoic metamorphic zircon growth event, nucleated on partially reset Archean cores.

Due to the lack of any primary structures, the protolith of this rock is difficult to determine. Due to its highly aluminous nature, as demonstrated by the presence of minerals such as cordierite, biotite, and feldspars, it is possible that this rock began as an aluminous sediment. However, it may also have been an Archean S-type granite.

The oldest model age observed in this sample is 2680 ± 10 Ma, belonging to the group of cores which spans a very broad range of time. One possibility is that these cores were gathered in a proximal, immature sediment, and were later lithified. Since the chemistry and microstructure of the cores is similar, they are probably eroded from a

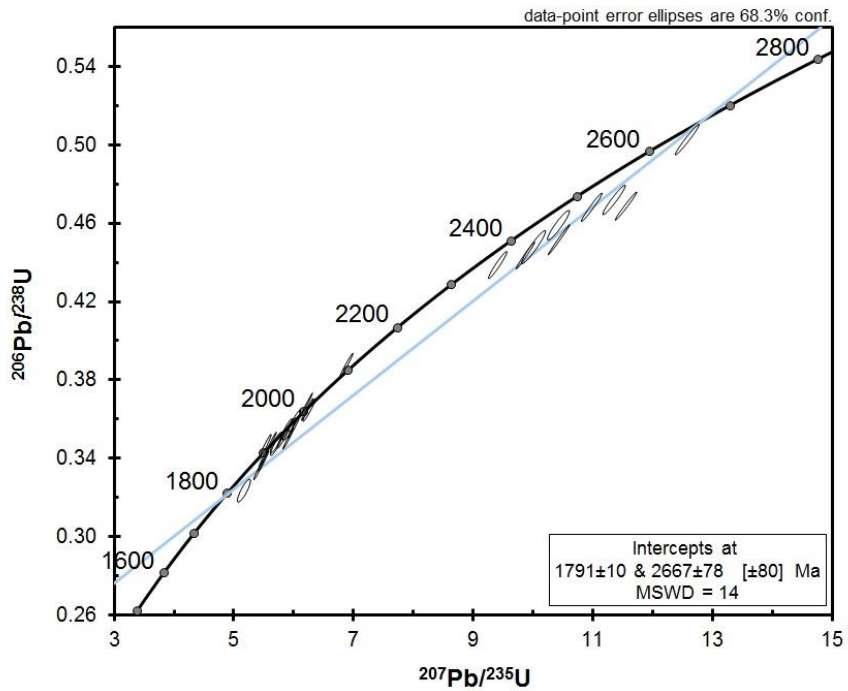
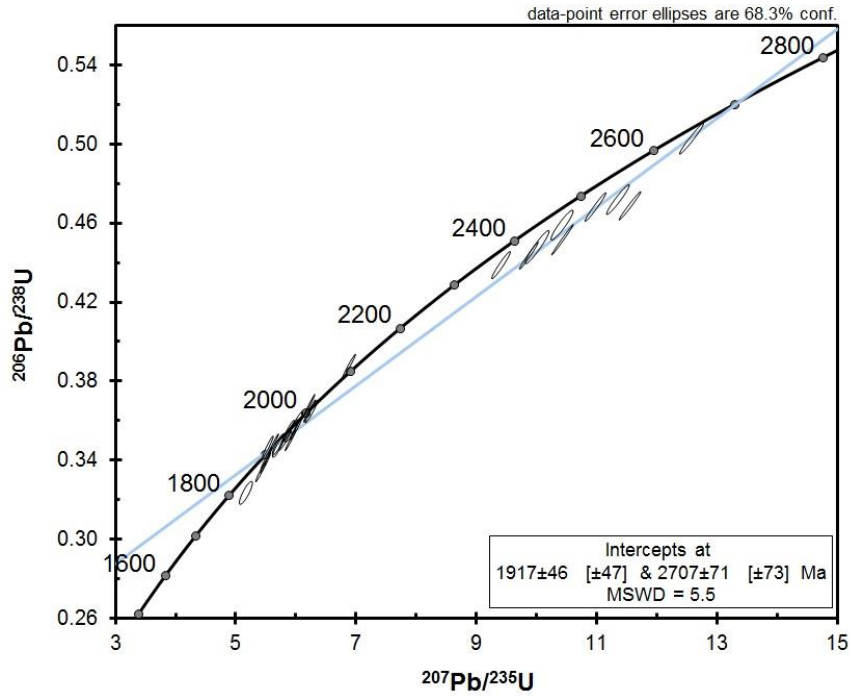


Figure 5.5 Top: Concordia plot for core analyses from sample 10645 with unforced intercepts showing the wide age variability of this group. Bottom: Concordia plot for core analyses from sample 10645 with a lower intercept forced at 1797 ± 12 Ma, the youngest model age of zircon growth in this sample. Data points which are greater than 5% discordant are excluded. Error ellipses are 1σ , ages are in Ma, black ellipses represent core analyses, red ellipses represent rim analyses.

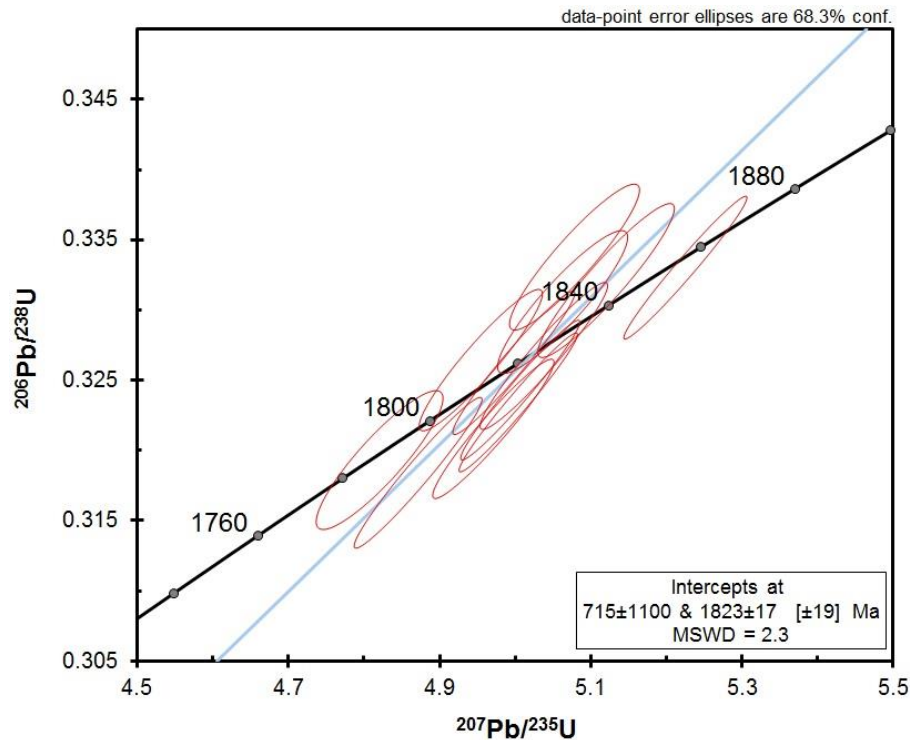


Figure 5.6 Concordia plot for rim analyses from sample 10645 with unforced intercepts. Data points which are greater than 5% discordant are excluded, along with the three mixed core-rim analyses. Error ellipses are 1σ , ages are in Ma, black ellipses represent core analyses, red ellipses represent rim analyses.

single source. Both sample suites 10644 and 10645 contain grains which have bright, planar to discontinuously zoned cores, surrounded by a dark, discontinuously zoned rims. If the microstructures observed in these cores is the same as those measured in sample 10644, it is possible that the protolith for 10644 may be the sediment source for this hypothetical immature sediment. The difference in model age could be explained by the obviously high degree of Pb loss and disturbance in this sample. If this is the case, then this implies that sample 10644 must have been at least partially exposed to the surface at some point after its crystallization in order to provide a sediment source for this rock.

Another possibility is that this rock formed as a result of partial melting of existing crust. Its aluminous composition and migmatitic texture suggest that it may have been an S-type granite. The orientation of migmatitic layering follows the regional

foliation trend, and could be syngenetic. In this case, the zircon grains would be inherited from the existing crust. If the heavily reset cores were inherited from sample 10644, then in this scenario it would not necessarily have had to been at the surface. This also means that the Proterozoic zircon grains may represent the age of formation of this rock.

5.1.3 History of Sample 10646 (G071A1)

The zircon population of sample 10646 cannot be separated into different groups, and is interpreted to represent a single zircon growth event. The $^{207}\text{Pb}/^{206}\text{Pb}$ model ages range from 1846 ± 6 Ma to 1800 ± 12 Ma, which gives a model age for the population as 1830 ± 6 Ma (see figure 5.7 for a concordia plot). It is important to note that all but one of the analyses for this sample are found on rims.

The only core domain from this sample (found in grain 42) that was analyzed gives an age much older than those of the rims, at 2022 ± 3 Ma (10% discordant). Many of the cores visible in colour-CL appear to be highly resorbed, and must represent some zircon growth and destruction/recrystallization events prior to the one measured in the rims of this sample. Texturally, the cores appear quite complex, and in some cases similar to grains with Archean model ages in sample 10644, as well as some of the highly disturbed cores of sample 10645. It is possible that further U-Pb analyses of some of the cores in this sample would result in data which resembles that of sample 10645, where the cores appear to represent one or more Archean zircon forming events. The cores may also be undisturbed, and appear more similar to those in sample 10644.

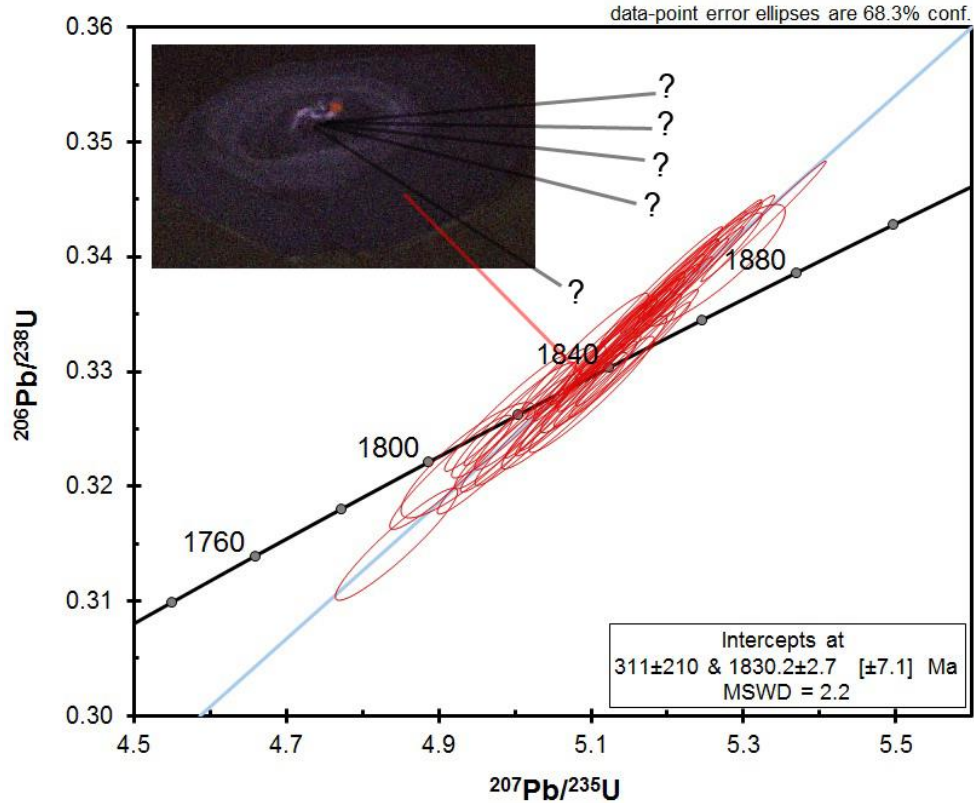


Figure 5.7 Concordia plot of Pb207/Pb206 model ages for sample 10646 with enforced intercepts. A grain with a measured rim and unknown core is overlain. At present, it is unclear how old the core might be, though it has most likely a member of an Archean population and has subsequently been partially reset. Data points which are greater than 5% discordant are excluded. Error ellipses are 1 σ , ages are in Ma, black ellipses represent core analyses, red ellipses represent rim analyses.

5.2 Chronology of the LIBZ

The oldest recorded activity in the LIBZ is the growth of igneous zircon ca. 2770 Ma. This event most likely terminated due to the cooling of the original magma body. If any Pb loss occurred after the cooling of the magma body, it was very minimal, as these grains are fairly concordant. It is possible that the magma body never really cooled prior to the 2670 metamorphic event. Approximately 100 million years later, ca. 2670 Ma, a metamorphic zircon growth event occurred, resulting in metamorphic rims around already existing igneous grains. This created the core-rim relationship which can be observed clearly in sample 10644. It may also be observable in samples 10645 and 10646, however this cannot be confirmed.

Sample 10645 contains Archean cores which have been reset to various degrees during Proterozoic metamorphism. Some of these cores appear to have similar core-rim structures to those observed in sample 10644, and may represent the same pair of Archean events, or may represent a different Archean event, evidence of which has been heavily disturbed. Available information does not appear to conclusively rule out either possibility. Sample 10646 also contains some cores with a similar appearance, however none of these have received U/Pb age analysis.

After the ca. 2670 Ma metamorphic zircon growth event, no new zircon growth occurred until the Proterozoic, and all samples appear to have experienced some degree of Pb loss. This means that the host lithologies must have been fairly cool, most likely situated above 10 km within the crust. Grains with analyzed cores from sample 10645 appear to have experienced highly variable degrees of Pb loss. This means that at some point between 2670 Ma and the Proterozoic, a fluid allowing for Pb solubility must have interacted with the host lithology.

Only one analysis was done on a core in sample 10646, revealing a likely highly reset age of 2022 ± 3 Ma, which is 10% discordant. It is probable that further analyses of this sample would show the same interaction with a fluid capable of transporting Pb. Many cores in sample 10646 are highly resorbed, which is unique to this sample. This suggests that a fluid allowing for Zr solubility interacted with the host lithology for sample 10646, but not with the host lithologies of the other two samples. The seemingly minimal amount of Pb loss, and lack of obvious resorbed cores in sample 10644 suggest that its host lithology had very limited interaction with fluids capable of transporting Pb or Zr in solution.

All three samples exhibit Paleoproterozoic metamorphic zircon growth events, which occur at slightly different times within each sample: at 1842 ± 7 Ma (sample 10644), 1830 ± 3 Ma (sample 10646), and 1822 ± 5 Ma (10645). Also present within sample 10644 is a younger, physically and chemically distinct event, at 1802 ± 5 Ma (sample 10644), which represents the youngest distinct zircon growth event in the LIBZ.

5.3 Relating the LIBZ to the Churchill Province

5.3.1 Archean Activity

The LIBZ belongs to the Rae sub-province of the Churchill Province, which contains a rich Archean tectonothermal history overprinted by Paleoproterozoic metamorphism. This complex history makes it difficult to accurately determine the events which led to the formation of the Archean crust found in the LIBZ, however broad similarities to Archean geology in the Churchill Province are apparent.

The oldest unit observed in the LIBZ is the 2770 ± 38 Ma granitoid from sample 10644. Around this time, there are several events which may be related. Martel et al., 2008 (and references therein) report a 2850 Ma thermal metamorphic event in the southern Rae sub-province, as well as igneous intrusions ca. 2735 Ma in the Snowbird Lake region, and 2728 Ma subvolcanic intrusions in the Prince Albert Group in the northern Rae. In the southern-central Rae, Zaleski et al. (2000) report detrital zircon in the Meadowbank River area ca. 2810 Ma. Bethune & Scammel, (2003) discuss an approximately 3000-2770 Ma orthogneiss complex in the Ege Bay region of Baffin Island, intruded by 2760-2725 Ma intermediate to felsic volcanics. They also report locally preserved 2740-2720 Ma supracrustal rocks of the Mary River Group on Baffin Island and the Prince Albert Group on the Melville Peninsula. Due to the character, timing, and proximity of the orthogneisses discussed in Bethune & Scammel (2003), these orthogneisses are most likely related to the ca. 2770 Ma granitoid unit in the LIBZ.

The second oldest Archean event recorded in the LIBZ occurs as ca. 2670 ± 36 Ma metamorphism expressed as zircon rims, observable in sample 10644. Martel et al. (2008) reports post-tectonic magmatic zircon growth in the Snowbird Lake region at 2668 Ma and 2661 Ma, attributed to the occurrence of a major deformation event throughout the Rae sub-province, and noting that this is a time of major global crustal formation. East of the Snowbird Lake region, near the northwest margin of the Hearne Province (Yathkyed, MacQuoid, Angikuni localities) is evidence for 2660-2610 Ma intrusions, regional crustal shortening, and greenschist to lower amphibolite metamorphism (MacLachlan et al., 2005; Davis et al., 2006). It is suggested that this

activity is related to the ca. 2650 Ma accretion of the Chesterfield Domain to the Rae sub-province (Martel et al., 2008), and such a significant event could easily cause enough disturbance along strike to generate new metamorphic zircon in the LIBZ.

5.3.2 Proterozoic Activity

Following the 2670 Ma metamorphism, the LIBZ experienced a prolonged period of inactivity where no new zircon populations were formed. This period of quiescence remained until the onset of the Trans Hudson Orogen and subsequent closing of the Manikewan Ocean began in the Paleoproterozoic as the Churchill and Superior Provinces collided (Corrigan et al., 2009). Various stages of these collisions are recorded in the LIBZ, producing several distinct metamorphic zircon growth events.

The first period of Proterozoic zircon growth in the LIBZ transpired at 1842 ± 14 Ma, as seen in sample 10644. Around this time, several regionally significant events were occurring. The period from 1865 Ma to 1850 Ma, (“Wathaman Orogeny” in Corrigan et al., 2009) is characterized by the emplacement of voluminous felsic plutons into an Andean-type continental margin setting.

From 1865-1850 Ma, Cumberland Batholith was in its waning stages of continental arc magmatism, producing high volumes of magma in the Meta Incognita micro-continent and the south-eastern margin of the Rae sub-province on central Baffin Island (Corrigan et al., 2009). Within the Sugluk block on Ungava Peninsula, the gneissic suite of the Narsajuaq arc contains similar rocks to those of the Cumberland Batholith, though slightly more intermediate in composition. These range in age from 1863 Ma to 1844 Ma, interpreted as the magmatic product of subduction beneath a tectonically attenuated continental margin containing an Archean crustal component. The subduction related magmatism likely stopped when the Parent-Spartan-Watts collage collided with the Sugluk Block ca. 1840 Ma, and reactivated the Bergeron Suture (Corrigan et. al., 2009).

The ca. 1842 Ma LIBZ population (as well as the 1830 ± 6 and 1823 ± 34 populations) may also be related to the 1840 Ma to 1820 Ma stage of “final magmatic

accretion” described in Corrigan et al. (2009). This period involved upper-plate continental arc-derived plutons in the Sugluk and Meta Incognita micro-continents, which terminated with the final closure of the Manikewan Ocean and amalgamation of the Superior craton.

The 1830 ± 6 , 1823 ± 34 , and 1802 ± 10 populations in the LIBZ may also have been related to the 1830 Ma to 1800 Ma “Terminal Collision” phase of the Trans Hudson, as the Superior craton consumed the Manikewan Ocean and docked with the Churchill Province (Corrigan et al., 2009). This terminal collision phase began in the Thompson Nickel Belt ca. 1830 Ma, getting progressively younger towards the northeast. It is recorded in the Cape Smith Belt ca. 1820 Ma, and the Core Zone ca. 1810 Ma. During this collisional phase, much of the Rae sub-province was reactivated, resulting in widespread peak to post-peak U-Pb titanite and monazite ages ranging from 1830 Ma to 1760 Ma (Corrigan et al., 2009; Gagne et al., 2009). This period marks the final period of metamorphic activity in the LIBZ, and is the current best estimate of the time of ductile strain. This possibly led to the crustal-scale disruption of the geophysical characteristics of the Rae lithosphere, as seen in the magnetotelluric transect.

5.4 Age Bracket on Ductile Strain in the LIBZ

Ductile deformation is difficult to date directly. However, by considering the igneous and metamorphic zircon chronology described above in the context of similar studies from surface samples and lower crustal xenoliths, some first order age constraints can be placed on the timing of displacement on the LIBZ. The deformation fabrics of the LIBZ and of the samples that were dated are defined by minerals of the upper amphibolite facies, conditions under which metamorphic zircon growth is widely observed (e.g. Bowman et al., 2011). The youngest metamorphic zircon therefore approximates the time when the fabrics and metamorphic minerals were last formed. In the case of the LIBZ, one of the three samples records an event at 1802 ± 10 Ma (sample 10644), and contains a veinlet of cross-cutting coarse-grained granite. If the vein is the same age as anatectic melting observed in the outcrop, this suggests that no appreciable strain occurred younger than 1802 ± 10 Ma. Hence 1802 ± 10 Ma can be taken as a minimum age for strain in the LIBZ at surface.

Regional geophysics profiling allows that the LIBZ is a crustal-scale boundary between two major blocks (see figure 5.8). The northwest side is considered to belong to the southern margin of the Rae craton, while the nature of the southeast side is more uncertain, although the most likely case is that it belongs to the Repulse Bay Block.

The history of the lower crust in the region also helps bracket LIBZ evolution. Two periods of Proterozoic metamorphic zircon growth are recognized in granulite-facies kimberlite xenoliths from the Repulse Bay block (Petts, 2012). Xenoliths from Repulse Bay and from the Rankin Inlet area 600 km to the south all exhibit 1750 to 1700 Ma growth. This late pan-Churchill lower crustal event is ascribed to Nueltin extension and magmatic underplating, and serves as a another lower (minimum) age bracket on LIBZ activity at a crustal-scale.

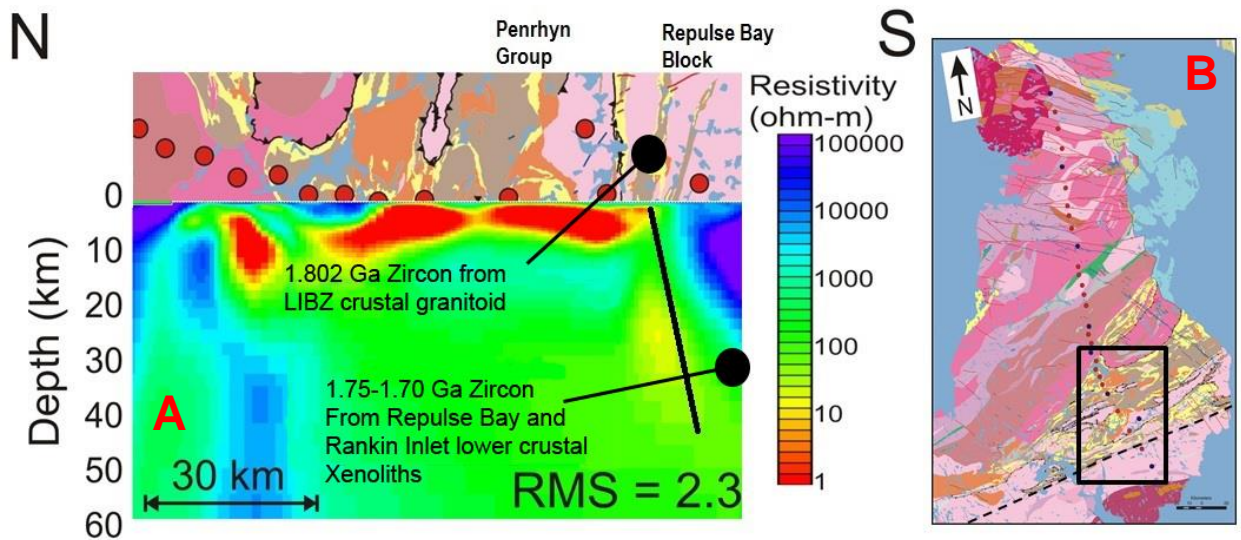


Figure 5.8 Magnetotelluric geophysical data (A) and accompanying index map (B) of the Melville Peninsula showing the location and depth of the crustal break which defines the LIBZ (modified from Corrigan, 2011, personal communication). The youngest zircon ages bracket ductile deformation in the LIBZ, and their relative locations in the crust are labeled.

5.5 Suggestions for Future Work

Future work in the LIBZ region could further the understanding of its evolution and relevance to the tectonothermal history of the western Churchill Province. More detailed mapping and sampling would be useful to further define and characterize the units. Further investigation of zircon *in-situ* in the K-feldspar rich veinlet in sample 10644 would be useful in order to test the hypothesis that it is the physical expression of the youngest activity in the LIBZ. This could be achieved by sampling these veinlets, carefully separating them from their host granitoid, and analyzing any U-Pb bearing minerals they contain. A second set of SHRIMP analyses for sample 10646 focusing on obtaining core ages and core-rim relationships would be useful to more closely investigate its Archean evolution. *In-situ* zircon and monazite dating could be used to help tighten the brackets on the timing of deformation and growth of individual mineral phases relative to metamorphic mineral growth. The Proterozoic history could benefit from U-Pb titanite dating of calc-silicates and ^{40}Ar - ^{39}Ar thermochronology to complement existing and new U-Pb data in order to develop a P-T path for the youngest cooling event. The Archean evolution of each sample could be enhanced by studying the oxygen isotopes of zircon grains to determine whether or not the protolith magma was equilibrated with mantle-derived or crustal-derived melts or fluids at the time of zircon crystallization.

6 Conclusions

6.1 Conclusions

A recently discovered crustal-scale boundary on the southern coast of the Melville Peninsula (Nunavut, Canada) was examined using mapping and U-Pb geochronology of zircon. The Lyon Inlet Boundary Zone is located in the Churchill Province, at the southern margin of the Rae sub-province, and likely represents the crustal expression of the amalgamation of the Repulse Bay Block to the southern Rae. Three representative samples from the LIBZ were analyzed in detail. The structural, petrographic, and geochemical data obtained from these samples led to the following major conclusions:

1. The average metamorphic grade of the study area is upper amphibolite facies, based on the dominant mineral assemblage of quartzo-feldspathic aluminous gneisses and migmatites, containing varying amounts of hornblende and biotite. Leucosomes often contain pockets of cordierite and garnet. Granitoid rocks are usually biotite and/or hornblende bearing. Although the northern portion of the map area contains a notable quantity of carbonate rocks (calc-silicate gneisses and marbles with varying amounts of calcite, diopside, graphite), these rocks received less scrutiny as they are less likely to contain high temperature dateable phases such as zircon and monazite. Aluminous gneisses and granitoids typically contained a variety of accessory phases including zircon, monazite, titanite, and apatite.
2. U-Pb geochronology revealed a complex Archean history in the LIBZ, which can be used to help constrain the Archean history of the Churchill Province, and broadly fit within known Churchill events:
 - a. A ca. 2770 Ma igneous zircon growth event (sample 10644) marking a major igneous episode, with little to no evidence for partial resetting or Pb-loss from this sample
 - b. A ca. 2670 Ma metamorphic zircon growth event (sample 10644), forming rims around pre-existing grains, which did not cause significant Pb-loss.

- c. Mixed Archean population(s) which are highly variable in model age (sample 10645, possibly sample 10646), due to either interaction with a fluid capable of leaching and transporting Pb, an origin as a detrital population, or both. Given the present day proximity of the samples, a Pb-leaching fluid would have been highly localized.
3. U-Pb geochronology also revealed an active Paleoproterozoic history, inferred to be a consequence of the poly-phasic Trans-Hudsonian Orogeny. Metamorphic zircon growth in the LIBZ is measured at ca. 1842 ± 14 (sample 10644), 1830 ± 6 Ma (sample 10646), 1823 ± 34 Ma (sample 10645) and 1802 ± 10 Ma (sample 10644).
4. The youngest zircon growth in the LIBZ is considered to be the result of a late cross-cutting K-feldspar bearing vein system, as seen in sample 10644. The 1802 ± 10 Ma population is thought to come from these veins, and represent the minimum age for ductile strain at the surface in the LIBZ, linking it to the terminal stages of Trans-Hudsonian mountain-building in arctic Canada. This is confirmed by zircon from lower crustal xenoliths, which confirm the cessation of collision and beginnings of extension and underplating by 1750-1700 Ma (Petts, 2012).

References

- Aspler, L.B., Cousins, B.L., and Chiarenzelli, J.R., 2002.* Griffin gabbro sills (2.11 Ga), Hurwitz Basin, Nunavut, Canada: long-distance lateral transport of magmas in western Churchill Province crust. *Precambrian Research*, v. 117, p. 269–294.
- Bethune, K.M., Scammell, R.J., 2003.* Distinguishing between Archean and Paleoproterozoic tectonism, and evolution of the Isortoq fault zone, Ege Bay area, north-central Baffin Island, Canada. *Canadian Journal of Earth Science*, v. 40, p. 1111-1135.
- Bowman, J.R., Moser, D.E., Valley, J.W., Wooden, J.L., Kita, N.T., Mazdar, F.K., 2011.* Zircon U-Pb Isotope, $\delta^{18}\text{O}$ and Trace Element Response to 80 M.y. of High Temperature Metamorphism in the Lower Crust: Sluggish Diffusion and new Records of Archean Craton Formation. *American Journal of Science*, v. 311, p.719-772.
- Cherniak, D.J., Watson, E.B., 2000.* Pb diffusion in zircon. *Chemical Geology*, v. 172, p. 5-24.
- Corrigan, D., Hajnal, Z., Németh, B., Lucas, S.B., 2005.* Tectonic framework of a Paleoproterozoic arc–continent to continent–continent collisional zone, Trans-Hudson Orogen, from geological and seismic reflection studies. *Canadian Journal of Earth Sciences*, v. 42., p 421-434.
- Corrigan, D., Pehrsson, S., Wodicka, N., 2009.* The Paleoproterozoic Trans-Hudsonian Orogen: a prototype of modern accretionary processes. *Geological Society of London, Special Publications*, v. 327, p.457-479.
- Davis, W.J., Hanmer, S., Tella, S., Sandeman, H.A., and Ryan, J.J., 2006.* U-Pb geochronology of the MacQuoid supracrustal belt and Cross Bay plutonic complex: Key components of the northwestern Hearne subdomain, western Churchill Province, Nunavut, Canada. *Precambrian Research*, v. 145, p. 53–80.
- Dredge, L.A., 2002.* Quaternary geology of southern Melville Peninsula, Nunavut. *Geological Survey of Canada, Bulletin 561*
- Flowers, R., Bowring, S.A., and Williams, M.L., 2006.* Timescales and significance of high-pressure, high-temperature metamorphism and mafic dike anatexis, Snowbird tectonic zone, Canada. *Contributions to Mineralogy and Petrology*, v. 151, p. 558–581.
- Gagne, S., Jamieson, R.A., MacKay, R., Wodicka, N., Corrigan, D., 2009.* Texture, Composition, and age variations in monazite from the lower amphibolite to the granulite facies, Longstaff Bluff Formation, Baffin Island, Canada. *The Canadian Mineralogist*, v. 47, p. 847-869.

Hanmer, S., Williams, M., Kopf, C., 1995. Striding-Athabasca mylonite zone: implications for the Archean and Early Proterozoic tectonics of the western Canadian Shield. Canadian Journal of Earth Science, v. 32, p. 178-196.

Harley, S.L., Kelly, N.M., 2007. Zircon, Tiny but Timely. Elements, v.3, p. 13-18.

*Henderson, J.R., 1983. Structure and metamorphism of the Aphebian basement complex in the Lyon Inlet area, Melville Peninsula. Geological Survey of Canada, Bulletin 324, 50 p. with map 1510A, scale 1:100 000. In: *Dredge, L.A., 2002. Quaternary geology of southern Melville Peninsula, Nunavut. Geological Survey of Canada, Bulletin 561.**

*Henderson, J.R., 1988. Geology, southeastern Melville Peninsula. Geological Survey of Canada, map 1655A, scale 1:100 000, 2 sheets. In: *Dredge, L.A., 2002. Quaternary geology of southern Melville Peninsula, Nunavut. Geological Survey of Canada, Bulletin 561.**

Klein, C., Hurlbut, C.S., 2001. The Manual of Mineral Science. Wiley, New York, USA.

MacLachlan, K., Davis, W.J., Relf, C., 2005. U/Pb geochronological constraints on Neoproterozoic tectonism: multiple compressional events in the northwestern Hearne Domain, Western Churchill Province, Canada. Canadian Journal of Earth Science, v. 42, p. 85-109.

Martel, E., van Breemen, O., Berman, R.G., Pehrsson, S., 2008, Geochronology and tectonometamorphic history of the Snowbird Lake area, Northwest Territories, Canada: New insights into the architecture and significance of the Snowbird tectonic zone. Precambrian Research, v. 161, p. 201-230.

*Maurice, Y.T., 1979. A preliminary assessment of the uranium potential of southern Melville Peninsula, District of Franklin. In: *Dredge, L.A., 2002. Quaternary geology of southern Melville Peninsula, Nunavut. Geological Survey of Canada, Bulletin 561.**

*Okulitch, A.V., Gordon, T.M., Henderson, J.R., Hutcheon, I.E., Turay, M., 1978a. Geology of the Barrow River map-area, Melville Peninsula, District of Franklin. In: *Dredge, L.A., 2002. Quaternary geology of southern Melville Peninsula, Nunavut. Geological Survey of Canada, Bulletin 561.**

*Okulitch, A.V., Gordon, T.M., Henderson, J.R., Reesor, J.E., Hutcheon, I.E., 1978b. Geology of the Barrow River and Hall Lake map-areas, Melville Peninsula, District of Franklin. In: *Dredge, L.A., 2002. Quaternary geology of southern Melville Peninsula, Nunavut. Geological Survey of Canada, Bulletin 561.**

Peterson, T.D., 2006. Geology of the Dubawnt Lake area, Nunavut-Northwest Territories. Geological Survey of Canada, Bulletin 580, 56p.

Petts, D.C., 2012. Deep Crustal Evolution of the Western Churchill Province, Nunavut, Canada: Isotopic (U-Pb, O), Trace Element and Micro-Structural Analysis of Zircon from Lower Crustal Xenoliths. (Doctoral Dissertation). 201p.

Rainbird, R.H., Davis, W.J., Stern, R.A., Peterson, T.D., Smith, S.R., Parrish, R.R., Hadlari, T., 2006. Ar-Ar and U-Pb Geochronology of a Late Paleoproterozoic Rift Basin: Support for a Genetic Link with Hudsonian Orogenesis, Western Churchill Province, Nunavut, Canada. *Journal of Geology*, v. 114, p. 1-17.

Reesor, J.E., LeCheminant, A.N., Henderson, J.N., 1975. Geology of the Penrhyn Group metamorphic complex, Melville Peninsula. In: *Dredge, L.A.*, 2002. Quaternary geology of southern Melville Peninsula, Nunavut. Geological Survey of Canada, Bulletin 561.

Sandeman, H.A., Brown, J., Studnicki-Gizbert, C., MacHattie, T., Hyde, D., Johnstone, S., Greiner, E., Plaza, D., 2001a, Bedrock mapping in the Committee Bay Belt, Laughland Lake area, central mainland, Nunavut. Geological Survey of Canada, Current Research, 2001-C12.

Sandeman, H.A., Studnicki-Gizbert, C., Brown, J., Johnstone, S., 2001b, Regional structural and metamorphic geology of the Committee Bay Belt, Laughland Lake area, central mainland, Nunavut. Geological Survey of Canada, Current Research, 2001-C13.

Sawyer, E.W., 2008. Atlas of Migmatites. The Canadian Mineralogist, Special Publication 9. Issued by: National Research Council Canada, Co-published by Mineral Association of Canada.

Wenk, H., Bulakh, A., 2004. Minerals: Their Constitution and Origin. Cambridge UP, New York, USA.

Winter, J.D., 2001. An introduction to igneous and metamorphic petrology. Prentice-Hall Inc, New Jersey, USA.

Zaleski, E., Pehrsson, S., Duke, N., Davis, W.J., L'Heureux, R., Greiner, E., Kerswill, J.A., 2000. Quartzite sequences and their relationships, Woodburn Lake group, western Churchill Province, Nunavut. Geological Survey of Canada Current Research 2000-C7, 10p.

Appendices

Appendix A - Thin Section Descriptions

Sample: G55-A1

Notes: Strong foliation defined by alignment of biotite and mineral segregation, heterogeneous zones of alteration with small zones of very fine grained k-spar and quartz along boundaries of larger grains.

Mineral Name	Modal %	Grain Shape	Grain Size (mm)	Notes
Quartz	40	Subhedral	<0.1-2	
K-Feldspar	50	Subhedral	<0.1-2.5	Heterogeneous alteration to ??
Biotite	7	Subhedral laths	<0.1-2	Pronounced pleochroism light yellow-brown to dark brick red
Amphibole	2	Anhedral	<0.1-1	Check: could be Bt @ different axis
Chlorite	1	Anhedral laths	<0.1-1	Occasionally intergrown with biotite
Opagues	<1	Anhedral	<0.1-1	
Accessories	<1			Zircon,

Sample: G51-A2

Notes: No foliation evident, heterogeneous alteration of plagioclase

Mineral Name	Modal %	Grain Shape	Grain Size (mm)	Notes
Quartz	20	anhedral	<1-2	
Plagioclase	25	anhedral	<1-2	Albite twinned
Biotite	5	Anhedral laths	<1-1.5	Pleochroic light-yellow-brown to dark red-brown
Hornblende	50	anhedral	<1-2	Pleochroic light yellow-brown to green, often highly fractured along cleavage planes
Opagues	<1	Anhedral	<1	
Accessories				

Sample: G53-A1

Notes: Strong foliation defined by alignment of biotite and mineral segregation. Thin band of (carbonate? Chlorite? Minor muscovite?) alteration approximately perpendicular to foliation – alteration extends outwards only a few grains from the source.

Mineral Name	Modal %	Grain Shape	Grain Size (mm)	Notes
Quartz	35	Anhedral	<1-1.5	
K-feldspar	25	Anhedral	<1-1	
Biotite	25	Subhedral laths	<1-1.5	
Hornblende	13	Anhedral	<1-1.5	
Opagues	2	anhedral	<1-1	Typically occur with Bt and/or Hbl
Accessories	<1			Zrc,

Sample: G56-A1 (small thin section)

Notes:

Mineral Name	Modal %	Grain Shape	Grain Size (mm)	Notes
Diopside	50	Anhedral	1-3	
Quartz?	30	anhedral	1-4	
Orthoamphibole?	20	anhedral	1-3	Often highly fractured
Accessories	<1			

Sample: G60-A1 (small thin section)

Notes: Weakly foliated, many grains quite fractured with recrystallization along fracture planes, especially feldspars

Mineral Name	Modal %	Grain Shape	Grain Size (mm)	Notes
Quartz	30	Anhedral	1-4	
K-feldspar	5	Anhedral	1-3	
Plagioclase	45	Anhedral	1-4	Occasionally myrmekitic, micropertitic
Biotite	5	Anhedral	<1-2	Pleochroic yellow-brown to blue-green
Hornblende	15	anhedral	<1-5	Pleochroic blue-green to green-brown
Opagues	<1	Anhedral	<1	
Accessories	<1			Zrc, Ttn

Sample: G60-A1 (large thin section)

Notes: Moderately foliated (thin bands of aligned bt and hbl)

Mineral Name	Modal %	Grain Shape	Grain Size (mm)	Notes
Quartz	40	anhedral	<1-4	
K-feldspar	5	anhedral	<1-2	
Plagioclase	35	anhedral	<1-4	Rare myrmekitic grains
Biotite	5	Anhedral	<1-2	Pleochroic yellow-brown to dark brown
Hornblende	15	Anhedral	<1-3	Pleochroic blue-green to green-brown
Opagues	<1	anhedral	<1	
Accessories	<1			Zrc, Ttn

Sample: G67-A1

Notes: Strongly foliated defined by Bt-alignment. Some areas appear more highly strained than others, with much finer grained bands.

Mineral Name	Modal %	Grain Shape	Grain Size (mm)	Notes
Quartz	40	anhedral	<1-2	
K-feldspar	5	anhedral	<1	
Plagioclase	20	anhedral	<1-3	
Biotite	30	anhedral	<1 - 2	Many contain inclusions w/ dark halos
Cordierite	5	anhedral	<1-2	Occasional inclusions w/ dark halos
Opagues	<1	anhedral	<1	
Accessories	<1			Zrc, Ttn

Sample: G71-A1

Notes: Weakly foliated (bt-alignment), some areas highly fractured.

Mineral Name	Modal %	Grain Shape	Grain Size (mm)	Notes
Quartz	45	anhedral	<1-4	
K-feldspar	5	anhedral	<1-2	
Plagioclase	20	anhedral	<1-3	Occasionally myrmekitic
Biotite	20	Anhedral to subhedral	<1-2	
Cordierite	5	anhedral	<1-2	
Opagues	5	anhedral	<1-1	
Accessories	<1			Zrc

Appendix B - SHRIMP U-Pb Data for Zircon

----- 204 corrected -----

Errors are 1σ unless otherwise s

Spot Name	ppm U	ppm Th	Th/U Ratio	4corr		4corr		4corr		204corr		207corr		208corr		204corr		204corr		204corr		Dis-corr-dant	
				% 206*	% 207*	% 207*	% 206*	err	err	err	err	err	err	err	err	err	err	err	err	err	err		err
10644-5.2	464	555	1.19	3.13	1.0	0.1097	0.30	4.84	1.1	0.320	1.0	0.96	1788	16	1787	18	1784	7	1810	22	1795	5	+0
10644-5.3	606	487	0.80	3.08	1.0	0.1099	0.27	4.92	1.0	0.325	1.0	0.97	1813	16	1815	18	1809	6	1842	23	1797	5	-1
10644-5.1	852	656	0.77	3.04	1.0	0.1102	0.30	5.00	1.1	0.329	1.0	0.96	1834	16	1839	19	1826	6	1915	25	1803	5	-2
10644-1.1	428	249	0.58	3.18	1.0	0.1107	0.33	4.79	1.1	0.314	1.0	0.95	1761	16	1755	18	1755	6	1833	31	1811	6	+3
10644-1.2	392	246	0.63	3.11	1.0	0.1107	0.31	4.91	1.1	0.321	1.0	0.96	1797	16	1795	18	1790	6	1869	27	1812	6	+1
10644-25.1	1955	181	0.09	3.02	1.0	0.1124	0.23	5.14	1.0	0.331	1.0	0.97	1846	16	1847	19	1845	5	1859	48	1839	4	-0
10644-15.1	2161	287	0.13	3.09	1.0	0.1125	0.28	5.02	1.0	0.324	1.0	0.96	1807	16	1802	18	1806	5	1882	43	1840	5	+2
10644-24.1	1510	157	0.10	2.97	1.0	0.1130	0.20	5.25	1.0	0.337	1.0	0.98	1870	16	1874	19	1870	6	1897	41	1848	4	-1
10644-27.1	1328	86	0.06	2.03	1.0	0.1759	0.17	11.93	1.0	0.492	1.0	0.99	2578	21	2562	30	2579	11	2503	57	2615	3	+2
10644-16.1	1035	117	0.11	2.07	1.0	0.1765	0.64	11.77	1.2	0.484	1.0	0.84	2543	21	2510	30	2548	10	2171	50	2620	11	+4
10644-24.2	769	155	0.20	2.07	1.0	0.1771	0.15	11.80	1.0	0.483	1.0	0.99	2540	21	2504	29	2536	10	2719	41	2626	2	+4
10644-4.1	1043	105	0.10	2.10	1.0	0.1774	0.17	11.64	1.0	0.476	1.0	0.99	2509	21	2461	28	2512	10	2304	54	2629	3	+5
10644-3.1	895	138	0.15	2.08	1.0	0.1783	0.18	11.83	1.0	0.481	1.0	0.98	2531	21	2488	29	2544	10	1825	44	2638	3	+5
10644-12.1	249	121	0.49	2.15	1.0	0.1792	0.31	11.51	1.1	0.466	1.0	0.96	2464	21	2395	28	2458	11	2572	62	2646	5	+8
10644-10.2	1216	58	0.05	1.95	1.0	0.1803	0.12	12.75	1.0	0.513	1.0	0.99	2688	22	2675	33	2688	11	2752	59	2656	2	-1
10644-10.1	1198	70	0.06	1.94	1.0	0.1805	0.12	12.84	1.0	0.516	1.0	0.99	2682	22	2694	34	2681	11	2761	59	2658	2	-1
10644-32.3	1319	108	0.08	1.92	1.0	0.1811	0.09	12.98	1.0	0.520	1.0	1.00	2699	22	2718	35	2698	12	2775	42	2663	2	-2
10644-28.4	1178	134	0.11	1.98	1.0	0.1813	0.10	12.64	1.0	0.506	1.0	1.00	2639	22	2627	32	2638	11	2724	38	2664	2	+1
10644-25.2	209	25	0.12	2.10	1.1	0.1815	0.41	11.92	1.1	0.476	1.1	0.93	2512	22	2449	29	2508	10	2795	130	2666	7	+7
10644-12.2	938	71	0.08	1.99	1.0	0.1826	0.16	12.65	1.0	0.503	1.0	0.99	2626	22	2602	31	2625	11	2652	70	2676	3	+2
10644-12.4	1057	58	0.05	1.94	1.0	0.1830	0.15	13.00	1.0	0.515	1.0	0.99	2679	22	2678	34	2678	11	2844	84	2680	2	+0
10644-2.1	2177	189	0.09	1.82	1.0	0.1849	0.31	14.02	1.1	0.550	1.0	0.96	2825	24	2910	44	2823	13	2969	43	2697	5	-6
10644-28.2	1158	38	0.03	1.92	1.0	0.1852	0.23	13.33	1.0	0.522	1.0	0.98	2707	23	2710	35	2707	12	2720	297	2700	4	-0
10644-19.1	499	133	0.27	2.03	1.0	0.1895	0.25	12.87	1.1	0.493	1.0	0.97	2582	22	2512	30	2576	11	2784	54	2738	4	+7
10644-20.1	406	125	0.31	1.92	1.1	0.1905	0.22	13.71	1.1	0.522	1.1	0.98	2708	25	2686	37	2707	12	2736	50	2747	4	+2
10644-12.3	276	131	0.47	2.01	1.0	0.1908	0.26	13.11	1.1	0.499	1.0	0.97	2607	22	2541	31	2603	12	2688	45	2749	4	+6
10644-14.1	311	180	0.58	1.92	1.0	0.1908	0.33	13.70	1.1	0.521	1.0	0.95	2701	23	2675	34	2697	13	2767	46	2749	5	+2
10644-28.3	190	102	0.54	1.83	1.1	0.1915	0.25	14.44	1.2	0.547	1.1	0.98	2812	26	2850	45	2816	14	2758	50	2755	4	-3
10644-17.1	590	430	0.73	1.87	1.0	0.1925	0.18	14.17	1.1	0.534	1.0	0.99	2758	23	2755	37	2753	13	2817	35	2764	3	+0
10644-9.1	4272	768	0.18	1.56	1.1	0.1927	0.49	17.04	1.2	0.641	1.1	0.92	3194	28	0	38	3194	17	3214	40	2766	8	-20
10644-34.2	244	193	0.79	1.87	1.1	0.1930	0.23	14.22	1.1	0.534	1.1	0.98	2760	25	2755	40	2756	14	2801	42	2768	4	+0
10644-11.1	280	167	0.60	2.05	1.1	0.1938	0.42	13.04	1.2	0.488	1.1	0.93	2562	23	2486	31	2546	12	2773	66	2775	7	+9
10644-18.1	76	40	0.53	2.02	1.3	0.1940	1.15	13.23	1.7	0.495	1.3	0.74	2591	27	2505	36	2568	14	2931	124	2776	19	+8
10644-35.2	323	259	0.80	1.88	1.1	0.1943	0.21	14.23	1.1	0.531	1.1	0.98	2747	24	2729	37	2743	14	2789	38	2779	3	+1
10644-18.2	86	40	0.47	1.82	1.1	0.1947	0.44	14.73	1.1	0.549	1.1	0.92	2819	24	2844	42	2811	14	2959	64	2782	7	-2
10644-13.1	75	37	0.48	1.86	1.4	0.1963	0.61	14.56	1.5	0.538	1.4	0.92	2775	31	2763	50	2769	14	2889	98	2796	10	+1

Spot Name	ppm U	ppm Th	Th/U Ratio	4corr				4corr				204corr				207corr				208corr				204corr				204corr				% Dis-corr-dant
				238/206*	% err	207*/206*	% err	4corr 207*/235	% err	4corr 206*/238	% err	204corr 238U/206Pb	% err	204corr 207Pb/238U	% err	204corr 208Pb/232Th	% err	204corr 206Pb/238U	% err	204corr 208Pb/232Th	% err	204corr 206Pb/238U	% err	204corr 208Pb/232Th	% err	204corr 206Pb/238U	% err	204corr 208Pb/232Th	% err	204corr 206Pb/238U	% err	
10645-80.1	284	13	0.05	2.56	1.1	0.1079	1.39	5.80	1.8	0.390	1.1	0.61	2123	20	2193	25	2132	7	510	451	1764	25	-24									
10645-56.1	811	14	0.02	3.13	1.0	0.1095	0.52	4.82	1.1	0.319	1.0	0.89	1786	16	1786	18	1789	5	626	392	1791	10	+0									
10645-59.1	303	27	0.09	2.78	1.0	0.1096	0.55	5.43	1.2	0.359	1.0	0.88	1978	18	2009	21	1983	6	1522	110	1793	10	-12									
10645-63.1	600	9	0.02	3.06	1.0	0.1101	0.38	4.95	1.1	0.326	1.0	0.94	1821	16	1824	18	1823	5	851	323	1801	7	-1									
10645-22.2	407	5	0.01	3.00	1.0	0.1104	0.44	5.08	1.1	0.334	1.0	0.92	1857	17	1864	19	1857	5	1523	461	1805	8	-3									
10645-7.2	312	17	0.05	2.83	1.0	0.1108	0.47	5.40	1.1	0.353	1.0	0.91	1950	17	1972	21	1952	6	1701	134	1812	8	-9									
10645-23.1	372	15	0.04	3.61	1.0	0.1109	0.77	4.23	1.3	0.277	1.0	0.80	1575	14	1549	16	1578	4	1113	166	1814	14	+15									
10645-25.1	525	52	0.10	3.35	1.1	0.1109	0.37	4.56	1.1	0.298	1.1	0.95	1682	16	1666	18	1682	5	1733	66	1814	7	+8									
10645-57.2	550	8	0.02	3.14	1.1	0.1110	0.27	4.87	1.1	0.318	1.1	0.97	1782	17	1777	20	1783	5	1492	187	1815	5	+2									
10645-56.2	1006	18	0.02	3.03	1.0	0.1111	0.47	5.06	1.1	0.331	1.0	0.91	1841	16	1845	19	1842	5	1243	292	1817	9	-2									
10645-63.2	616	9	0.01	3.07	1.0	0.1111	0.26	5.00	1.1	0.326	1.0	0.97	1820	16	1821	19	1820	5	1713	199	1818	5	-0									
10645-25.2	346	31	0.09	3.01	1.1	0.1118	0.41	5.12	1.2	0.332	1.1	0.94	1849	18	1851	20	1848	5	1913	83	1829	7	-1									
10645-8.1	417	6	0.01	3.06	1.1	0.1118	0.32	5.04	1.1	0.327	1.1	0.96	1823	17	1822	19	1823	5	1326	253	1829	6	+0									
10645-20.1	613	15	0.02	3.08	1.0	0.1120	0.23	5.01	1.0	0.324	1.0	0.97	1811	16	1808	18	1810	5	2122	99	1832	4	+1									
10645-32.1	831	86	0.10	3.11	1.0	0.1121	0.31	4.97	1.1	0.322	1.0	0.96	1797	16	1792	18	1797	5	1846	49	1834	6	+2									
10645-23.3	266	11	0.04	3.36	1.0	0.1121	1.24	4.60	1.6	0.297	1.0	0.65	1678	15	1659	17	1677	4	1826	477	1834	22	+10									
10645-58.1	359	49	0.14	2.46	1.0	0.1122	0.97	6.29	1.4	0.407	1.0	0.73	2200	20	2279	25	2203	8	2022	172	1835	18	-23									
10645-14.1	827	10	0.01	3.09	1.0	0.1122	0.22	5.00	1.0	0.323	1.0	0.98	1806	16	1802	18	1807	5	1604	175	1836	4	+2									
10645-29.1	912	55	0.06	3.00	1.0	0.1138	0.21	5.23	1.0	0.333	1.0	0.98	1853	16	1852	19	1851	5	2052	58	1861	4	+0									
10645-101.1	530	22	0.04	2.89	1.0	0.1141	0.24	5.45	1.1	0.346	1.0	0.97	1918	17	1926	20	1916	6	2181	82	1866	4	-3									
10645-52.1	464	27	0.06	2.95	1.0	0.1141	0.34	5.33	1.1	0.339	1.0	0.95	1880	17	1883	19	1879	6	2042	97	1866	6	-1									
10645-17.1	368	13	0.04	2.94	1.2	0.1148	0.50	5.39	1.3	0.340	1.2	0.92	1889	19	1891	22	1887	6	2234	245	1877	9	-1									
10645-1.1	802	46	0.06	2.88	1.0	0.1157	0.27	5.53	1.1	0.347	1.0	0.97	1920	17	1924	20	1917	6	2274	124	1891	5	-2									
10645-18.1	451	117	0.26	3.09	1.2	0.1159	0.72	5.17	1.4	0.323	1.2	0.86	1807	19	1794	21	1804	6	1877	68	1894	13	+5									
10645-67.1	1120	227	0.20	2.87	1.0	0.1172	0.17	5.62	1.0	0.348	1.0	0.99	1925	17	1927	20	1922	6	2043	31	1914	3	-1									
10645-67.2	948	160	0.17	2.93	1.0	0.1172	0.22	5.51	1.1	0.341	1.0	0.98	1892	17	1888	20	1892	6	1869	37	1914	4	+1									
10645-1.1.2	854	41	0.05	2.99	1.0	0.1175	0.24	5.42	1.0	0.334	1.0	0.97	1859	16	1849	19	1859	5	1809	72	1919	4	+4									
10645-67.2.2	947	167	0.18	2.95	1.0	0.1177	0.21	5.49	1.0	0.339	1.0	0.98	1880	16	1873	19	1880	6	1860	35	1922	4	+2									
10645-1.1.3	731	29	0.04	3.07	1.1	0.1179	0.21	5.29	1.1	0.326	1.1	0.98	1817	18	1801	20	1817	5	1856	70	1925	4	+6									
10645-27.1	1506	343	0.23	2.87	1.0	0.1189	0.52	5.71	1.1	0.348	1.0	0.89	1925	17	1923	20	1921	6	2080	30	1940	9	+1									
10645-7.1	229	90	0.39	2.88	1.0	0.1194	0.49	5.71	1.1	0.347	1.0	0.91	1920	17	1915	20	1916	7	1985	47	1947	9	+2									
10645-42.1	659	195	0.30	2.82	1.0	0.1201	0.36	5.88	1.1	0.355	1.0	0.94	1957	17	1957	20	1956	6	1994	33	1958	6	+0									
10645-95.1	557	92	0.17	2.85	1.1	0.1204	0.39	5.82	1.1	0.351	1.1	0.94	1939	18	1935	21	1937	6	2041	60	1962	7	+1									
10645-58.2	181	133	0.73	2.82	1.1	0.1211	0.53	5.92	1.2	0.355	1.1	0.89	1958	18	1955	21	1946	8	2071	42	1972	9	+1									
10645-22.1	1715	939	0.55	2.78	1.0	0.1214	0.41	6.01	1.1	0.359	1.0	0.93	1978	17	1978	20	1974	7	2036	31	1978	7	-0									
10645-36.1	463	189	0.41	2.81	1.1	0.1223	0.24	6.01	1.1	0.356	1.1	0.98	1964	19	1960	22	1963	7	1993	32	1990	4	+1									

10645-27.2	1394	538	0.39	2.86	1.0	0.1224	0.16	5.91	1.0	0.350	1.0	0.99	1935	17	1925	20	1934	6	1952	27	1992	3	+3
10645-39.1	1643	492	0.30	2.72	1.0	0.1226	0.13	6.22	1.0	0.368	1.0	0.99	2018	18	2023	21	2015	7	2092	26	1995	2	-1
10645-18.2	186	119	0.64	2.95	1.1	0.1227	1.02	5.74	1.5	0.339	1.1	0.73	1883	18	1865	20	1883	7	1886	40	1995	18	+6
10645-46.1	670	463	0.69	2.74	1.0	0.1238	0.19	6.23	1.0	0.365	1.0	0.98	2006	17	2004	21	2001	7	2050	26	2011	3	+0
10645-12.1	348	235	0.68	2.74	1.0	0.1244	0.31	6.26	1.1	0.365	1.0	0.96	2004	18	2001	21	2001	8	2036	44	2021	6	+1
10645-75.1	995	113	0.11	2.58	1.0	0.1287	0.19	6.88	1.0	0.388	1.0	0.98	2112	19	2118	23	2107	7	2466	48	2081	3	-2
10645-77.1	507	63	0.12	2.74	1.2	0.1336	0.43	6.72	1.2	0.365	1.2	0.94	2005	20	1977	23	1997	7	2504	87	2146	8	+8
10645-101.2	174	73	0.42	2.49	1.1	0.1448	0.65	8.00	1.2	0.401	1.1	0.85	2173	19	2146	24	2161	8	2390	56	2285	11	+6
10645-70.1	571	76	0.13	2.46	1.0	0.1491	0.21	8.37	1.0	0.407	1.0	0.98	2202	19	2167	23	2196	8	2556	50	2336	4	+7
10645-98.1	1051	517	0.49	2.37	1.0	0.1552	0.21	9.04	1.0	0.422	1.0	0.98	2271	19	2233	24	2264	9	2379	31	2404	4	+7
10645-57.1	888	170	0.19	2.28	1.0	0.1555	0.29	9.41	1.1	0.439	1.0	0.96	2345	20	2326	26	2337	9	2690	40	2407	5	+3
10645-52.2	312	83	0.27	2.46	1.1	0.1576	0.35	8.85	1.2	0.407	1.1	0.96	2203	21	2143	26	2195	8	2427	59	2430	6	+11
10645-37.1	1061	381	0.36	2.38	1.0	0.1579	0.13	9.15	1.0	0.420	1.0	0.99	2261	19	2212	24	2253	8	2417	29	2433	2	+8
10645-98.2	837	278	0.05	2.25	1.0	0.1614	0.17	9.87	1.0	0.444	1.0	0.99	2367	20	2333	26	2364	9	2431	36	2470	3	+5
10645-31.1	1409	38	0.03	2.23	1.2	0.1620	0.41	10.01	1.3	0.448	1.2	0.95	2386	25	2356	32	2385	9	2510	78	2477	7	+4
10645-64.1	1148	61	0.05	2.18	1.1	0.1647	0.42	10.42	1.2	0.459	1.1	0.93	2435	22	2411	29	2435	9	2442	78	2504	7	+3
10645-19.1	1571	901	0.57	2.21	1.1	0.1675	0.13	10.43	1.1	0.452	1.1	0.99	2402	23	2358	29	2380	10	2710	33	2533	2	+6
10645-55.1	353	137	0.39	2.14	1.0	0.1701	0.22	10.98	1.0	0.468	1.0	0.98	2476	21	2445	28	2470	10	2594	40	2558	4	+4
10645-30.2	642	298	0.46	2.25	1.1	0.1703	0.24	10.43	1.1	0.444	1.1	0.98	2370	22	2306	28	2353	10	2651	37	2561	4	+9
10645-61.1	236	49	0.21	2.12	1.1	0.1744	0.30	11.35	1.1	0.472	1.1	0.96	2492	22	2450	29	2492	10	2481	66	2601	5	+5
10645-38.1	183	84	0.46	2.20	1.0	0.1751	0.36	10.96	1.1	0.454	1.0	0.94	2413	21	2344	27	2398	10	2669	52	2607	6	+9
10645-30.1	550	310	0.56	2.13	1.0	0.1787	0.17	11.55	1.0	0.469	1.0	0.99	2478	21	2415	27	2475	11	2528	32	2641	3	+7
10645-8.2	516	382	0.74	2.10	1.3	0.1787	0.23	11.72	1.3	0.475	1.3	0.98	2507	26	2453	35	2501	11	2565	39	2641	4	+6
10645-16.1	346	440	1.27	1.99	1.0	0.1814	0.22	12.57	1.0	0.503	1.0	0.98	2626	22	2607	32	2605	14	2745	33	2666	4	+2
10645-23.2	250	86	0.35	2.06	1.2	0.1830	0.33	12.24	1.3	0.485	1.2	0.97	2550	26	2494	35	2544	11	2683	64	2680	5	+6

10646-29.1	986	13	0.01	3.05	1.0	0.1122	0.18	5.07	1.0	0.327	1.0	0.98	1826	16	1825	18	1826	5	1915	123	1835	3	+1
10646-99.1	445	16	0.04	2.95	1.0	0.1122	0.27	5.24	1.1	0.339	1.0	0.97	1880	17	1887	19	1880	6	1748	88	1836	5	-3
10646-18.1	667	21	0.03	3.02	1.0	0.1123	0.22	5.14	1.0	0.332	1.0	0.98	1846	16	1848	19	1846	5	1935	92	1838	4	-1
10646-58.1	723	12	0.02	3.05	1.0	0.1124	0.21	5.09	1.0	0.328	1.0	0.98	1829	16	1828	18	1829	5	1877	105	1839	4	+1
10646-36.2	771	18	0.02	3.05	1.0	0.1125	0.23	5.08	1.0	0.328	1.0	0.98	1827	16	1825	18	1827	5	1939	116	1839	4	+1
10646-3.1	397	22	0.06	2.95	1.0	0.1125	0.56	5.26	1.2	0.339	1.0	0.88	1883	17	1890	19	1884	6	1831	175	1840	10	-3
10646-1.1	401	23	0.06	3.06	1.0	0.1125	0.33	5.07	1.1	0.327	1.0	0.95	1822	16	1819	19	1822	5	1816	84	1840	6	+1
10646-33.1	406	15	0.04	3.03	1.0	0.1125	0.32	5.12	1.1	0.330	1.0	0.95	1837	16	1837	19	1838	5	1695	112	1841	6	+0
10646-51.1	2222	16	0.01	2.91	1.0	0.1126	0.12	5.33	1.0	0.343	1.0	0.99	1901	17	1911	19	1901	6	1915	86	1842	2	-4
10646-21.1	918	115	0.13	3.03	1.0	0.1127	0.19	5.13	1.0	0.330	1.0	0.98	1839	16	1839	18	1839	5	1863	35	1843	3	+0
10646-88.1	820	60	0.07	3.01	1.0	0.1127	0.19	5.16	1.0	0.332	1.0	0.98	1848	16	1849	19	1848	5	1868	45	1843	3	-0
10646-32.2	400	28	0.07	3.05	1.0	0.1128	0.30	5.10	1.1	0.328	1.0	0.96	1829	16	1826	19	1827	5	2070	75	1845	5	+1
10646-16.1	967	35	0.04	3.02	1.0	0.1129	0.17	5.15	1.0	0.331	1.0	0.99	1843	16	1843	19	1843	5	1842	57	1846	3	+0
10646-42.2	1217	59	0.05	3.01	1.0	0.1245	0.16	5.70	1.0	0.332	1.0	0.99	1849	16	1822	18	1846	5	2376	57	2022	3	+10

Curriculum Vitae

Name: Nikolas Ganderton

Post-secondary Education and Degrees: The University of Western Ontario
London, Ontario, Canada
2006-2010 B.Sc.

The University of Western Ontario
London, Ontario, Canada
2010-2013 M.Sc.

Honours and Awards: GAC Jerome H. Remick Poser Award (Honourable Mention)
GAC-MAC 2011, Ottawa, Ontario, Canada

Related Work Experience Teaching Assistant
The University of Western Ontario
2010-2012

Geological Survey of Canada
Research Affiliate Program (RAP)
2009-2012